UNIVERSIDAD
NACIONAL
DE COLOMBIA

Scaling of Bubbling Fluidized Bed Reactors

Robert José Macías Naranjo

Universidad Nacional de Colombia
Facultad de Minas, Departamento de Procesos y Energía
Medellín, Colombia
2020

Scaling of Bubbling Fluidized Bed Reactors

Robert José Macías Naranjo

A dissertation submitted to the Facultad De Minas of Universidad Nacional de Colombia-Medellín in partial fulfillment of the requirements for the Degree of

Doctorado en Ingeniería – Sistemas Energéticos

Advisor:

Ph.D. Farid Chejne Janna

Co-Advisor:

Ph.D. Juan Carlos Maya López

Investigation line:

Energy Systems

Research group:

Applied thermodynamics and alternative energies TAYEA

Universidad Nacional de Colombia

Facultad de Minas, Departamento de Procesos y Energía

Medellín, Colombia

2020

“Science enhances the moral value of life, because it furthers a love of truth and reverence—love of truth displaying itself in the constant endeavor to arrive at a more exact knowledge of the world of mind and matter around us, and reverence, because every advance in knowledge brings us face to face with the mystery of our own being.”

Max Planck

Declaración de obra original

Yo declaro lo siguiente:

He leído el Acuerdo 035 de 2003 del Consejo Académico de la Universidad Nacional. «Reglamento sobre propiedad intelectual» y la Normatividad Nacional relacionada al respeto de los derechos de autor. Esta disertación representa mi trabajo original, excepto donde he reconocido las ideas, las palabras, o materiales de otros autores.

Cuando se han presentado ideas o palabras de otros autores en esta disertación, he realizado su respectivo reconocimiento aplicando correctamente los esquemas de citas y referencias bibliográficas en el estilo requerido.

He obtenido el permiso del autor o editor para incluir cualquier material con derechos de autor (por ejemplo, tablas, figuras, instrumentos de encuesta o grandes porciones de texto).

Por último, he sometido esta disertación a la herramienta de integridad académica, definida por la universidad.

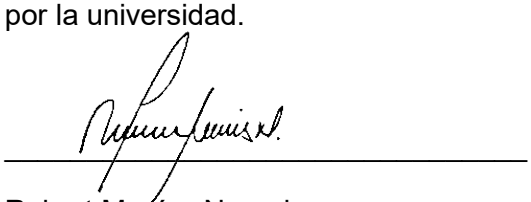

Robert Macías Naranjo

14/12/2020

Acknowledgments

First and foremost I am extremely grateful to my supervisors, Prof. Farid Chejne Janna and Juan Carlos Maya for their invaluable advice, continuous support, and patience during my Ph.D. study. Their immense knowledge and plentiful experience have encouraged me all the time of my academic research and daily life. I would like to thank all the members of the TAYEA Group. It is their kind help and support that have made my study and life in the Facultad de Minas a wonderful time. Finally, I would like to express my gratitude to my mother Janette, my sisters Sandra y Valentina and, my girlfriend Valentina Sierra. Without their tremendous understanding and encouragement in the past few years, it would be impossible for me to complete my study.

The author would like to thank call 785 of Colciencias “Convocatoria de Doctorados Nacionales 2017”. To Universidad Nacional de Colombia and Universidad de Zaragoza for their support. Furthermore, the author wants to thank the project "Strategy of transformation of the Colombian energy sector in the horizon 2030", funded by call 788 of Minciencias Scientific Ecosystem. Contract number FP44842-210-2018.

Abstract

Scaling of Bubbling Fluidized Bed Reactors

This thesis presents a novel mathematical model for coal char activation with CO_2, steam, and a CO_2/steam mixture. The main contribution of this model is that CO_2 and steam react with distinct active sites, considered by attributing a unique char structure effect to each gasifying agent; the CO_2-char reaction increases the pore length, whereas the steam-char reaction increases the pore radius. Moreover, in this work proposes a novel population-balance based model for a bubbling fluidized bed reactor. This model considers two continuum phases: bubble and emulsion. The evolution of the bubble size distribution was modeled using a population balance, considering both axial and radial motion. This sub-model involves a new mathematical form for the aggregation frequency, which predicts the migration of bubbles from the reactor wall towards the reactor center. Additionally, the reacting particles were considered as a lagrangian phase, which exchanges mass with the emulsion phases. For each particle, the variation of the pore size distribution was also considered. The model presented here accurately predicted the experimental data for biochar gasification in a lab-scale bubbling fluidized bed reactor. Finally, a new strategy for the scaling of bubbling fluidized bed reactors is presented. This strategy is based on the bubble size distribution, bubble coalescence phenomenon, and the chemical reactivity, allowing to deduct a dimensionless number Φ that must remain constant at different scales to guarantee the fluidization regime. The proposed strategy is validated from computational simulations carried out at different operating conditions. Additionally, limits for the validity of this scaling strategy were determined, which agrees with those reported in the literature.

Keywords: Scaling, Fluidized bed reactor, Gasification, Population balance, Mathematical modelling

Resumen

Escalado de reactores de gasificación de lecho fluidizado

Esta tesis presenta un modelo matemático novedoso para la activación de carbón con CO_2, vapor y una mezcla de CO_2 / vapor. La principal contribución de este modelo es que el CO_2 y el vapor reaccionan con distintos sitios activos, lo que se considera atribuyendo un efecto de estructura de carbón único a cada agente gasificante; la reacción CO_2-carbón aumenta la longitud de los poros, mientras que la reacción vapor-carbón aumenta el radio de los poros. Además, en este trabajo se propone un nuevo modelo basado en el balance de población para un reactor de lecho fluidizado burbujeante. Este modelo considera dos fases continuas: burbuja y emulsión. La evolución de la distribución del tamaño de las burbujas se modeló utilizando un balance de población, considerando tanto el movimiento axial como el radial. Este submodelo implica una nueva forma matemática para la frecuencia de agregación, que predice la migración de burbujas desde la pared del reactor hacia el centro del reactor. Además, las partículas que reaccionan fueron consideradas como una fase lagrangiana, que intercambia masa con la fase emulsión. Para cada partícula, también se consideró la variación de la distribución del tamaño de poro. El modelo presentado aquí predijo con precisión los datos experimentales para la gasificación de biochar en un reactor de lecho fluidizado burbujeante a escala de laboratorio. Finalmente, se presenta una nueva estrategia para el escalado de reactores de gasificación de lecho fluidizado burbujeante. Esta estrategia se basa en la distribución del tamaño de las burbujas, el fenómeno de coalescencia de las burbujas y la reactividad química, lo que permite deducir un número adimensional Φ que debe permanecer constante a diferentes escalas para garantizar el régimen de fluidización y los rendimientos. La estrategia propuesta se valida a partir de simulaciones computacionales realizadas en diferentes condiciones de operación. Adicionalmente, se determinaron límites para la validez de esta estrategia de escalado, lo que concuerda con lo reportado en la literatura.

Palabras clave: gasificación, modelo matemático, reactor de lecho fluidizado, escalado, balances de población.

Table of content

Pag.

Abstract..... IX

List of figures..... XIII

List of tables XV

1. General introduction 1
1.1 Scientific contributions..... 4
References 9

2. On the evolution of pore microstructure during coal char activation with steam/CO_2 mixtures. 15
2.1 Introduction 16
2.2 Experimental 18
2.2.1 Determination of chemical control conditions 19
2.2.2 Evolution of the PSD and specific surface area..... 19
2.3 The model 20
2.3.1 Model assumptions..... 20
2.3.2 Model Development..... 21
2.3.3 Pore overlapping..... 22
2.4 Analysis and results 25
2.4.1 Chemically controlled conditions..... 25
2.4.2 Intraparticle gradients 32
2.5 Concluding remarks 36
References 37

3. Integration of the different scales: Bubble, Particle, and Reactor 43
3.1 Introduction 43
3.2 Mathematical model 47
3.2.1 Particle Model..... 47
3.2.2 Pore overlapping..... 49
3.2.3 Two-phase reactor model 50
3.3 Population balance for the bubble size distribution..... 51
3.3.1 Aggregation frequency..... 53
3.3.2 Solution method and scales connection strategy 56
3.4 Results and discussion..... 59
3.4.1 Another simulations 67
3.5 Conclusion 71
3.6 Notation..... 72

References 74

4. Scaling strategy 79
4.1 Introduction 79
4.2 Fluidized beds modelling for scaling 82
4.3 Dimensionless numbers and scaling methodology 85
4.3.1 Limits of the scaling methodology 88
4.4 Scaling strategy 90
4.5 Concluding remarks 94
References 95

A. Appendix: Pearson's correlation coefficient 101

List of figures

Figure 1-1. Graphic representation of the integration of different scales. 2
Figure 1-2. Reaction scheme. 4
Figure 1-3. Representation of the aggregation frequency 5
Figure 1-4. Scaling results 6
Figure 1-5. Detail of signal pressure over time. 7
Figure 2-1. Scheme of the different scales in a bubbling fluidized bed reactor. 15
Figure 2-2. Evolution of PSD during activation with CO_2 for a) C1; b) C2; and c) C3. 27
Figure 2-3. Evolution of PSD during activation with steam for a) C1; b) C2; and c) C3. . 29
Figure 2-4. Evolution of PSD during activation with a CO_2/steam mixture for a) C1; b) C2; and c) C3 31
Figure 2-5. Evolution of specific surface area for the activation of C1 with a) CO_2; b) steam; and c) a CO_2/steam mixture. 34
Figure 3-1. Scheme of fluid dynamics processes in a bubbling fluidized bed reactor. 47
Figure 3-2. Representation of the aggregation frequency 53
Figure 3-3. Bubble frequency predictions 59
Figure 3-4. Bubble size predictions 60
Figure 3-5. Bubble rise velocity predictions 61
Figure 3-6. Diagram of fluidized bed experimental setup 63
Figure 3-7. a) Evolution of specific surface area with conversion. b) Evolution of char conversion over time. 64
Figure 3-8. (a) Porosity distribution and (b) Average bubble size with radial position for various fluidization velocities 65
Figure 3-9. Emulsion temperature profiles 66
Figure 3-10. Evolution of pressure over time at z=0.3 m. 66
Figure 3-11. Evolution over time of pressure fluctuations at different minimum velocities of fluidization. 67
Figure 3-12. Detail of signal pressure over time 68
Figure 3-13. Profile of porosity of the bubbling fluidized bed 69
Figure 3-14. Profile of average bubble radius in the bubbling fluidized bed 69
Figure 3-15. Profile of numbers of bubbles in the bubbling fluidized bed 70
Figure 3-16. Terminal velocity of particles at different minimum velocities of fluidization 71
Figure 4-1. Fluidization chart. Adapted from [57] 88
Figure 4-2. Study cases 91
Figure 4-3. Scaling results 93

List of tables

Table 2-1: Proximate analysis of coal samples. 19
Table 3-1. Parameters of simulations. 57
Table 3-2. Characterization of char sample 62
Table 4-1. Sets of scaling law in literature. 83
Table 4-2. Scaling limits 89
Table 4-3. Scaling results 92

1. General introduction

The interest in combining and/or replacing fossil fuels in recent years has raised attention to alternative energy sources such as the ones derived from some residual biomass and coal thermochemical processes. The main thermochemical processes currently used at industrial level for the generation of energy are torrefaction, pyrolysis, gasification, and combustion.

Gasification is a technology that has gained relevance in the last years and appears as a partial alternative supply for conventional fuels, since its derived products are similar to those of oil [1]. The gasification process consists of a set of thermochemical reactions that occur in a poor oxygen environment; the carbonaceous material formed mainly by coal and/or biomass is subjected to the action of heat and transformed into a combustible gas of energy interest called poor gas, which according to its composition is used in the production of thermal or electrical energy[2]. The gases obtained in the combustion of organic solids contain mainly carbon monoxide, hydrogen, methane, water vapor, nitrogen, carbon dioxide, and CnHm. These products can be given in very variable compositions, this result is due to the type of coal and/or biomass, the operating conditions (temperature and pressure), the type of process used, the use (or not) of catalysts and the gasification agent used [3].

One of the most important technologies is bubbling fluidized bed, which has been extensively explored in both experimental and theoretical approaches and many industries as a source of energy generation [4]. In a fluidized bed, particles such as char or biomass are kept suspended due to gas entering the reactor and forming a mixture between the solid phase and the gas phase (emulsion), their behavior is similar to a fluid. The excess gas is transformed into bubbles that rise through the bed, constantly mixing the different phases. This allows the solid-gas contact to be improved, increasing the mass transfer and, in addition, keeps the temperature in the bed almost homogeneous [5].

Given the significance of these types of technologies, it is important to develop a scaling strategy, which was the aim of this thesis. The basic main difficulty in the scaling of this type of reactors is that that both multiscale and multiphase phenomena take place. In Figure 1-1, it can be seen the importance of developing models coupling what happens inside the particle, the impact of the bubbles, and the connection with the continuous phase in the reactor.

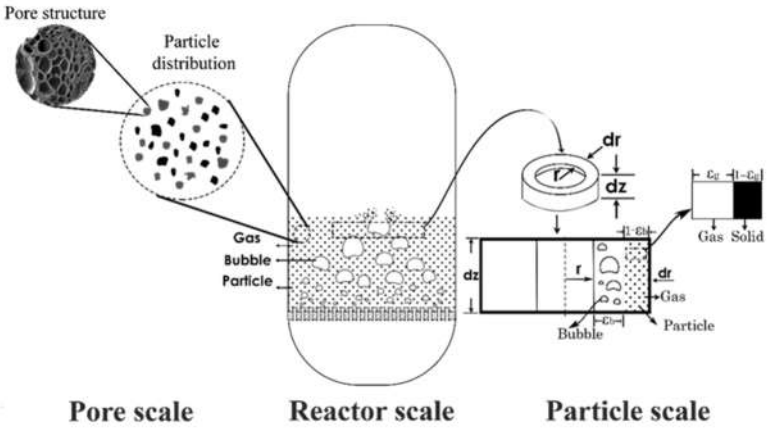

Figure 1-1. Graphic representation of the integration of different scales.

On the other hand, several authors have classified the phases of bubbling fluidized beds into two types; the emulsion phase formed by gas and solid particles, and the bubble phase[6–12]. The emulsion phase has been widely explored by several authors[11,13–19], however, although approximate kinetic models and particle models such as the Shrinking Core have been developed[20–23], these models represent solid-gas interface, boundary layer and mass transfer, but the behavior of intra-particles phenomena and their effect into the bed are not considered. Similarly, models have been proposed to predict the reactivity and internal behavior of the particles, as is the case of activated carbon in fluidized beds such as those developed by [24–29]; however, these models have not been integrated into the global process, that is, coupled in the same model to the mass transfer that occurs within the bed. On the other hand, several authors have developed models based on population balances to predict the evolution of the porous structure in the particles taking into account the kinetics and initial pore distribution[22,24,25,30–32]. In the same way, these models have been applied to model the behavior of bubbles in fluidized bed reactors[33,34].

The bubbles in a fluidized bed reactor rise in the form of a gas bag through the bed, so various heterogeneous reactions occur during their rise in the solid-gas interface. Authors such as Lim. *et.al* and Medrano. *et.al* [13,35–37] have described the behavior of bubbles through image analysis techniques, finding that they increase in size and as they rise, and move in axial and radial directions. The size increase is due to the pressure gradients which the gas bag is subjected to and the interaction between bubbles, the latter phenomenon has been called coalescence and occurs when two or more bubbles combine to form a larger bubble[34,38–45]. Krishna *et.al.*[33,34,46] have developed bubble coalescence models based on population balances. However, these models describe bubbles fusion only in axial direction, that is, the model takes into account a bubble that rises in the bed on an imaginary vertical band and combines with the bubbles it finds in its path, neglecting the radial movement of the bubbles which has been demonstrated by various authors. This behavior is extremely complex to model since the bubble distribution of the surroundings and the movement of the bubble towards the center of the reactor must be taken into account.

In accordance with the above, due to the heterogeneous nature of the fluidized beds and the strong interaction between hydrodynamics, the kinetics of the reactions and, the heat and mass transfer phenomena, it is difficult to describe them and it has been necessary to use empirical correlations for having an approximate behavior[47]. However, these correlations are the product of many years of experimentation and modelling processes, in particular, these correlations fail at the time of being applied to other scales and do not consider the transfer phenomena simultaneously. In that sense, the scale-up or scale-down of bubbling fluidized bed reactors becomes a complex and troublesome endeavor.

Maintaining the hydrodynamic regime and the adequate conversion of the particles within the bed depends on many variables that can affect the performance of the reactor and the economy at the time of operation. Therefore, one of the main challenges of scaling fluidized bed gasification reactors is to identify the interaction, dependence, and variation of the operating parameters with the reactor scale.

In that sense, this work aims to develop a mathematical model that integrates the intraparticle phenomena, the kinetics of reactions, mass transfer and, bubble phase to global bed hydrodynamics for bringing new information about the actual behavior of fluidized bed reactors at different scales and proposing a new scaling strategy.

1.1 Scientific contributions

To carry out this task, a new mathematical model for coal/biochar activation with CO_2/steam mixtures was developed that considers the pore overlapping phenomenon that strongly affects the development of both porosity and specific surface area during the physical activation process. Furthermore, this new model, for the very first time, takes into account the longitudinal pore growth caused by the CO_2/char reaction. Thus, the change in pore length and pore radius is respectively expressed by

$$\frac{dl}{dt} = \frac{k1(C_{CO_2})}{\rho_m} \tag{1-1}$$

$$\frac{dr_p}{dt} = \frac{k2(C_{H_2O})}{\rho_m} \tag{1-2}$$

In Figure 1-2, the behavior predicted by the model is schematized. First, under a CO_2 atmosphere, the model predicts a monotonically growth in pore length. Secondly, under a steam atmosphere, the model predicts a growing in pore radius without increase in pore length. Finally, under an atmosphere made up of a CO_2/steam mixture, both phenomena (pore radius and pore length growth) take place.

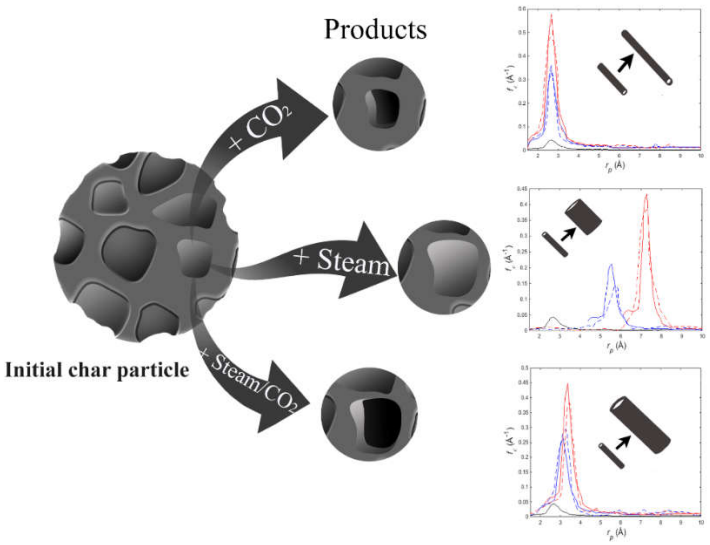

Figure 1-2. Reaction scheme.

From the comparison of model prediction with experimental data, it was demonstrated that the CO_2-char reaction increases the pore length, whereas the steam-char reaction increases the pore radius. Moreover, this mathematical model is fundamental for the understanding of the phenomena that occur at different scales and is then integrated to a reactor-scale model.

Another important contribution consist on the development of a novel mathematical model for bubbling fluidized bed gasifiers that couples different scales: bubble, particle, and reactor scale, which had not been achieved so far (see Figure 1-1). The model integrates simultaneously reactivity, hydrodynamics, and energy and mass balances. Additionally, the model consider coalescence of bubbles and their movement from the wall towards the reactor center, which it has been observed experimentally but never modelled (see Figure 1-3)

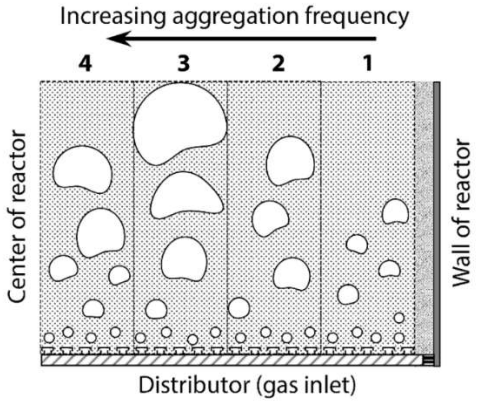

Figure 1-3. Representation of the aggregation frequency

For this, a new mathematical form for the aggregation frequency a_{gf} was proposed, which involves the probability of coalescence among different bibs within the reactor domain:

$$a_{gf_1,i} = a_{g0} * M_{0,i} \tag{1-3}$$

$$a_{gf_2,i} = a_{g0} * \left(M_{0,i-1} + M_{0,i+1}\right) \tag{1-4}$$

This new expression for the aggregation frequency constitutes a significant advance on the modelling of fluidized bed reactors and also allows to relate the aggregation frequency with

the reactor size, making that this parameter can be used for scaling fluidized bed reactors. In this way, a new dimensionless number for scaling fluidized bed reactors ($\boldsymbol{\Phi}$) is proposed:

$$\Phi = \frac{u_{g0}\dot{\gamma}_0'' S}{C_{e0} u_{b_0} \overline{a_{gf}} f_{b_0} \overline{r_{b_0}}} \tag{1-5}$$

This proposed parameter integrates both reactivity and hydrodynamics of bubbling fluidized bed reactors, which had not been proposed to date. Furthermore, the dimensionless numbers proposed here contain the most used scaling parameters and reported in the literature. The applicability of this new scaling methodology was also validated by means of simulations for different reactor sizes and particle sizes, resulting in a constant value for $\boldsymbol{\Phi}$, which confirm the hypothesis of this work (see Figure 1-4).

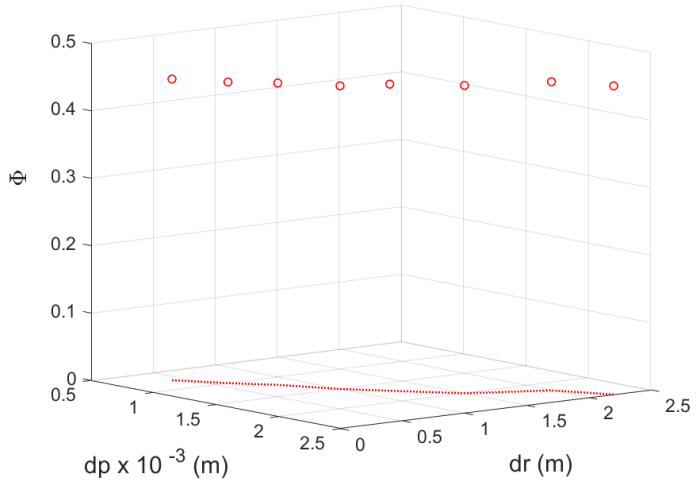

Figure 1-4. Scaling results

Hence, Figure 1-4 shows that the $\boldsymbol{\Phi}$ number remains constant for the scaling of reactors ranging from 0.4 m to 2.2 m with variations in particle size, which also allows the reactor conversion to be maintained. In addition, Figure 1-4 constitutes an important tool to scale-up or scale down within the established limits.

In addition, the model mentioned above allowed to describe the behavior of the pressure signal of a bubbling fluidized bed due to changes in the porosity of the bed (see Figure 1-5). That is, to the change in the distribution of the size of the bubbles represented in the model as $\frac{4}{3}\pi * M_3$.

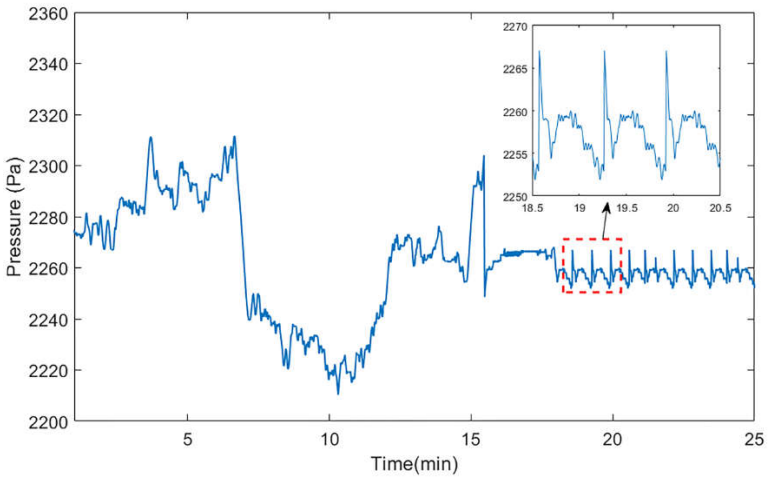

Figure 1-5. Detail of signal pressure over time.

In order to bring clarity about the sequence in this work, the chapters that constitute it and a brief description are given below. The thesis is divided into three sections:

First section (Chapter 2). Particle modelling. In this section, a novel mathematical model for coal/biochar activation with CO2, steam and a CO2/steam mixture is developed. The main hypothesis of this model is that CO2 and steam react on different active sites, which was considered by attributing different effects on the char structure to each gasifying agent. On the one hand, it is supposed that CO2-char reaction mainly increases pore length whereas the steam-char reaction increases the pore radius. Additionally, the pore overlapping effect was taken into account and the radial pore growth was computed by means of a population balance equation. **Second section (Chapter 3)**. Mathematical modelling of fluidized bed reactor. A novel population balance-based model for a bubbling fluidized bed reactor is proposed. This model takes into account two continuum phases: bubble and emulsion (bubble-gas-particles). The bubble size distribution was modeled using a population balance inside the reactor, in which the motion in both axial and radial directions was considered. This sub-model involves a new mathematical form for the aggregation frequency, which allows predicting the migration of bubbles located close to the reactor wall towards the reactor center. **Third section (Chapter 4)**. Scaling strategy. In this chapter, a new strategy of scaling for fluidized bed reactors based on the a-dimensional numbers (Macias-Maya-Chejne) that couple physical phenomena such as bubble dynamics and kinetics of particles during the gasification process was developed.

The main results of this work are presented in the following scientific publications

Published papers and books

- Robert J. Macías, Juan C. Maya and Farid Chejne, J. Arauzo, Zainab Afailal. Modelling a fluidized bed reactor by integrating various scales: pore, particle, and reactor. AIChE Journal.2020.
- J. C. Maya, Robert J. Macías, C. A. Gómez, and F. Chejne. On the evolution of pore microstructure during coal char activation with steam/CO_2 mixtures, Carbon N. Y., vol. 158, pp. 121–130, Mar. 2020.
- La gasificación: alternativa de generación de energía y productos con alto valor agregado para la industria En: Colombia 2016. ed:Editorial Universidad Nacional De Colombia Sede Medellin. ISBN: 978-958-775-932-7
- Juan C. Maya, Robert Macías, Carlos A. Gómez, and Farid Chejne. On the modelling of the peripheral fragmentation during the coal char gasification with CO_2

Papers submitted

- Robert J. Macías, Juan C. Maya and Farid Chejne. Strategy of scaling of bubbling fluidized bed reactors. AIChE Journal.2020

Events

- A Novel Population Balance-Based Model For Bubbling Fluidized Bed Reactor. 13th International Conference on Fluidized Bed Technology (CFB-13). Vancouver, Canada 2021.

Software

- PopFlow 1.0. Robert J Macías, Juan C. Maya, Farid Chejne, Carlos A. Gómez, Carlos M. Ceballos. Dirección Nacional de Derechos de Autor. Register 13-75-353. Sept 2019.

References

1. Meerman JC, Knoope M, Ramírez A, Turkenburg WC, Faaij APC. The Techno-Economic Potential of Integrated Gasification Co-Generation Facilities with CCS Going from Coal to Biomass. Energy Procedia. 2013;37:6053-6061.

2. Higman C, van der Burgt M. Gasification.; 2003.

3. Basu P. Biomas Gasification and Pyrolysis: Practical Design. Elsevier, ed. Published online 2010.

4. Basu P. Front Matter. In: Basu P, ed. Biomass Gasification Design Handbook. Vol 45. Elsevier; 2010:i-i.

5. Rüdisüli M, Schildhauer TJ, Biollaz SM a., van Ommen JR. Scale-up of bubbling fluidized bed reactors — A review. Powder Technology. 2012;217:21-38.

6. Ellis N, Briens LA, Grace JR, Bi HT, Lim CJ. Characterization of dynamic behaviour in gas-solid turbulent fluidized bed using chaos and wavelet analyses. Chemical Engineering Journal. 2003;96(1-3):105-116.

7. Grace JR, Shemilt LW, Bergougnou MA, Engineering Foundation (U.S.). Fluidization VI : Proceedings of the International Conference on Fluidization. Engineering Foundation; 1989.

8. Sit SP, Grace JR. Effect of bubble interaction on interphase mass transfer in gas fluidized beds. Chemical Engineering Science. 1981;36(2):327-335.

9. Grace JR. An evaluation of models for fluidized bed reactors.Fluidization fundamental studies, solid-fluid reactions, and applications. American Institute of Chemical Engineers. Published online 1971:159-157.

10. Hernández-Jiménez F, Gómez-García A, Santana D, Acosta-Iborra A. Gas interchange between bubble and emulsion phases in a 2D fluidized bed as revealed by two-fluid model simulations. Chemical Engineering Journal. 2013;215-216(January):479-490.

11. Davidson JF (John F, Harrison D (David). Fluidised Particles,. University Press;

1963.

12. Chejne F, Hernandez JP. Modelling and simulation of coal gasification process in fluidised bed. Fuel. 2002;81(13):1687-1702.

13. Medrano JA, Gallucci F, Boccia F, Alfano N, van Sint Annaland M. Determination of the bubble-to-emulsion phase mass transfer coefficient in gas-solid fluidized beds using a non-invasive infra-red technique. Chemical Engineering Journal. 2017;325:404-414.

14. Cui H, Mostoufi N, Chaouki J. Characterization of dynamic gas-solid distribution in fluidized beds. Chemical Engineering Journal. 2000;79(2):133-143.

15. Chejne F, Hernandez JP. Modelling and simulation of coal gasification process in fluidised bed. Fuel. 2002;81(13):1687-1702.

16. Vale HM, McKenna TF. Modeling particle size distribution in emulsion polymerization reactors. Progress in Polymer Science. 2005;30(10):1019-1048.

17. Jain AA, Mehra A, Ranade V V. Modeling and simulation of a fluidized bed gasifier. Asia-Pacific Journal of Chemical Engineering. 2018;13(1):1-17.

18. Abba IA, Grace JR, Bi HT, Thompson ML. Spanning the flow regimes: Generic fluidized-bed reactor model. AIChE Journal. 2003;49(7):1838-1848.

19. Mayerhofer M, Fendt S, Spliethoff H, Gaderer M. Fluidized bed gasification of biomass – In bed investigation of gas and tar formation. Fuel. 2014;117:1248-1255.

20. Zheng H, Vance Morey R. An unsteady-state two-phase kinetic model for corn stover fluidized bed steam gasification process. Fuel Processing Technology. 2014;124:11-20.

21. Heesink ABM, Klaus J, van Swaaij WPM. The influence of particle residence time distribution on the reactivity in fluidized bed reactors. Chemical Engineering Science. 1994;49(14):2243-2261.

22. Hashimoto K, Silveston PL. Gasification: Part I. Isothermal, kinetic control model for a solid with a pore size distribution. AIChE Journal. 1973;19(2):259-268.

23. Shuai W, Guodong L, Huilin L, Juhui C, Yurong H, Jiaxing W. Fluid dynamic

simulation in a chemical looping combustion with two interconnected fluidized beds. Fuel Processing Technology. 2011;92(3):385-393.

24. Maya JC, Janna FC. Novel model for non catalytic solid-gas reactions with structural changes by chemical reaction and sintering. Chemical Engineering Science. 2016;142:258-268.

25. Maya JC, Chejne F, Bhatia SK. Novel model for the sintering of ceramics with bimodal pore size distributions: Application to the sintering of lime. AIChE Journal. 2017;63(3):893-902.

26. Efthimiadis EA, Sotirchos S V. Effects of pore structure on the performance of coal gas desulfurization sorbents. Chemical Engineering Science. 1993;48(11):1971-1984.

27. Verkoeijen D, Pouw GA, Meesters GMH, Scarlett B. Population balances for particulate processes—a volume approach. Chemical Engineering Science. 2002;57(12):2287-2303.

28. Sotirchos S V, Yu H-C. Mathematical modelling of gas-solid reactions with solid product. Chemical Engineering Science. 1985;40(11):2039-2052.

29. Maya JC, Macías R, Gómez CA, Chejne F. On the evolution of pore microstructure during coal char activation with steam/CO2 mixtures. Carbon. 2020;158:121-130.

30. Ramkrishna D. Population Balances Theory and Applications to Particulate Systems in Engineering. Academic Press; 2000.

31. Natale G, Galgano A, Di Blasi C. Modeling particle population balances in fluidized-bed wood gasifiers. Biomass and Bioenergy. 2014;62:123-137.

32. Alexopoulos AH, Roussos A, Kiparissides C. Part V: Dynamic evolution of the multivariate particle size distribution undergoing combined particle growth and aggregation. Chemical Engineering Science. 2009;64(14):3260-3269.

33. Sweet IR, Gustafson SS, Ramkrishna D. Population balance modelling of bubbling fluidized bed reactors—I. well-stirred dense phase. Chemical Engineering Science. 1987;42(2):341-351.

34. Muralidhar R, Gustafson S, Ramkrishna D. Population balance modelling of bubbling fluidized beds. II. Axially dispersed dense phase. Sadhana. 1987;10(1-2):69-86.

35. Lim CN, Gilbertson MA, Harrison AJL. Bubble distribution and behaviour in bubbling fluidised beds. Chemical Engineering Science. 2007;62(1-2):56-69.

36. Almendros-Ibáñez JA, Pallarès D, Johnsson F, Santana D. Voidage distribution around bubbles in a fluidized bed: Influence on throughflow. Powder Technology. 2010;197(1-2):73-82.

37. Lim KS, Agarwal PK, O'neill BK. Measurement and modelling of bubble parameters in a two-dimensional gas-fluidized bed using image analysis. Powder Technology. 1990;60(2):159-171.

38. Glicksman LR, McAndrews G. The effect of bed width on the hydrodynamics of large particle fluidized beds. Powder Technology. 1985;42(2):159-167.

39. WELUDA KD, SCHÜTTE K, WITTLER W, WINGELSDORF R, SCHÜGERL K. INVESTIGATIONS OF THE BUBBLE PHASE BEHAVIOR IN A HIGH TEMPERATURE FLUIDIZED BED REACTOR WITH COALCOMBUSTION. Chemical Engineering Communications. 1987;62(1-6):161-185.

40. Rüdisüli M, Schildhauer TJ, Biollaz SMA, Van Ommen JR. Radial bubble distribution in a fluidized bed with vertical tubes. Industrial and Engineering Chemistry Research. 2012;51(42):13815-13824.

41. Allahwala SA, Singh B, Potter OE. Bubble frequency and distribution in fluidized beds. Chemical Engineering Communications. 1981;11(4-5):255-280.

42. Chiba T, Terashima K, Kobayashi H. Behaviour of bubbles in gas-solids fluidized beds: initial formation of bubbles. Chemical Engineering Science. 1972;27(5):965-972.

43. Shah BH, Ramkrishna D, Borwanker JD. Simulation of bubble populations in a gas fluidized bed. Chemical Engineering Science. 1977;32(12):1419-1425.

44. Darton R, LaNauze R, Davidson J, Harrison D. Bubble growth due to coalescence in fluidised beds. Transcripts of the Institute of Chemical Engineering. 1977;55:274-280.

45. Bokkers GA, Laverman JA, van Sint Annaland M, Kuipers JAM. Modelling of large-scale dense gas-solid bubbling fluidised beds using a novel discrete bubble model. Chemical Engineering Science. 2006;61(17):5590-5602.

46. Bhole MR, Joshi JB, Ramkrishna D. Population balance modeling for bubble columns operating in the homogeneous regime. AIChE Journal. 2007;53(3):579-588.

47. Horio M, Nonaka A, Sawa Y, Muchi I. A new similarity rule for fluidized bed scale-up. AIChE Journal. 1986;32(9):1466-1482.

2. On the evolution of pore microstructure during coal char activation with steam/CO_2 mixtures.

The present chapter develops a novel mathematical model for coal char activation with CO_2, steam, and a CO_2/steam mixture. This as part of the understanding of the phenomena that occur at different scales, in this case at a particle scale. As can be seen in Figure 2-1. The integration of the phenomena that occur on a particle scale such as the development of porosity will serve to determine with greater precision the conversion of the particles and therefore the mass transfer phenomena that occur within the bed to later be integrated into a complete model that allows scaling up bubbling fluidized bed gasification reactors.

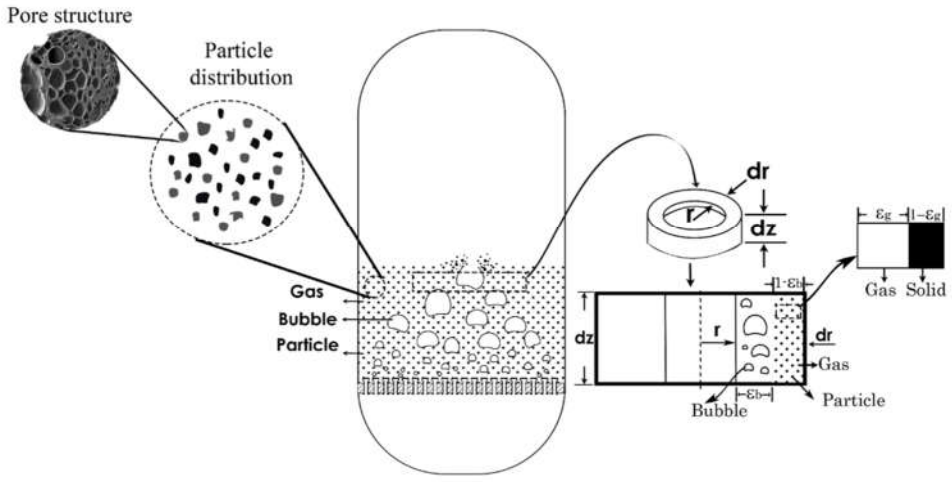

Figure 2-1. Scheme of the different scales in a bubbling fluidized bed reactor.

In this sense, the main hypothesis of this model is that CO_2 and steam react with distinct active sites, considered by attributing a unique char structure effect to each gasifying agent; the CO_2-char reaction increases the pore length, whereas the steam-char reaction increases the pore radius. Additionally, the pore overlapping effect was taken into account

and the radial pore growth was computed by means of a population balance equation. Model predictions of both the pore size distribution and specific surface area changes were compared with experimental data, resulting in an outstanding fit. This supports the model's main hypothesis, which reconciles discrepancies between various authors regarding the overall reaction velocity during activation of coal chars with CO_2/steam mixtures. Finally, the maximum specific surface area occurs under chemically-controlled conditions, where all particle zones reach their maximum areas simultaneously, while for activation with diffusional limitations each particle zone attains its maximum specific surface area at a different time.

2.1 Introduction

Activation of carbonaceous materials by partial gasification has been widely studied for its applications in wastewater treatment processes [1], the removal of undesirable tastes, colors, and odors, solvent recovery, and recently in the pharmaceutical industry for toxin removal [2]. In this process, a gas penetrates through the pores of the char and reacts with the carbon located at the pore surface, which produces a change in the microstructure of the solid. During the initial stage of activation, there is an increase in both pore volume and specific surface area; however, at some point, a maximum specific surface area is reached. This maximum value is mainly determined by the char's initial microstructure and the gasifying agent. Therefore, understanding the development of the microstructure during the activation process is fundamental to producing high quality activated carbon.

Two of the most commonly used gasifying agents are steam and CO_2, which is why a large number of experimental and theoretical studies on gasification with these molecules can be found in the scientific literature. Most of these works study gasification with either steam or CO_2, while few works study gasification with steam/CO_2 mixtures. Roberts and Harris [3] found that for gasification with a steam/CO_2 mixture at high pressures, the char-CO_2 and char-steam reactions take place in common active sites. Similarly, Umemoto et al. [4] proposed a reaction model assuming that CO_2 and steam share active sites, obtaining good agreement with experimental data. On the other hand, several authors [5–10] found that for gasification with steam/CO_2 mixtures at atmospheric pressure, the char-CO_2 and char-steam reactions occur at distinct active sites, such that the overall reaction rate can be

expressed as the sum of the reaction rate of each gas. Furthermore, Arenas and Chejne [11] found that CO_2 elongates pores whereas steam widens pores. That is, CO_2 increases the average pore length while steam increases the average pore radius.

To better understand the behavior of the microstructure during the activation process, it is necessary to develop particle models that adequately predict structural variables such as specific surface area, porosity, and Pore Size Distribution (PSD). Essentially, a particle model starts with a geometric description of the particle and its internal structure, i.e. the porous structure. Probably the simplest model is the so-called Shrinking Core Model (SCM), in which the solid particle reacts, generating a layer of solid product through which gases are diffused. Although the SCM can appropriately describe the overall activation kinetics [12], this model is only valid for non-porous materials and it does not describe the internal structure of the particle, which defines the quality of the activated carbon. Another model simulating char gasification kinetics is the Single Pore Model [13], in which the particle is described by a set of pores of uniform size that grow due to the chemical reaction. On the other hand, the so-called grain model describes the particle as a population of uniform grains that react following an SCM mechanism. The latter two models adequately describe the evolution of conversion over time and also consider the existence of concentration gradients in the particle. However, they predict a monotonic variation of the specific surface area, which is not in accordance with physical reality.

The pores grow in the early stage of activation, which causes an increase in the specific surface area of the reactant particle. However, as the activation progresses, the growing pores intersect with adjacent pores. Therefore, the specific surface area increases due to the growth of the pores, and decreases due to the intersection of adjacent pores. Eventually the specific surface area reaches a maximum, after which the pore intersection dominates, leading to a monotonic decrease of the surface area until the char is completely consumed. To simulate the phenomenon described above, some authors proposed models based on population balances that predict the Pore Size Distribution [14–16]. These models assume that the reactant solid is formed of a population of cylindrical pores that grow and coalesce due to the gasification reaction. Nonetheless, these models require the adjustment of a parameter known as aggregation frequency, which lacks physical meaning in the case of the activation process. In addition, pore coalescence does not adequately represent the

real phenomenon, which is pore intersection; that is, although the pores intersect, they do not lose their identity. In order to represent the effect of pore intersection, the so-called pore overlapping models [17] were developed, of which the most widely used is the Random Pore Model (RPM) [18] and its derivatives [19–21]. These models assume that the particle is formed of cylindrical pores that grow and overlap randomly as the gasification reaction proceeds. Nevertheless, the overlapping models consider that the pores grow only radially, which may not be the case, as experimental data show that pore growth during gasification may be longitudinal [14,22–24], especially for the CO_2-char reaction.

The most commonly used models to describe the gasification reaction with steam/CO_2 mixtures are the Random Pore Model [25], the Shrinking Core Model, and the so-called volumetric model [26], which does not take into account the microstructure of the reactant particle. Thus, although these models have been able to properly describe the overall kinetics of the reaction with steam/CO_2 mixtures, the evolution of the microstructure, or PSD, of the solid has not been predicted. Furthermore, at present, the models for gasification only consider radial pore growth.

Consequently, this work presents a mathematical model that elucidates the effect of steam/CO_2 mixtures on the microstructure (PSD) evolution of coal char during activation by partial gasification. This model takes into account the pore overlap phenomenon and both radial and longitudinal pore growth, and is validated with experimental data taken by both porosimetry and thermogravimetry. The proposed model prioritizes involving the minimum number of parameters necessary to fit. Lastly, the effect of intraparticle concentration gradients on the evolution of the specific surface area is also considered.

2.2 Experimental

Three samples of Colombian coals were used, designated as C1, C2, and C3. The proximate analysis of these three coals is shown in Table 2-1

Table 2-1: Proximate analysis of coal samples.

Coal	C1	C2	C2
Ash (%)	2.2	4.1	3.7
Moisture (%)	11.1	8.6	7.9
Volatile matter (%)	42.3	40.7	38.6
Fixed carbon (%)	44.4	46.6	49.8

2.2.1 Determination of chemical control conditions

The present chapter studies the evolution of the PSD and specific surface area during activation, under both chemical control conditions and with intraparticle gradients. Therefore, it was initially necessary to determine under which particle size and gas flow conditions chemical control is achieved. Several experiments varying the particle size and gas flow were carried out in a LINSEIS STA PT1600 thermogravimetric balance. Intraparticle gradients were found to disappear for average particle sizes smaller than or equal to 0.07 mm. Additionally, the external mass transfer resistance was negligible for gas flows larger than 100 mL STP/min.

2.2.2 Evolution of the PSD and specific surface area

The coals were both devolatilized and activated using a heating muffle. The sample was spread on a ceramic plate inside the heating muffle at room temperature in a pure N_2 atmosphere. Subsequently, the muffle was heated up to a temperature of 850 °C, which was held for 90 min to ensure complete devolatilization. The muffle was then turned off, maintaining the pure N_2 atmosphere until returning to room temperature. The sample was withdrawn from the heating muffle in order to measure its weight and the initial pore size distribution of the coal char. Each coal char sample was then reheated in the muffle to a temperature of 850 °C in a N_2 atmosphere. The gasifying agent was injected up to the desired concentration in the gasification atmosphere. After a specific time, the atmosphere

was returned to pure N_2 and the muffle was turned off. Upon reaching room temperature, the sample was taken from the muffle to be weighed, sieved, and used for the specific surface area and porosimetry measurements. The specific surface area and porosimetry measurements were performed by means of CO_2 adsorption using a Micrometrics TriStar II Plus surface and porosity analyzer. The Pore Size Distribution (PSD) was calculated using the Non-Local Density Functional Theory (NLDFT) method, and the specific surface area was calculated using the Dubinin-Radushkevich equation (each measurement of specific surface area was performed three times and an average was taken). A previous work [27] reports that the activated carbon produced from the coals of this work are microporous, signifying that characterization by CO_2 adsorption should properly describe the solid microstructure.

2.3 The model

2.3.1 Model assumptions

The following assumptions were made in the development of this model:

- The reactions to be modelled are

$$C + CO_{2(g)} \rightarrow 2CO_{(g)}$$

$$C + H_2O_{(g)} \rightarrow CO_{(g)} + H_{2(g)}$$

- The reactant particle is spherical and formed by cylindrical pores that grow axially when reacting with steam and longitudinally when reacting with CO_2.
- The particle maintains its spherical shape and radius throughout the reaction.
- Two resistances to activation are considered: diffusion within pores, and surface chemical reactions.
- At the beginning of the reaction, pore radii are distributed non-uniformly.
- The process is considered isothermal in the model proposed herein. Intraparticle temperature gradients have been reported to be negligible for experimental conditions similar to those used in this work [28].
- A non-steady state is considered.
- Pore overlapping is considered.

2.3.2 Model Development

In the present work's model, the reacting particle is described by a population of cylindrical pores with non-uniform initial radii that grow lengthwise due to the CO_2-char reaction and radially due to the steam-char reaction. Consequently, the intrinsic reaction rates for the CO_2-char and steam-char reactions may be expressed in terms of the change in mean pore length and pore radius, respectively:

$$\frac{dl}{dt} = \frac{k1(C_{CO_2})}{\rho_m} \tag{2-1}$$

$$\frac{dr_p}{dt} = \frac{k2(C_{H_2O})}{\rho_m} \tag{2-2}$$

where ρ_m is the molar density of the reactant solid, l is the mean pore length, r_p is the pore radius, C_{CO_2} is the CO_2 concentration, C_{H_2O} is the steam concentration, and $k1$ and $k2$ are the reaction kinetic constants for the CO_2-char and the steam-char reactions, respectively. The mass balances for the particle, taking into account the mass transfer by diffusion and the chemical reaction, are given by:

$$\varepsilon \frac{\partial C_i}{\partial t} = \frac{1}{R^2}\frac{\partial}{\partial R}\left(D_{e,i}R^2\frac{\partial C_i}{\partial R}\right) - \dot{r}_i \tag{2-3}$$

where ε is the porosity, R is the radial coordinate within the particle, C_i, $D_{e,i}$, and $\dot{r}_i$ are the concentration, the effective diffusivity, and the volumetric reaction rate, respectively, which are associated with each component $i = CO_2, H_2O$. For the sake of simplicity, the sub-index i always refers to variables related to both the CO_2 and steam. Eq. (2-3) is subject to the following boundary conditions

$$\frac{\partial C_i}{\partial R} = 0 \quad \text{at} \quad R=0$$

$$C_i = C_{i,b} \quad \text{at} \quad R=R_p$$

where $C_{i,b}$ is the concentration in the bulk phase. The volumetric reaction rates for both CO_2 and steam are functions of their intrinsic reaction rates and their specific surface areas:

$$\dot{r}_{CO_2} = v_C\,\rho_m\frac{dl}{dt}S_{CO_2} \tag{2-4}$$

$$\dot{r}_{H_2O} = v_C\,\rho_m\frac{dr_p}{dt}S_{H_2O} \tag{2-5}$$

where v_C is the volumetric fraction of carbon in the particle, and S_{CO_2} and S_{H_2O} are the specific surface area of the CO_2-char and steam-char reactions, respectively. On the one hand, since it is assumed that the steam-char reaction increases the pore size, the surface reaction must take place at the pore walls; therefore, S_{H_2O} gives the pore wall surface area per unit volume. On the other hand, because it is assumed that the CO_2-char reaction increases the pore length, the CO_2 must react with the bottom surfaces of the dead-end pores; therefore, S_{CO_2} is the area of the pore ends per unit volume. The effective diffusivity is expressed as follows [29]

$$D_{e,CO_2} = \varepsilon^2 D_{g,CO_2} \tag{2-6}$$

where D_{g,CO_2} is the pore diffusivity of CO_2, which is calculated from the combination of molecular diffusivity and Knudsen diffusivity [30]. The local conversion is expressed as a function of initial and current porosities

$$X(R,t) = 1 - \frac{(1-\varepsilon) - v_{ash}}{(1-\varepsilon_0) - v_{ash}} \tag{2-7}$$

where v_{ash} is the volumetric fraction of ash. The average conversion is computed by integrating local conversion over the entire particle radius as follows

$$\bar{X}(t) = \frac{\int_0^{R_P} 4\pi R^2 X(R,t) dR}{{}^4/_3 \pi {R_P}^3} \tag{2-8}$$

2.3.3 Pore overlapping

As pore length and radius grow due to the CO_2/steam activation reaction, the pores begin to overlap. For a non-overlapped pore system, the cumulative pore volume distribution function is defined as follows

$$F_e = \int_0^{r_p} f_{\varepsilon,e}(r_p{}') \, dr_p{}' \tag{2-9}$$

where $f_{\varepsilon,e}(r_p)$ and F_e are the porosity density distribution function and the cumulative pore distribution, respectively, for the non-overlapped pore population. Avrami [31] found that the

differential change of a population of objects randomly overlapped in space is proportional to the fractional differential change of the correspondent non-overlapped system:

$$dF = (1 - F)dF_e \tag{2-10}$$

where F and F_e are the cumulative fraction of pore volume occupied by the overlapped and non-overlapped pore systems, respectively. Similar expressions were used in the development of RPM, which assumes radial pore growth [18]. However, the concept of pore overlapping is also valid for longitudinally varying pore systems. Thus, Eq (2-10) is solved by the expression

$$F = 1 - \exp(-\int_0^{r_p} f_{\varepsilon,e}(r_p')\, dr_p') \tag{2-11}$$

The porosity density distribution function of the non-overlapped porous system $f_{\varepsilon,e}(r_p)$ is computed as

$$f_{\varepsilon,e}(r_p) = \pi r^2 f(r_p) l \tag{2-12}$$

where $f(r_p)$ is the pore radius density distribution function. For instance, $f(r_p)\, dr_p$ gives the number of pores per unit volume belonging to the radius range $[r_p, r_p + dr_p]$. From Eq.(2-11), it is possible to derive an equation for the porosity density distribution function of the overlapped porous system. By definition, the density and cumulative distributions are related by

$$\frac{dF}{dr_p} = f_\varepsilon(r_p) \tag{2-13}$$

where $f_\varepsilon(r_p)$ is the porosity density distribution function of the non-overlapped porous system. Hence, by differentiating Eq. (2-11) with respect to r_p, we obtain

$$f_\varepsilon(r_p) = f_{\varepsilon,e}(r_p) \times \exp(-\int_0^{r_p} f_{\varepsilon,e}(r_p')\, dr_p') \tag{2-14}$$

From Eq. (2-11), the total porosity of the sample can be readily calculated as follows

$$\lim_{r_p \to \infty} F = \int_0^{\infty} f_{\varepsilon}\left(r_p\right) dr_p = \varepsilon = 1 - \exp(-\varepsilon_e) \tag{2-15}$$

where ε_e is the porosity of the non-overlapped system, which is given by

$$\varepsilon_e = \int_0^{\infty} f_{\varepsilon,e}\left(r_p\right) dr_p \tag{2-16}$$

To derive expressions for S_{CO_2} and S_{H_2O}, the cylindrical pores of the non-overlapped system are taken to grow radially by a differential amount dr_p, leading to the following expression

$$d\varepsilon_e = S_{e,H_2O}\, dr_p \tag{2-17}$$

where S_{e,H_2O} is the specific surface area of the pore walls for the non-overlapped system. Similarly, for an overlapped system with radial pore growth, we have

$$d\varepsilon = S_{H_2O}\, dr_p \tag{2-18}$$

Deriving Eq. (2-15) with respect to ε_e and combining with Eqs. (2-17) and (2-18) gives

$$S_{H_2O} = S_{e,H_2O}\,(1 - \varepsilon) \tag{2-19}$$

If the cylindrical pores grow in the axial direction a differential amount dl, the following relations must be satisfied for the non-overlapped, Eq. (2-20), and the overlapped, Eq. (2-21), systems

$$d\varepsilon_e = S_{e,CO_2} dl \tag{2-20}$$

$$d\varepsilon = S_{CO_2}\, dl \tag{2-21}$$

where S_{e,CO_2} is the specific surface area of pore ends for the non-overlapped system. Following a similar procedure to that for deriving S_{H_2O} leads to

$$S_{CO_2} = S_{e,CO_2}(1 - \varepsilon) \tag{2-22}$$

The total specific surface area S is given by the sum of S_{H_2O} and S_{CO_2} as

$$S = S_{CO_2} + S_{H_2O} \tag{2-23}$$

The specific surface area of the pore walls for the non-overlapped system is given by

$$S_{e,H_2O} = \int_0^\infty 2\pi l r_p f(r_p)\, dr_p \tag{2-24}$$

while the specific surface area of the pore ends for the non-overlapped system is given by

$$S_{e,CO_2} = \int_0^\infty \pi {r_p}^2 f(r_p)\, dr_p \tag{2-25}$$

Finally, $f(r_p)$ is calculated from the following population balance

$$\frac{\partial f}{\partial t} = -\frac{\partial}{\partial r_p}\left[\left(\frac{dr_p}{dt}\right) f\right] \tag{2-26}$$

The model described above was solved using the ordinary differential equations solver ode15s from Matlab (R2017a), and the population balance Eq.(2-26) was computed using a variation of the so-called Extended Method of Moments (EMOM), which is described elsewhere [29]. The initial porosity, PSD, and specific surface area were determined by CO_2 adsorption at 273 K. The reaction kinetic constants were fitted from the experiments under chemical control carried out in the thermogravimetric balance. Both the initial mean pore length and the pore radius density distribution functions were obtained by following the procedure described by Gavals (1980) [17].

2.4 Analysis and results

2.4.1 Chemically controlled conditions

The predictions of the model proposed herein were analyzed and compared with experimental data on the evolution of the PSD under chemically-controlled conditions for various atmospheres and char samples. Figure 2-2 a), b), and c) show the PSD evolution during activation with CO_2 (90% CO_2, 10% N_2, T=850 °C) for C1, C2, and C3, respectively. In these figures, the model predictions properly fit the experimental data and the PSD tends to grow in the y-axis direction. The latter indicates that the cylindrical pores increase in length with CO_2-gasification, without a significant variation in radius, which supports the hypothesis of this work.

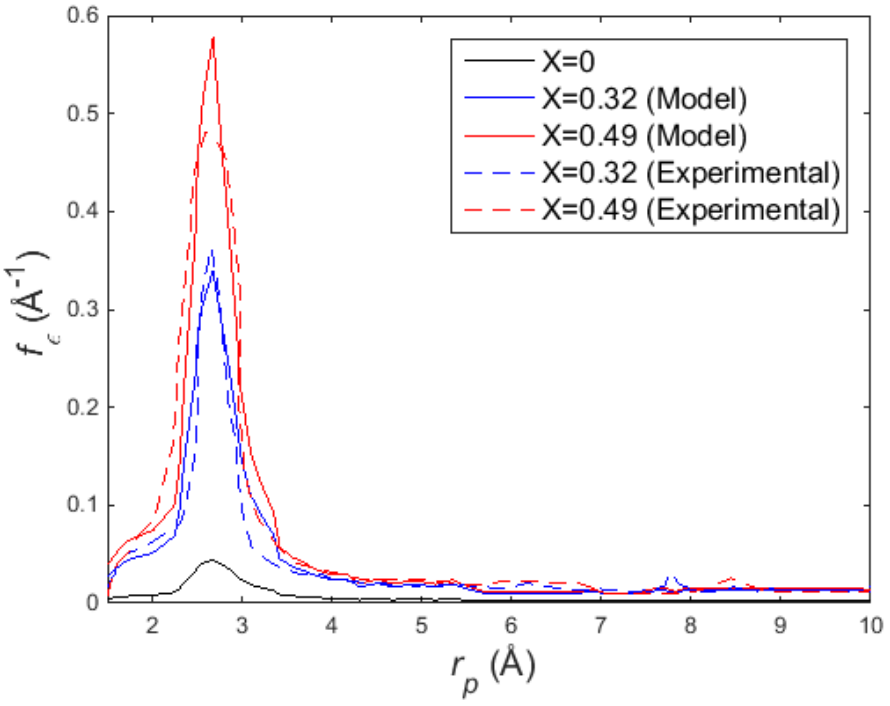
X=0
X=0.32 (Model)
X=0.49 (Model)
X=0.32 (Experimental)
X=0.49 (Experimental)
f_ϵ (Å^{-1})
r_p (Å)

a)

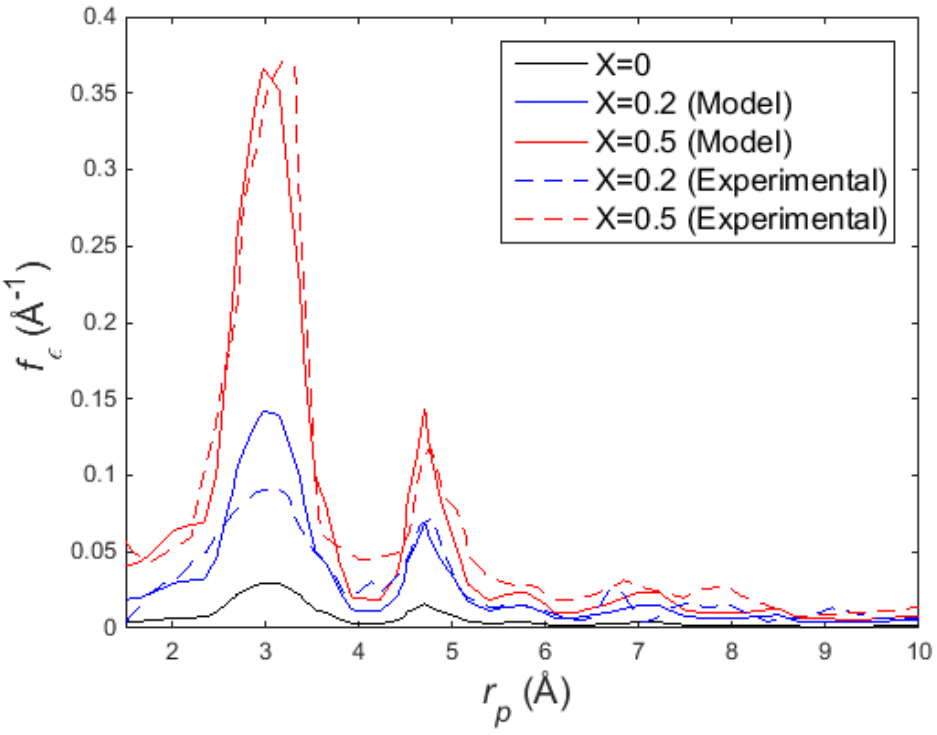
X=0
X=0.2 (Model)
X=0.5 (Model)
X=0.2 (Experimental)
X=0.5 (Experimental)
f_ϵ (Å^{-1})
r_p (Å)

b)

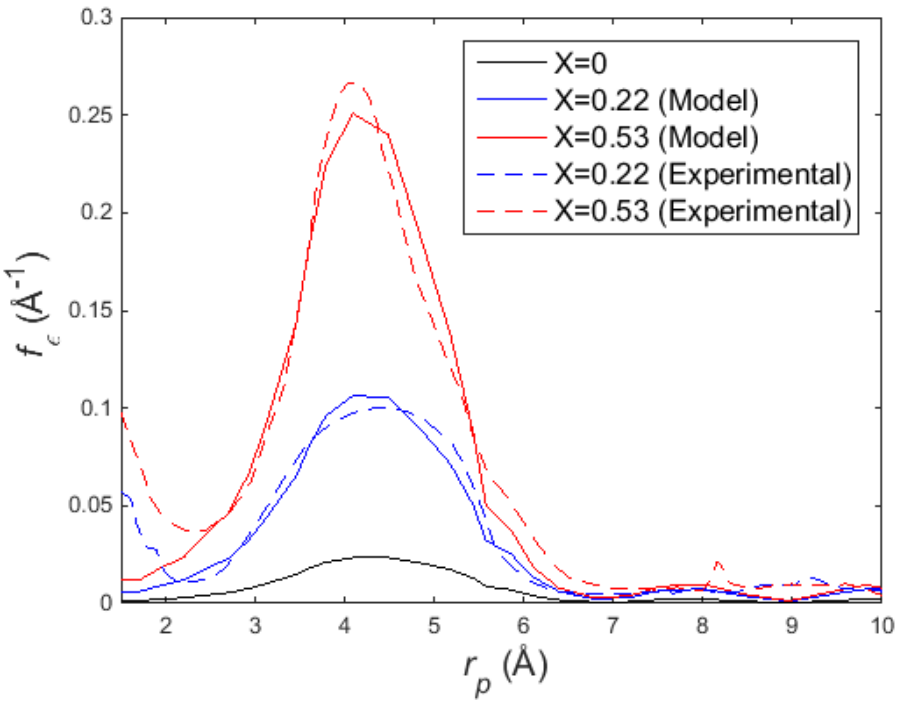

c)

Figure 2-2. Evolution of PSD during activation with CO_2 for a) C1; b) C2; and c) C3.

On the other hand, the model proposed here fails to predict the evolution of the smallest micro pores (r_p=1.5 Å-2.5 Å) of the PSD for C3. This behavior can be explained by experimental observations showing that CO_2 opens the closed micropores initially present in some coal-chars [32]. This behavior could be modeled mathematically in a similar way to a nucleation phenomenon [15]. However, this requires additional parameters describing the kinetics of the appearance of pores, which is not compatible with this work's goal of modelling coal char microstructure development with the minimum number of parameters.

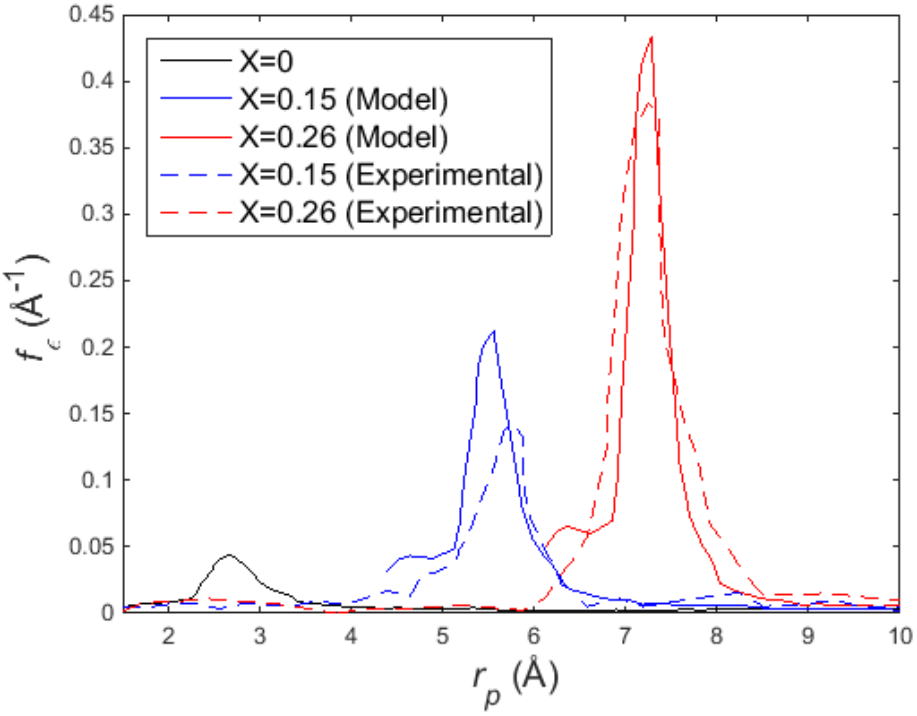
X=0
X=0.15 (Model)
X=0.26 (Model)
X=0.15 (Experimental)
X=0.26 (Experimental)
f_ϵ (Å^{-1})
r_p (Å)

a)

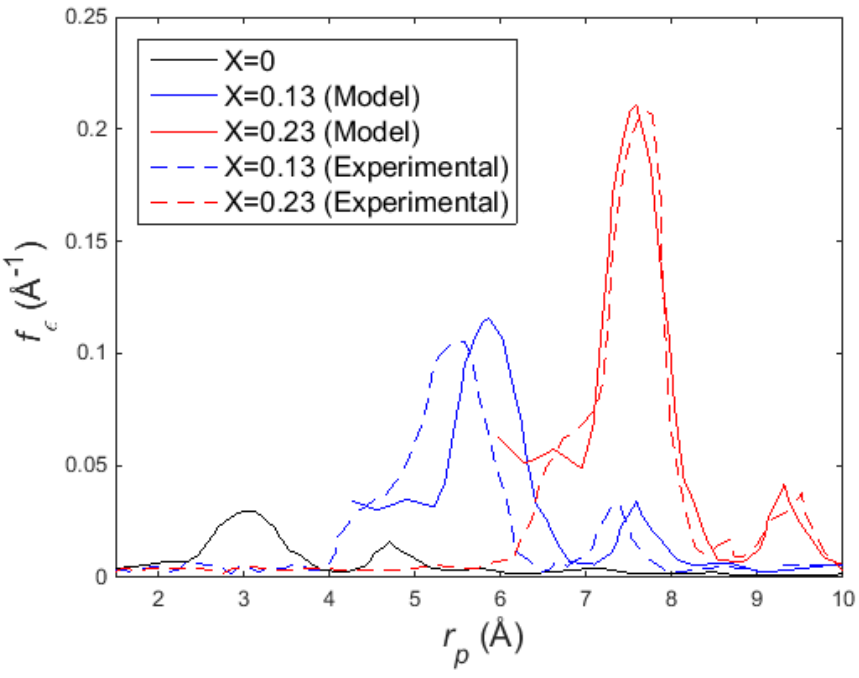
X=0
X=0.13 (Model)
X=0.23 (Model)
X=0.13 (Experimental)
X=0.23 (Experimental)
f_ϵ (Å^{-1})
r_p (Å)

b)

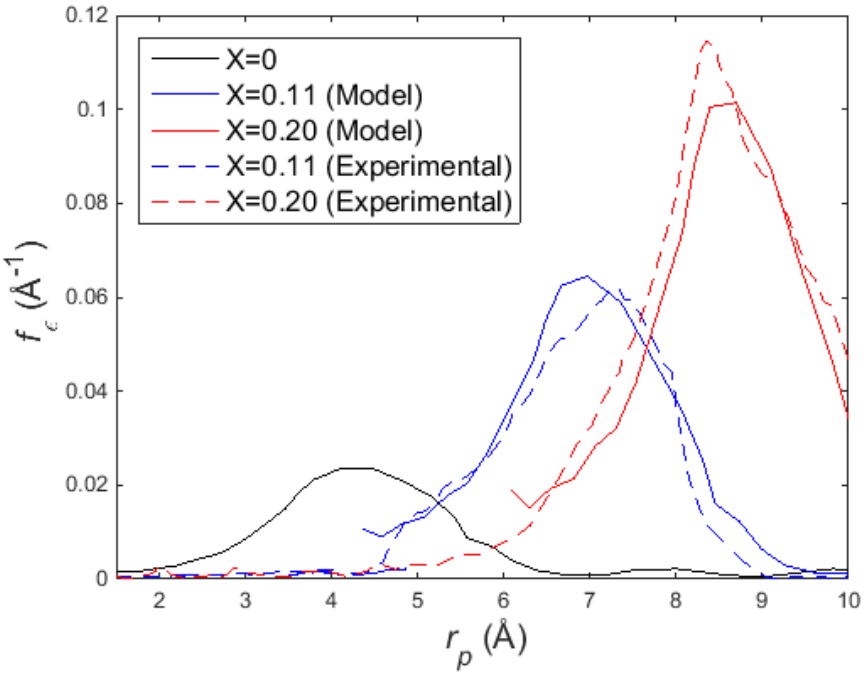

c)

Figure 2-3. Evolution of PSD during activation with steam for a) C1; b) C2; and c) C3.

Figure 2-3 a), b), and c) show the evolution of PSD during steam activation (10% steam, 90 % N_2, T = 850 °C) for C1, C2, and C3, respectively. The model predictions agree with experimental data. Moreover, the PSD tends to move toward the right side of the x-axis as the reaction takes place. This confirms past observations [11,32] and the model's assumption that steam's main effect on the coal-char microstructure during activation is the increase in pore radius. However, the model overpredicts the PSD at X=0.13 for C2. This may be due to three main reasons. Firstly, it is likely that the kinetic constant of the reaction varies during steam-C2 activation as steam gasification is an endothermic reaction (+131 kJ/mol [33]), which can result in a transient reduction of the kinetic constant during early stages of the process where the reaction rate is faster [34]. Secondly, it has been reported that the thermal annealing decreases the reaction rates during gasification due to a reduction in reactive sites [11,35]. Finally, the model developed herein does not consider the occurrence of homogeneous reactions (e.g., water-gas shift reaction), which can also affect the fit between the model predictions and experimental data.

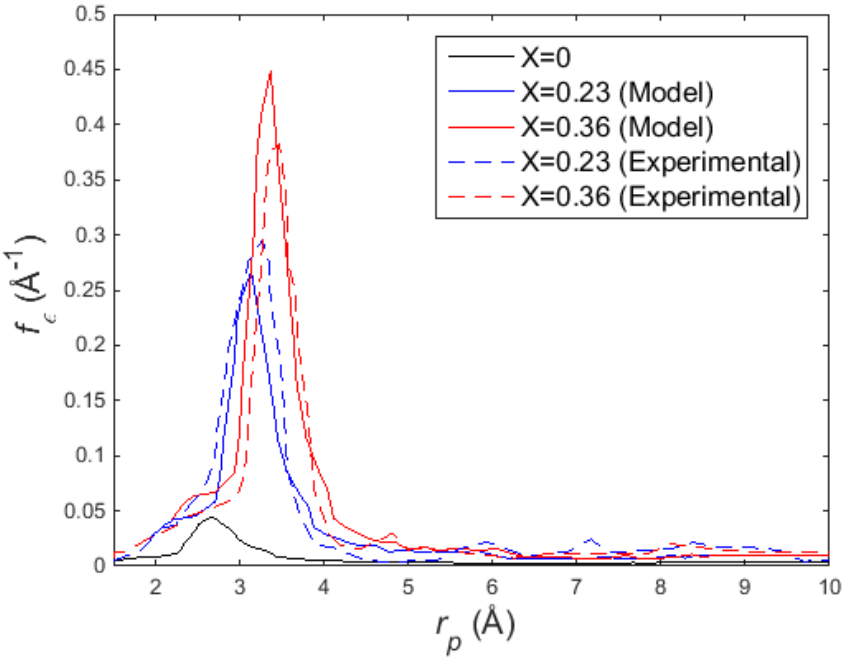
X=0
X=0.23 (Model)
X=0.36 (Model)
X=0.23 (Experimental)
X=0.36 (Experimental)
f_ϵ (Å^{-1})
r_p (Å)

a)

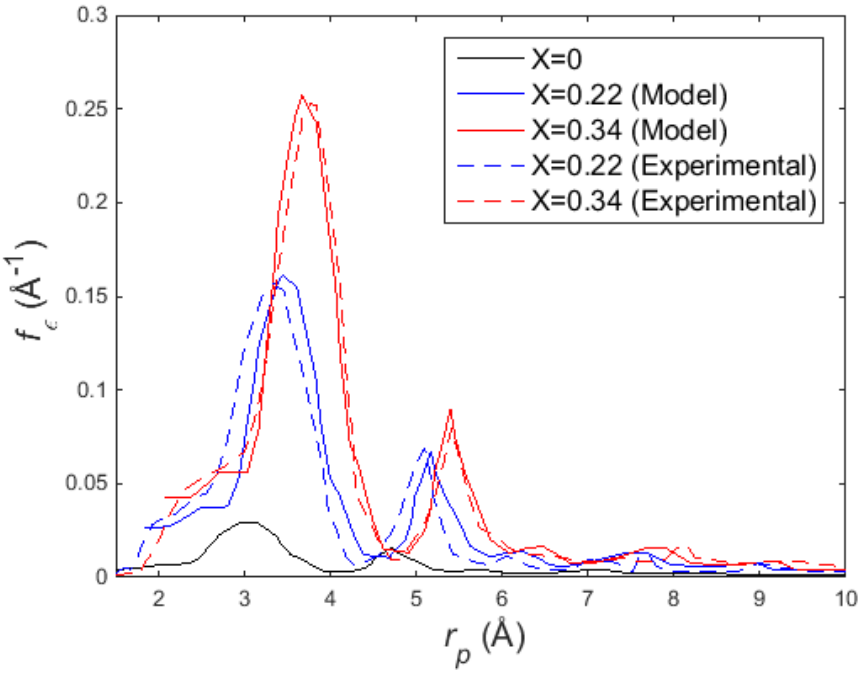
X=0
X=0.22 (Model)
X=0.34 (Model)
X=0.22 (Experimental)
X=0.34 (Experimental)
f_ϵ (Å^{-1})
r_p (Å)

b)

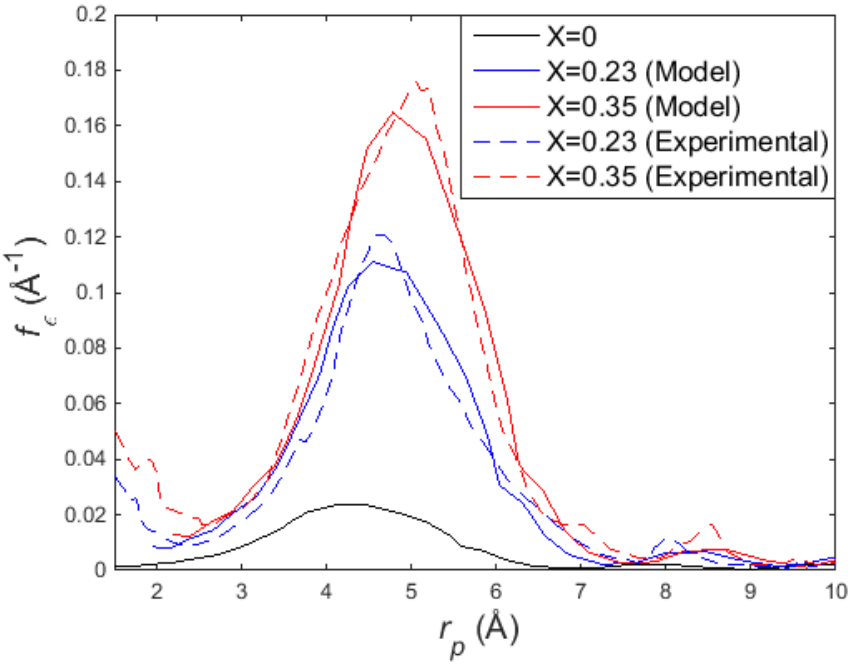

c)

Figure 2-4. Evolution of PSD during activation with a CO_2/steam mixture for a) C1; b) C2; and c) C3.

Figure 2-4 a), b), and c) show the evolution of PSD during CO_2/steam activation (10% steam, 90% CO_2, T =850 °C) for C1, C2, and C3, respectively. In these figures, the PSD moves to the right on the x-axis due to the effect of steam and up on the y-axis due to the effect of CO_2. Thus, the model predicts the tendency of all distributions, confirming the hypothesis that during coal-char activation with steam/CO_2 mixtures, each gasifying agent reacts on different active sites, such that the overall reaction rate is the sum of the reaction rates of each agent. Nevertheless, it must be said that this conclusion is only valid for the experimental conditions of this work. These results show that pore size may be controlled during char activation by using CO_2/steam mixtures. For instance, it is common for the adsorption process to require the existence of large pores that facilitate transport within the char particle and micropores that provide sufficient surface area for adsorption to occur [36]. In this case, the appropriate concentration of steam in the mixture allows the pore size to be increased to the desired value so that the final activated carbon contains both mesopores and micropores for transport and adsorption, respectively.

It is important to analyze why other authors [3,4] came to the conclusion that CO_2 and steam share active sites during coal char activation. First, Roberts & Harris [3] conducted their experiments under high pressures, while those carried out in this work were conducted under atmospheric pressure. Secondly, the work of Umemoto et al. [4] presents two significant sources of error: (1) the specific surface area used for the reaction rate calculations was taken from the RPM, which only considers radial pore growth; and (2), the authors used different values of the RPM parameter Ψ for the CO_2-char and the steam-char reactions. However, this parameter only depends on the initial pore structure of the char, which implies that it should have the same value regardless of the reaction taking place.

2.4.2 Intraparticle gradients

The effect of the concentration gradients within the particle on the development of the specific surface area during coal char activation with CO_2, steam, and a CO_2/steam mixture was analyzed. An average particle size of 2 mm was used during the activation test at 850 °C. Figure 2-5 a), b), and c) show the evolution of the specific surface area with respect to the conversion of C1 for activation with CO_2, steam, and CO_2/steam, respectively. Each figure presents the model predictions and the experimental data under both chemical control and diffusional limitations**.** The so-called percolation threshold, defined as the critical porosity at which the porous matrix can no longer maintain its structure and fragments into smaller particles, is an important characteristic. For reactions with diffusive limitations, the particle size decreases as gasification occurs due to peripheral fragmentation. However, in order to take this phenomenon into account, two parameters are required [37]: the critical porosity ε_c at which fragmentation occurs, and the critical porosity gradient $\nabla\varepsilon_c$. Critical porosity may vary over a wide range ($\varepsilon_c \approx 0.2 - 0.99$ [38]), whereas the critical porosity gradient must be determined using experimental data for each coal char sample. However, due to the objective of modelling coal char activation using the least number of parameters, the percolation threshold was not taken into account. Consequently, only experimental data exhibiting no significant sample fragmentation was considered. On the other hand, the percolation threshold does not affect the chemically-controlled reactions due to negligible porosity gradients; therefore, the fragmentation phenomenon does not occur [37].

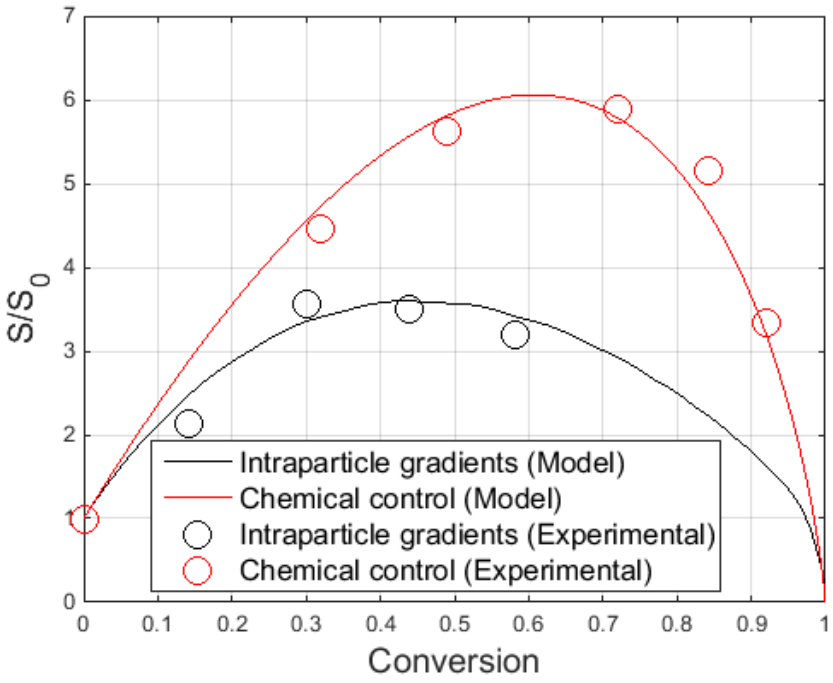
S/S0
Conversion
Intraparticle gradients (Model)
Chemical control (Model)
Intraparticle gradients (Experimental)
Chemical control (Experimental)

a)

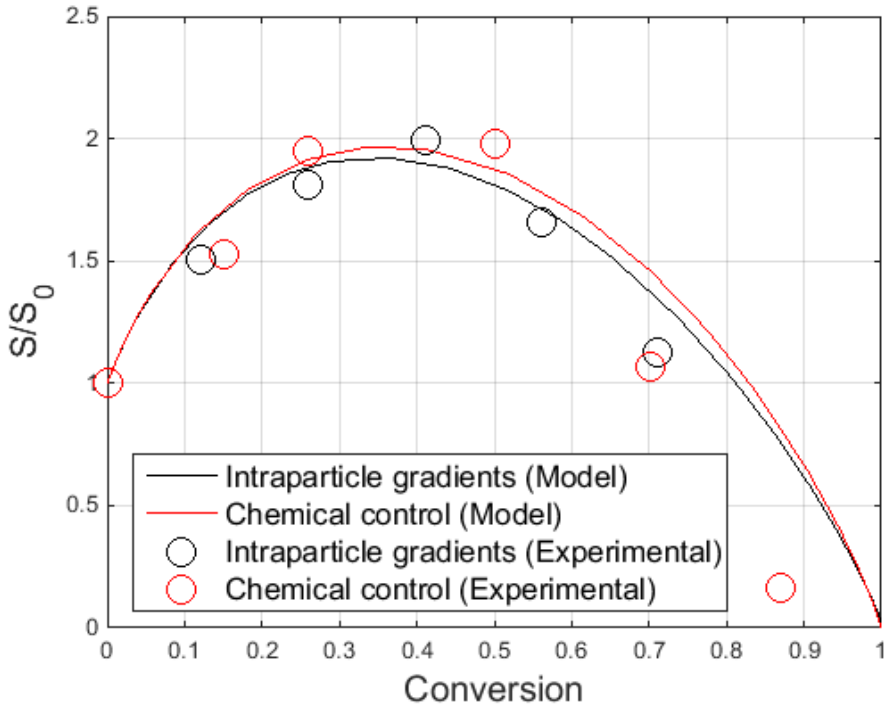
S/S0
Conversion
Intraparticle gradients (Model)
Chemical control (Model)
Intraparticle gradients (Experimental)
Chemical control (Experimental)

b)

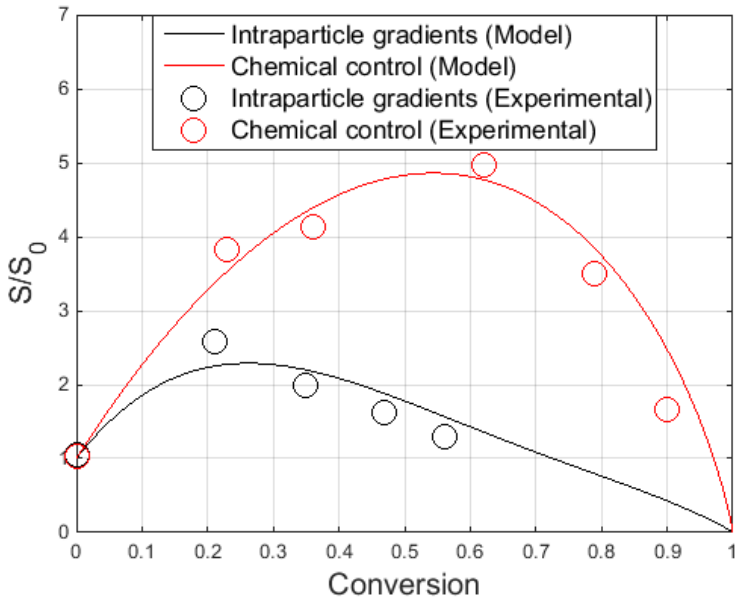

c)

Figure 2-5. Evolution of specific surface area for the activation of C1 with a) CO_2; b) steam; and c) a CO_2/steam mixture.

Figure 2-5 a) shows that chemical control conditions lead to a specific surface area larger than that for the CO_2-char reaction with intraparticle gradients. The latter is better understood by defining the following dimensionless variable

$$\theta = \frac{\tau_D}{\tau_C} \tag{2-27}$$

where τ_C and τ_D are the complete conversion times (X=99.9 %) for chemical control conditions and intraparticle gradients, respectively. The parameter θ quantifies the relative effect of diffusive limitations on the overall reaction kinetics. Thus, as θ tends to one, the intraparticle pore diffusional resistance becomes negligible. Conversely, as θ becomes larger than one, the relative importance of pore diffusion on the overall kinetics increases. The present work found θ to be 1.77, meaning that pore diffusion resistance causes the gasification with intraparticle gradients to take almost twice as long to complete as the chemically controlled reaction. In other words, the particle center takes about two times longer to complete the reaction than the periphery. This signifies that when the particle

center reaches its maximum specific surface area, the overlap effect has already reduced the specific surface area of the outermost layer of the particle to below its maximum. Consequently, for the experimental conditions of this work, the maximum specific surface area obtained by CO_2 activation with diffusional limitations cannot be as large as that achieved with chemical control conditions.

Figure 2-5 b) shows that the maximum specific surface areas for steam activation with chemical control conditions and with intraparticle gradients are very similar. In this case, θ was found to be 1.1, indicating that diffusive limitations are smaller than those of the CO_2-char reaction, Figure 2-5 a). This behavior can be explained by the steam increasing the radius of the pores as the reaction progresses, whereas for the CO_2-char reaction the pores maintain an almost constant radius. Therefore, the fluid-pore wall interactions [30,39] of CO_2 are stronger than those of steam, with an effective CO_2 diffusivity significantly smaller than that of steam. This is illustrated by defining the mean effective diffusivity $\overline{D_{eff,i}}$, which is calculated by averaging the effective diffusivity over time and space as follows

$$\overline{D_{eff,i}} = \frac{1}{{}^4/_3\,\pi\,{R_p}^3 \times\, t_f} \int_0^{t_f} \int_0^{R_p} D_{eff,i}(t,R)\; 4\pi R^2 dR\; dt \tag{2-28}$$

where t_f is the simulation time. The calculated mean effective diffusivity for steam activation was $1.3*10^{-5}$ m^2/s, whereas for CO_2 activation it was $3.2*10^{-7}$ m^2/s. On the other hand, the model fails to fit the experimental specific surface area for the steam-char reaction with intraparticle gradients at later stages. This is due to the fact that CO_2 is only capable of measuring microporosity under typical adsorption conditions (T=273 K). The specific surface area predictions for the CO_2-char reactions are in agreement with experimental data over the whole conversion range; the CO_2 does not significantly increase the pore radius, leaving the char microporous during all reaction stages. Conversely, steam-char activation increases the pore radius as the reaction progresses, leading to wide pores at late reaction stages which cannot be measured by CO_2 adsorption.

Figure 2-5 c) shows that the maximum specific surface area for the reactions with intraparticle gradients is much smaller than that of the chemically-controlled reactions. This difference is the most pronounced with the mixed agents, followed by the case of CO_2 activation, Figure 2-5 a). This is expected since the gas mixture produces a higher reactivity

than that obtained using each gas separately. For steam/CO_2 mixture activation with chemical control, the calculated initial reactivity $\frac{dX}{dt}$ is 0.029 min^{-1}, while for steam and CO_2 activation, $\frac{dX}{dt}$ is 0.009 min^{-1} and 0.019 min^{-1}, respectively. This increase in reactivity causes diffusive phenomena to gain importance, leading to a θ of 2, implying that diffusive limitations are more significant for activation with CO_2/steam mixtures than for activation with either gas separately.

2.5 Concluding remarks

The present work develops a new mathematical model for coal char activation with CO_2/steam mixtures. It considers the pore overlapping phenomenon that strongly affects the development of both porosity and specific surface area during the physical activation process. Radial pore growth associated with the steam-char reaction was taken into account using a population balance equation. Additionally, the longitudinal pore growth associated with the CO_2-char reaction was also considered, which had not been done so far.

The model predictions were compared with experimental data of both PSD and specific surface area development. Even though the model only requires the fitting of two parameters (the reaction kinetic constants for booth CO_2-char and steam-char reactions), a remarkable agreement between experimental data and simulations was observed. This indicates that, for the experimental conditions of this work, the two main hypotheses of this model are correct: (1) the effect of CO_2 on the char microstructure during activation is the increase in pore length; and (2) the main effect of steam is the increase in pore radius. Therefore, pore size may be controlled during char activation by using the proper concentration of steam in the CO_2/steam mixture. This can be applied when designing activated carbons since it is known that the adsorption process requires both micropores and mesopores for adsorption and transport, respectively.

The experimental data for char activation with the CO_2/steam mixture were suitably predicted by taking the overall reaction rate to be the sum of the reaction rates of the CO_2-char and steam-char reactions. This supports the idea that steam and CO_2 react on different

active sites for the experimental conditions of this work. Similarly, no inhibition or synergy effects were observed.

Intraparticle concentration gradients during activation reactions reduce the maximum obtainable specific surface area to less than that achievable under chemical control conditions due to a mismatch in timing. By the time the inner zone of the particle reaches its maximum specific surface area, the specific surface area of the periphery has already begun to decrease below its maximum value due to the overlapping effect.

References

1. Bhatnagar A, Hogland W, Marques M, Sillanpää M. An overview of the modification methods of activated carbon for its water treatment applications. Chemical Engineering Journal. 2013;219:499-511.

2. Danish M, Ahmad T. A review on utilization of wood biomass as a sustainable precursor for activated carbon production and application. Renewable and Sustainable Energy Reviews. 2018;87:1-21.

3. Roberts DG, Harris DJ. Char gasification in mixtures of CO2 and H2O: Competition and inhibition. Fuel. 2007;86(17):2672-2678.

4. Umemoto S, Kajitani S, Hara S. Modeling of coal char gasification in coexistence of CO2 and H2O considering sharing of active sites. Fuel. 2013;103:14-21.

5. Nilsson S, Gómez-Barea A, Ollero P. Gasification of char from dried sewage sludge in fluidized bed: Reaction rate in mixtures of CO2 and H2O. Fuel. 2013;105:764-768.

6. Huang Z, Zhang J, Zhao Y, et al. Kinetic studies of char gasification by steam and CO2 in the presence of H2 and CO. Fuel Processing Technology. 2010;91(8):843-847.

7. Everson RC, Neomagus HWJP, Kasaini H, Njapha D. Reaction kinetics of pulverized coal-chars derived from inertinite-rich coal discards: Gasification with carbon dioxide and steam. Fuel. 2006;85(7-8):1076-1082.

8. Tay H-L, Kajitani S, Zhang S, Li C-Z. Effects of gasifying agent on the evolution of char structure during the gasification of Victorian brown coal. Fuel. 2013;103:22-28.

9. Guizani C, Escudero Sanz FJ, Salvador S. The gasification reactivity of high-heating-rate chars in single and mixed atmospheres of H2O and CO2. Fuel. 2013;108:812-823.

10. Jayaraman K, Gokalp I. Effect of char generation method on steam, CO2 and blended mixture gasification of high ash Turkish coals. Fuel. 2015;153:320-327.

11. Arenas E, Chejne F. The effect of the activating agent and temperature on the porosity development of physically activated coal chars. Carbon. 2004;42(12-13):2451-2455.

12. Liu Q, He H, Li H, et al. Characteristics and kinetics of coal char steam gasification under microwave heating. Fuel. 2019;256:115899.

13. Fatehi H, Bai X-S. Structural evolution of biomass char and its effect on the gasification rate. Applied Energy. 2017;185:998-1006.

14. Navarro M, A. Seaton N, M. Mastral A, Murillo R. Assessment of the development of the pore size distribution during carbon activation: A population balance approach. Studies in Surface Science and Catalysis - STUD SURF SCI CATAL. 2007;160:551-558.

15. Hashimoto K, Silveston PL. Gasification: Part I. Isothermal, kinetic control model for a solid with a pore size distribution. AIChE Journal. 1973;19(2):259-268.

16. SIMONS GA. The Structure of Coal Char: Part II.— Pore Combination. Combustion Science and Technology. 1979;19(5-6):227-235.

17. Gavals GR. A random capillary model with application to char gasification at chemically controlled rates. AIChE Journal. 1980;26(4):577-585.

18. Bhatia SK, Perlmutter DD. A random pore model for fluid-solid reactions: I. Isothermal, kinetic control. AIChE Journal. 1980;26(3):379-386.

19. Gupta JS, Bhatia SK. A modified discrete random pore model allowing for different

initial surface reactivity. Carbon. 2000;38(1):47-58.

20. Singer SL, Ghoniem AF. An Adaptive Random Pore Model for Multimodal Pore Structure Evolution with Application to Char Gasification. Energy & Fuels. 2011;25(4):1423-1437.

21. Cai J, Wang S, Kuang C. A Modified Random Pore Model for Carbonation Reaction of CaO-based Limestone with CO2 in Different Calcination-carbonation Cycles. Energy Procedia. 2017;105:1924-1931.

22. Navarro MV, Seaton NA, Mastral AM, Murillo R. Analysis of the evolution of the pore size distribution and the pore network connectivity of a porous carbon during activation. Carbon. 2006;44(11):2281-2288.

23. Karaman I, Yagmur E, Banford A, Aktas Z. The effect of process parameters on the carbon dioxide based production of activated carbon from lignite in a rotary reactor. Fuel Processing Technology. 2014;118:34–41.

24. Guizani C, Jeguirim M, Gadiou R, Escudero Sanz FJ, Salvador S. Biomass char gasification by H2O, CO2 and their mixture: Evolution of chemical, textural and structural properties of the chars. Energy. 2016;112:133-145.

25. Li J, Qiao Y, Chen X, et al. Steam gasification of land, coastal zone and marine biomass by thermal gravimetric analyzer and a free-fall tubular gasifier: Biochars reactivity and hydrogen-rich syngas production. Bioresource Technology. 2019;289:121495.

26. Preciado-Hernandez J, Zhang J, Zhu M, Zhang Z, Zhang D. An experimental study of CO2 gasification kinetics during activation of a spent tyre pyrolysis char. Chemical Engineering Research and Design. 2019;149:129-137.

27. Chejne et al. F. Obtencion de Carbones Activados a Partir de Carbones Colombianos. Final Technical Report.; 2001.

28. Lee S, Angus JC, Edwards R V, Gardner NC. Noncatalytic coal char gasification. AIChE Journal. 1984;30(4):583-593.

29. Maya JC, Chejne F. Novel model for non catalytic solid–gas reactions with structural changes by chemical reaction and sintering. Chemical Engineering Science. 2016;142:258-268.

30. Yuan J, Sundén B. On mechanisms and models of multi-component gas diffusion in porous structures of fuel cell electrodes. International Journal of Heat and Mass Transfer. 2014;69(0):358-374.

31. Avrami M. Kinetics of Phase Change. II Transformation-Time Relations for Random Distribution of Nuclei. The Journal of Chemical Physics. 1940;8(2):212.

32. Rodríguez-Reinoso F, Molina-Sabio M, González MT. The use of steam and CO2 as activating agents in the preparation of activated carbons. Carbon. 1995;33(1):15-23.

33. Slezak R, Krzystek L, Ledakowicz S. Steam gasification of pyrolysis char from spent mushroom substrate. Biomass and Bioenergy. 2019;122:336-342.

34. Fong GH, Jorgensen S, Singer SL. Pore-resolving simulation of char particle gasification using micro-CT. Fuel. 2018;224:752-763.

35. Zolin A, Jensen AD, Jensen PA, Dam-Johansen K. Experimental study of char thermal deactivation. Fuel. 2002;81(8):1065-1075.

36. Ding LP, Bhatia SK, Liu F. Kinetics of adsorption on activated carbon: Application of heterogeneous vacancy solution theory. Chemical Engineering Science. 2002;57(18):3909-3928.

37. Golfier F, Van de steene L, Salvador S, Mermoud F, Oltean C, Bues MA. Impact of peripheral fragmentation on the steam gasification of an isolated wood charcoal particle in a diffusion-controlled regime. Fuel. 2009;88(8):1498-1503.

38. Feng B, Bhatia SK. Percolative Fragmentation of Char Particles during Gasification. Energy & Fuels. 2000;14(2):297-307.

39. Gao X, Diniz da Costa JC, Bhatia SK. Understanding the diffusional tortuosity of porous materials: An effective medium theory perspective. Chemical Engineering Science. 2014;110:55-71.

3. Integration of the different scales: Bubble, Particle, and Reactor

This work proposes a novel population-balance based model for a bubbling fluidized bed reactor. This model considers two continuum phases: bubble and emulsion. The evolution of the bubble size distribution was modeled using a population balance, considering both axial and radial motion. This sub-model involves a new mathematical form for the aggregation frequency, which predicts the migration of bubbles from the reactor wall towards the reactor center. Additionally, the reacting particles were considered as a lagrangian phase, which exchanges mass with the emulsion phases. For each particle, the variation of the pore size distribution was also considered. The model presented here accurately predicted the experimental data for biochar gasification in a lab-scale bubbling fluidized bed reactor. Finally, the aggregation frequency is shown to serve as a scaling parameter.

3.1 Introduction

Gasification has gained relevance in recent years and appears as an alternative for partially replacing conventional fuels since it has compounds similar to those of oil[1]. Gasification is the process of transforming coal or biomass carbonaceous material into a gaseous fuel by thermochemical reactions in various types of reactors[2]. One of the most common is bubbling fluidized bed reactor, which has been extensively researched both experimentally and theoretically and has been used by many industries for the production of energy and high added-value products[3]. In a fluidized bed, particles such as char or biomass are suspended due to gas entering the reactor, forming a mixture of solid and gas phases with a behavior similar to that of a fluid. The excess gas produces bubbles that rise through the bed, constantly mixing the different phases, this improves the solid-gas contact, increasing the mass transfer and maintaining an almost homogenous temperature in the bed[4].

Due to the heterogeneous nature of the fluidized beds and the strong interaction between hydrodynamics, chemical kinetics, and heat and mass transfer phenomena, it has been necessary to use empirical dimensionless group models[5] to predict the temperature and concentration profiles, char conversion, specific surface area, and porosity. However, these expressions do not consider the interaction between different phenomena and are only valid for limited reactor scales. In addition, the bubble size distribution, which is given by the characteristic bubble interactions inside the bed, is not considered by most of these models.

The first models describing the behavior of fluidized beds date back to the 50s and 70s, where the two-phase theory by Toomey and Johnstone[6] and the first fluidized-bed reactor model by Shen and Johnstone were described[7]. Subsequently, many models were published, which can be classified into two groups[8]: the simple models and the bubbling bed models. The former assume a monophasic system with three or more variables, while the latter considers the formation of bubbles, their properties, and increasing bubble size. Horio and Wen[9] proposed a model considering two phases with adjustable parameters, which are fitted using experimental data from the center of the reactor, neglecting wall effects. Another assumption made by this model is how the variables change with vertical position within the bed. However, the model does not consider particle size distribution. Comparing this model with experimental data allowed predicting that it strongly depends on the adjustable experimental parameters; consequently, this model lacks generality.

In 1986, Grace[10] analyzed the performance of fluidized bed gasifiers with respect to some variables such as temperature, operating scale, heat transfer, and pressure drop. He classified the models according to the number of phases (one, two, or three) and proposed some simple expressions for the first-order chemical kinetics.

In 2003, Ho[11] stated that fluidized bed gasification reactor models can be categorized into two classes: The first class refers to models based on a pseudo-homogeneous approach assuming ideal flows, a homogeneous dispersion of particles, and constant temperatures; the second class refers to models considering two phases (bubble and emulsion), where a governing equation for each phase describes the mass and energy exchange between phases. These two-phase models have demonstrated a remarkable fit between predictions and experimental data, thus becoming the most accepted. A general expression for the mass transfer between the two phases was proposed by Wen and Fang[12]. The most used

model is the so-called two-phase model proposed by Davison and Harrison[13]; this model incorporates essential phenomena such as mass transfer, hydrodynamics, bubble dynamics, and diffusion between phases. However, it assumes a homogenous bubble size distribution throughout the bed and is based on multiple semi-empirical correlations[6].

Over the last few years, several modifications have been introduced to the classical two-phase model[7,14]; these modifications include the modelling of bubble sizes and velocities, new equations predicting mass transfer between phases, complex particle reactions, as well as sub-models for describing devolatilization phenomena and char conversion. Nevertheless, these models assume steady-state conditions, which do not fully represent the reality of fluidized bed gasifiers. Furthermore, certain emulsion phase particles experience intraparticle mass transfer phenomena and changes in porosity and reactivity[4,14,15] which these models do not account for.

The most common particle models do not take into consideration the effect of non-uniformity on the overall reaction rate. Recently, Maya et al. [16–19] presented several models based on population balances for predicting the evolution of microstructures during solid-gas reactions. However, these models have been used only at particle scale without considering effects appearing at reactor scale.

A large number of correlations have been reported in the literature for predicting the evolution of the average bubble size, and mass transfer, heat transfer, and diffusion coefficients. However, these correlations have not been generalized and consequently lead to predictions far from experimental results when applied to the different reactors and operating conditions of the fluidized bed gasifiers[20]. The behavior of bubbles depends on multiple operating parameters such as the reactor geometry, configuration of the distributor, and the gas velocity, physicochemical properties, density, and viscosity. The bubble size distribution determines the dispersion of solid particles and gas within the bed, affecting the mass, heat, and momentum transfers. The above-mentioned bubble size distribution can be characterized by population balance models considering phenomena of coalescence, rise, growth, and dispersion within the bed[21].

Several authors have explored modelling fluidized beds using population balances[20–23]. Models like the one proposed by Ramkrishna[24], contemplate the growth, coalescence, and

rise of bubbles within the bed. The model proposed by Ramkrishna considers that coalescence only occurs in the axial direction. However, it has been demonstrated that bubbles coalesce in both axial and radial directions by migrating towards the center of the reactor; that is, larger bubbles are concentrated in the reactor center whereas smaller bubbles are found closer to the reactor wall[25].

Bubble coalescence has been modeled using population balance equations by means of birth and death terms, which involves the use of a parameter known as aggregation frequency. Some authors have proposed aggregation frequencies based on the coalescence probability as a function of vertical bubble separation[23,24,26,27]; however, this approach cannot be used for modelling radial coalescence.

Based on the above, the main shortcomings of the fluidized bed reactor models developed thus far can be summarized as: (i) omitting intra particle phenomena during gasification and (ii) omitting radial coalesce. In consequence, the present work develops a bubbling fluidized bed model that incorporates the migration of bubbles to the reactor center due to coalescence. A population-balance based coalescence model is coupled with mass and heat transfer equations for both emulsion and bubble phases. Furthermore, this model considers changes in particle structure and intraparticle mass transfer phenomena. Finally, the model presents a novel mathematical form for the aggregation frequency and modified birth and death terms in the population balance equation. The model is validated with experimental data.

3.2 Mathematical model

The correct modelling of bubbling fluidized beds implies mathematical models at various scales. Accordingly, a mathematical model predicting the behavior of CO_2 gasification in a bubbling fluidized bed reactor was proposed. Figure 3-1 presents a scheme of the model, which considers a dispersed phase formed by bubbles and a homogeneous phase consisting of gases and particles (emulsion).

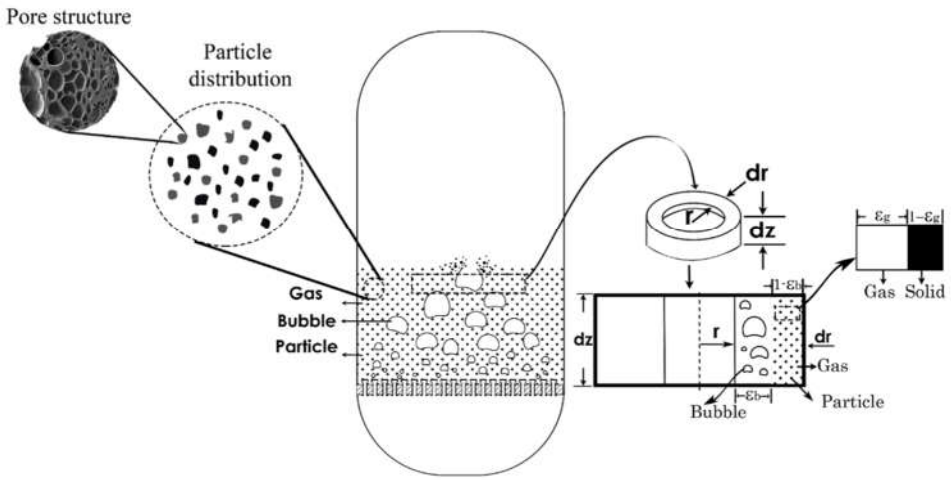

Figure 3-1. Scheme of fluid dynamics processes in a bubbling fluidized bed reactor.

The particles inside the emulsion were considered as a phase that reacts to produce a variation in pore size distribution. The evolution of the bubble size distribution was modeled using population balances, considering the rising of bubbles in the bed and both axial and radial motion. Mass and energy balances for each phase, as well as transfer terms between phases, were included.

3.2.1 Particle Model

These reacting particles transfer mass to both the emulsion and bubble phases along the bed. The particle model is based on that developed by Maya et al.[19], which assumes that CO_2 reacts with the bottom surfaces (approximately equal to the cross-sectional area of the pore) of the dead-end pores, producing an increase in their length.

The reaction between CO_2 and char is given by Eq.(3-1), and the intrinsic reaction rate is expressed in terms of the change in the mean pore length as is shown in Eq.(3-2).

$$C + CO_{2(g)} \rightarrow 2CO_{(g)} \tag{3-1}$$

$$\frac{dl}{dt} = \frac{k(C_{CO_2})^n}{\rho_m} \tag{3-2}$$

where l is the mean pore length, k is the kinetic constant for the CO_2-char reaction, C_{CO_2} is the CO_2 concentration, and ρ_m is the molar density of the solid reactant. The particle mass balance is calculated as:

$$\varepsilon_p \frac{\partial C_{CO_2}}{\partial t} = \frac{1}{R^2}\frac{\partial}{\partial R}\left(D_{eff,\mathrm{CO_2}} R^2 \frac{\partial C_{CO_2}}{\partial r_p}\right) - \dot{r}_{\mathrm{CO_2}}''' \tag{3-3}$$

$$\dot{r}_{\mathrm{CO_2}}''' = v_C\, \rho_m \frac{dl}{dt} S \tag{3-4}$$

These equations account for mass transport by diffusion and chemical reaction, where ε_p is the particle porosity, $R, C_{CO_2}, D_{eff,\mathrm{CO_2}}$ and $\dot{r}_{\mathrm{CO_2}}'''$ are the radial coordinate of the particle, the CO_2 concentration, the effective diffusivity, and the volumetric reaction rate of the CO_2, respectively. The boundary conditions for Eq. (3-3) are:

$$\frac{\partial C_{CO_2}}{\partial r_p} = 0 \quad \text{at} \quad R\text{=}0$$

$$C_{CO_2} = C_{CO_2,e} \quad \text{at} \quad R\text{=}R_0$$

The effective diffusivity is expressed as a function of the porosity [28]

$$D_{e,CO_2} = \varepsilon^2 D_{g,CO_2} \tag{3-5}$$

where D_{g,CO_2} is the pore diffusivity of CO_2, which is calculated from

$$D_{g,CO_2} = \left(\frac{1}{D_{M,CO_2}} + \frac{1}{D_K}\right) \tag{3-6}$$

where D_{M,CO_2} is the molecular diffusion coefficient of CO_2, and D_K is the Knudsed diffusivity, which is expressed as

$$D_K = 97\bar{r_p}\sqrt{\frac{T}{M_{CO_2}}} \tag{3-7}$$

where $M_{CO_2}$is the molecular weight of CO_2, T is the temperature of the particle, and $\bar{r_p}$ is the average pore radius, which is given by

$$\bar{r_p} = 2\frac{\varepsilon}{S} \tag{3-8}$$

For the particle model, the conversion is expressed as a function of porosity as follows:

$$X(R,t) = 1 - \frac{(1-\varepsilon) - v_{ash}}{(1-\varepsilon_0) - v_{ash}} \tag{3-9}$$

where v_{ash} is the ash volume fraction and ε_0 is the initial porosity of the particle. The average conversion is calculated by Eq.(3-10).

$$\bar{X}(t) = \frac{\int_0^{R_0} 4\pi R^2 X(R,t) dR}{{}^4/_3\,\pi {R_0}^3} \tag{3-10}$$

3.2.2 Pore overlapping

During the reaction process, CO_2 reacts with the carbon located at pore ends. Consequently, the pores increase in length, which increases the specific surface area of the first stage of the reaction with CO_2. As the reaction proceeds, pores begin to overlap, reaching a maximum specific surface area followed by a monotonic decrease until the end of the reaction. In the scientific literature, there are several works on pore overlap models, among which the works of Gavalas [29], and Bhatia & Perlmutter [30,31] stand out. However, these models assume that pores growth is radial. In the model used in this paper it is supposed that pores grow longitudinally; thus, the evolutions of porosity and specific surface area are given by Eqs. (3-11) and (3-12), respectively.

$$\varepsilon(t) = 1 - \exp\left[-\int_0^{\infty} f_{\varepsilon,e}(r_p')\, dr_p' \left(1 + \frac{k\, C_{CO_2}}{l_0\, \rho_m} t\right)\right] \tag{3-11}$$

$$S(t) = (1-\varepsilon)\left[\frac{S(0)}{(1-\varepsilon_0)}\left(1 + \frac{k\, C_{CO_2}}{l_0\, \rho_m} t\right) - \frac{k\, C_{CO_2}}{l_0\, \rho_m} t \int_0^{\infty} \frac{f_{\varepsilon,e}(0, r_p)}{l_0} dr_p\right] \tag{3-12}$$

where l_0 is the initial mean pore length and $f_{\varepsilon,e}(0, r_p)$ is the initial porosity density distribution function of the overlapped porous system, which is calculated from

$$f_{\varepsilon,e}(0, r_p) = \frac{f_{\varepsilon}(0, r_p)}{1 - \int_0^{r_p} f_{\varepsilon 0}(0, r_p')\, dr_p} \tag{3-13}$$

where $f_{\varepsilon}(0, r_p)$ is the initial porosity density distribution function, which is experimentally determined. Finally, it must be said that $f_{\varepsilon,e}(0, r_p)$ may be alternately calculated by the procedure proposed by Gavalas [29].

3.2.3 Two-phase reactor model

The balance equations are based on the generic fluidized bed model proposed by Grace and Abba[32], which takes into account different fluidization regimes such as bubbling fluidized bed, dispersed flow at low velocities, and core-annular flow at high velocities. The mass balance for both emulsion and bubble phases include terms of accumulation, convection, axial diffusion, interphase mass transfer, and chemical reaction. For each phase, the model considers both mass and energy transfers for predicting the evolution of both the concentration and temperature profiles over time. The equations for the emulsion and bubble phases are given by Eqs.(3-14) and (3-15), respectively.

$$\frac{\partial \mathbb{C}_{i,e}}{\partial t} = -u_g \frac{\partial\, \mathbb{C}_{i,e}}{\partial z} + k_{E-B} a \left(\frac{\mathbb{C}_{i,b}(1-\epsilon_b)(\epsilon_{mf})}{\epsilon_b} - \mathbb{C}_{i,e} \right) + \frac{D_{g,e}}{\epsilon_{mf}} \frac{\partial}{\partial r} \left(r \frac{\partial \mathbb{C}_{i,e}}{\partial r} \right) + \sum_j \ddot{\Gamma}_j \alpha_{i,j} + \dot{N}'''_{p-e,i} \tag{3-14}$$

$$\frac{\partial (\mathbb{C}_{b,i})}{\partial t} = -u_b \frac{\partial (\mathbb{C}_{bi})}{\partial z} + k_{E-B} a \left(\frac{\mathbb{C}_{e,i}\epsilon_b}{(1-\epsilon_b)\epsilon_{mf}} - \mathbb{C}_{b,i} \right) + D_{g,b} \frac{\partial}{\partial r} \left(r \frac{\partial \mathbb{C}_{i,b}}{\partial r} \right) + \sum_j \ddot{\Gamma}_j \alpha_{i,j} \tag{3-15}$$

where $\mathbb{C} = (C_{ei}(1-\epsilon_b)(\epsilon_{mf}))$ and $\dot{N}'''_{p-e,i}$ are the gas mass flow coming from the particles that reacting, given by:

$$\dot{N}'''_{p-e,i} = 4\pi \int_0^{\infty} -r_{p_0}^2 f_{p(r_{p_o})} D_{eff,i} \left. \frac{dC_{co_2}}{dr_p} \right|_{r_{p_o}} dr_{p_o} \tag{3-16}$$

The energy balance equation for the emulsion phase and bubble phase are given by Eqs.(3-17) and (3-18), respectively.

$$\frac{\partial T_e}{\partial t} = -u_g \frac{\partial T_e}{\partial z} + \frac{h_{be}}{\rho_e C p_e} a(T_b - T_e) + D_{Tg,e} \frac{\partial}{\partial r}\left(r \frac{\partial T_e}{\partial r}\right) + \sum_j \ddot{\Gamma}_j \Delta H_j + \sum_j \dot{N}'''_{p-e,i} * h_i \quad (3\text{-}17)$$

$$\frac{\partial T_{i,b}}{\partial t} = -u_b \frac{\partial T_b}{\partial z} + \frac{h_{be}}{\rho_b C p_b} a(T_e - T_b) + D_{Tg,b} \frac{\partial}{\partial r}\left(r \frac{\partial T_b}{\partial r}\right) + \sum_j \ddot{\Gamma}_j \Delta H_j \quad (3\text{-}18)$$

3.3 Population balance for the bubble size distribution

The model proposed in this work developed a population balance for the bubbles within the bed. This model explains the dynamic evolution of the bubble size distribution as a function of operating conditions. In the case of a fluidized bed reactor, the bubble size distribution may change due to coalescence between adjacent bubbles, the rising of bubbles, and the growth produced by chemical reactions. Solving the population balance equation is a difficult task; hence, this work applies the method of moments to the bubble size distribution for evaluating its effect on the surface area of bubbles per unit volume and the volume fraction of bubbles within the reactor. The moment of the bubble size distribution function is given by:

$$M_n = \int_0^\infty f_b {r_b}^n \, dr_b \quad (3\text{-}19)$$

If one cylinder-shaped reactor element of cross-sectional area *Ac* and height Δz is considered, the following balance can be made:

$$(M_n V)_{acum} = (M_n V)_{in} - (M_n V)_{out} + (M_n V)_{gen} \quad (3\text{-}20)$$

where $(M_n V)_{in}$ is the quantity $(M_n V)$ entering the system of volume $V = Ac \times \Delta z$, per unit time. Similarly, $(M_n V)_{out}$, $(M_n V)_{gen}$, and $(M_n V)_{acum}$ are the leaving, generation, and accumulation of quantity $(M_n V)$ of volume V in the system per time unit, respectively. The convective flux of quantity $(M_n V)$ is given by:

$$(\dot{M_n V})'' = M_n u_b \quad (3\text{-}21)$$

Thus, by substituting Eq. (3-21) in (3-20), we obtain:

$$\frac{\Delta(M_n V)}{\Delta t} = (M_n u_b)_z \times Ac - (M_n u_b)_{z+\Delta z} \times Ac + (M_n V)_{gen} \tag{3-22}$$

Dividing both sides by V, Eq. (3-22) yields

$$\frac{\Delta(M_n)}{\Delta t} = \frac{(M_n u_b)_z - (M_n u_b)_{z+\Delta z}}{\Delta z} + (M_n)_{gen} \tag{3-23}$$

Taking the limit when both Δz and Δt tend to zero, we obtain:

$$\frac{\partial(M_n)}{\partial t} = \frac{-\partial(M_n u_b)}{\partial z} + (M_n)_{gen} \tag{3-24}$$

$(M_n)_{gen}$ appears due to coalescence and bubble growth. This term is defined elsewhere[28]:

$$(M_n)_{gen} = n \int_0^\infty {r_b}^{n-1} \frac{dr_b}{dt} f_b dr_b + \int_0^\infty {r_b}^n (B - D)\, dr_b \tag{3-25}$$

Where B and D are the birth and death terms respectively. B and D are given by:

$$B = a_{gf} \left[\frac{1}{2} \int_0^\infty f_b \left({r_b}^3 - {r_b'}^3 \right)^{1/3} f_b\,(r_b') dr_b' + f_{b\,i-1}\,(r_b) \int_0^\infty f_{b\,i-1}\,(r_b') dr_b' \right] \tag{3-26}$$

$$D = a_{gf} \left[f_b\,(r_b) \int_0^\infty f_b\,(r_b') dr_b' + f_{b\,i} \int_0^\infty f_{b\,i}\,(r_b') dr_b' \right] \tag{3-27}$$

Finally, by combining Eqs. (3-24) and (3-25), we obtain:

$$\frac{\partial(M_n)}{\partial t} = \frac{-\partial(M_n u_b)}{\partial z} + n \int_0^\infty {r_b}^{n-1} \frac{dr_b}{dt} f_b dr_b + \int_0^\infty {r_b}^n (B - D)\, dr_b \tag{3-28}$$

where $M_{n,i}$ is the moment *n*, M_0 is the density (number of bubbles per unit volume), M_1 is the sum of all radius of bubbles (m of bubbles per unit volume), M_2 is proportional to the surface area of bubbles (m^2 of bubbles per unit volume), and M_3 is proportional to the porosity inside the bed (m^3 of bubble per unit volume). In addition, $\frac{dr_b}{dt}$ is the rate of change of the bubble radius due to the mass transfer between the emulsion and the bubble phase and is given by:

$$\frac{P}{RT_b} \frac{dr_b}{dt} = k_{E-B} a \left(\frac{\mathbb{C}_{e,i} \epsilon_b}{(1 - \epsilon_b)\epsilon_{mf}} - \mathbb{C}_{b,i} \right) \tag{3-29}$$

where the specific surface area a and the volume fraction of the bubbles are expressed as follows:

$$a = 4\pi M_2 \tag{3-30}$$

$$\epsilon_b = \frac{4}{3}\,\pi M_3 \tag{3-31}$$

Furthermore, an equation for both the growth and coalescence of bubbles based on a novel form for the aggregation frequency was proposed. This model assumes that the coalescence probability of a given bubble depends on the number of bubbles that surround it, and that bubbles migrate toward the center of the rector as coalescence takes place[33], as shown in Figure 3-2.

3.3.1 Aggregation frequency

The mathematical form for the aggregation frequency proposed in this work is based on the following assumptions.

(i) Two types of bubble coalescence: intra-element and inter-element coalescence. The former involves bubbles belonging to the same differential element, and the latter considers bubbles belonging to adjacent differential elements.

(ii) The intra-element aggregation frequency is assumed to be proportional to the bubble density in the given differential element, whereas the inter-element aggregation frequency is considered to be proportional to the sum of the densities of the adjacent differential elements. The latter indicates that bubbles located closer to the reactor center have a larger aggregation frequency than those located closer to the reactor wall.

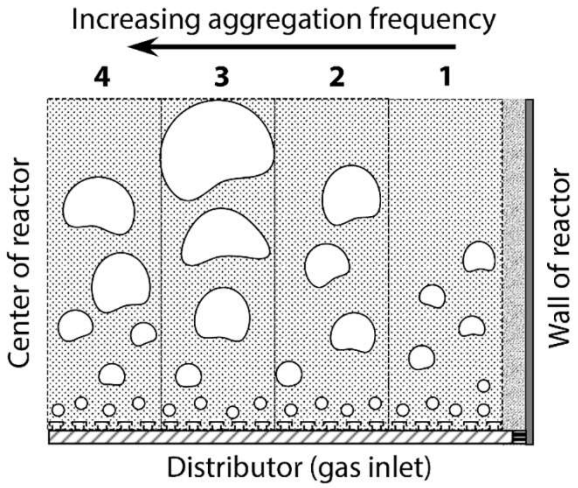

Figure 3-2. Representation of the aggregation frequency

The inter-element bubble coalescence phenomenon is represented by new terms of birth and death, the fifth and sixth RHS terms of Eq.(3-32). The birth term is due to the death of bubbles in the adjacent element closer to the wall. The death term is due to the coalescence of bubbles located in a given element with bubbles of the adjacent element closer to the reactor center. Therefore, it can be inferred that inter-element coalescence always drives bubbles towards the reactor center. After some mathematical manipulation, Eq. (3-28) takes the form of Eq.(3-32).

$$\begin{aligned}\frac{\partial M_{n,i}}{\partial t} = -\vec{u}_b \frac{\partial M_{n,i}}{\partial z} + n\frac{dr_b}{dt} M_{n-1,i} + \frac{a_{g0} M_0}{2} \sum_{i=0}^{n} \binom{n}{i} M_{n-i} M_i \\ - a_{g0} M_0 (M_0 M_n) + \left[a_{g0}\left(M_{0,i-2} + M_{0,i}\right) M_{0,i-1} M_{n,i-1}\right] \\ - \left[a_{g0}\left(M_{0,i-1} + M_{0,i+1}\right) M_{0,i} M_{n,i}\right]\end{aligned} \tag{3-32}$$

The aggregation frequency a_{gf} has different mathematical forms depending on the class of coalescence. Thus, we will define the variables a_{gf_1} and a_{gf_2}, which are the intra-element and inter-element aggregation frequencies, respectively, and can be calculated from:

$$a_{gf_1,i} = a_{g0} * M_{0,i} \tag{3-33}$$

$$a_{gf_2,i} = a_{g0} * \left(M_{0,i-1} + M_{0,i+1}\right) \tag{3-34}$$

where a_{g0} is a constant that must be fitted experimentally . Thus, Eq. (3-32) implies that the aggregation frequency near the reactor walls is smaller than that close the reactor center. Interestingly, this fact allows an approximation to scaling bubbling fluidized bed reactors. First, consider the following continuity equation for the bubble size distribution function.

$$\frac{\partial f}{\partial t} + \frac{\partial (u_b f_b)}{\partial z} = B - D \tag{3-35}$$

by assuming a steady-state and replacing B and D from Eqs. (3-26) and (3-27), we obtain

$$\frac{\partial(u_b f_b)}{\partial z} = \overline{a_{gf}}\left[\left(\frac{1}{2}\int_0^{\infty} f_b\left({r_b}^3 - {r_b'}^3\right)^{1/3} f_b\left(r_b'\right)dr_b' + f_{b\,i-1}\left(r_b\right)\int_0^{\infty} f_{b\,i-1}\left(r_b'\right)dr_b'\right) - \left(f_b\left(r_b\right)\int_0^{\infty} f_b\left(r_b'\right)dr_b' + f_{b\,i}\int_0^{\infty} f_{b\,i}\left(r_b'\right)dr_b'\right)\right] \tag{3-36}$$

It must be said that in this case average aggregation frequency $\overline{a_{gf}}$ is for the sake of deriving dimensionless parameters useful for the scaling up process. The average aggregation frequency is defined by:

$$\overline{a_{gf}} = \frac{\int_0^{r_0} a_{gf}\big|_{z=0} 2\pi r dr}{\pi {r_0}^2} \tag{3-37}$$

From Eq.(3-37) it is inferred that as the reactor radius increases, the average aggregation frequency also increases. Conversely, as the reactor radius decreases, the average aggregation decreases as well. The latter suggest that the average aggregation frequency can be used in the scaling up process. Now, the following set of dimensionless variables is defined.

$${r_b}'^* = \frac{r_b'}{\overline{r_{b_0}}}\ ; \qquad {u_b}^* = \frac{u_b}{u_{b\,0}}\ ; \qquad z^* = \frac{z}{H}\ ; \qquad {r_b}^* = \frac{r_b}{\overline{r_{b_0}}}\ ; \qquad {f_b}^*(r_b) = \frac{f_b\left(r_b\right)}{f_{b\,0}} \tag{3-38}$$

where $\overline{r_{b_0}}$, $u_{b\,0}$ and $f_{b\,0}$ are the average bubble radius, bubble velocity, and bubble radius distribution function at $z = 0$, respectively. By substituting variables of Eq. (3-38) in Eq. (3-36), we have:

$$\frac{\partial(u^* {f_b}^*)}{\partial z^*} = \frac{\overline{a_{gf}} H f_{b_0} \overline{r_{b_0}}}{u_{b0}}\left[\left(\frac{1}{2}\int_0^{\infty} {f_b}^*\left({r_b}^3 - {r_b'}^3\right)^{1/3} {f_b}^*\left(r_b'\right)dr_b'^* + {f_{b\,i-1}}^*\left(r_b\right)\int_0^{\infty} {f_{b\,i-1}}^*\left(r_b'\right)dr_b'^*\right) - \left({f_b}^*(r_b)\int_0^{\infty} {f_b}^*(r_b')dr_b'^* + {f_{b\,i}}^*\int_0^{\infty} {f_{b\,i}}^*\left(r_b'\right)dr_b'^*\right)\right] \tag{3-39}$$

In Eq. (3-39) a dimensionless number appears, it is defined as follows:

$$\psi = \frac{\overline{a_{gf}} H f_{b_0} \overline{r_{b_0}}}{u_{b_0}} \tag{3-40}$$

This dimensionless number ψ relates the characteristic time for bubble rising $\tau_u = \frac{H}{u_{b_0}}$ with the characteristic time for bubble coalescence $\tau_a = \frac{1}{\overline{a_{gf}} f_{b_0} \overline{r_{b_0}}}$ as follows:

$$\psi = \frac{\tau_u}{\tau_a} \tag{3-41}$$

Thus, the dimensionless number ψ allows to relate the forces involved with bubble rising and those related to the bubble migration from the reactor walls to the center. In this sense, it is expected that maintaining this dimensionless number the bubbling regime will be conserved. The above dissertation does no pretend to establish a new validated scaling up process but to demonstrate the possibility to explore new alternatives for scaling up bubbling fluidized bed reactors from the population balance modelling.

3.3.2 Solution method and scales connection strategy

The present mathematical model was solved using the ode15s software by Matlab R2019b, a solver of stiff ordinary differential equations that allows coupling algebraic equations. Partial spatial derivatives are discretized by centered finite differences for diffusive terms and by the upwind scheme for convective terms.

The energy and mass balance equations for all the phases and population balances of bubbles were coupled. The emulsion phase was coupled to the bubble phase by the second RHS term of Eqs.(3-14), (3-15), (3-17) and (3-18). The emulsion phase was coupled to the particles by the fifth RHS term of Eqs. (3-14) and (3-17). Finally, the population balance was connected by Eqs. (3-30) and (3-31). Additionally, in the Table 3-1, the values of the parameters used in the simulations are presented.

Table 3-1. Parameters of simulations.

Parameter	Symbol	Value	Unit
Design parameters			
Minimum fluidization velocity	U_{mf}	0.1 – 0.25	m/s
Height of bed	H	0.2 – 0.5	m
Reactor radius	r_0	0.1 – 0.5	m
Temperature at the distributor	T_{in}	300	K
Wall reactor temperature	T_w	1,123	K
Pressure	P	101.325	kPa
Emulsion phase parameters			
Gas velocity at distributor	u_{g0}	0.7-1.3	m/s
Dispersion coefficient of emulsion phase[34]	$D_{g.e}$	0.01	m^2/s
Parameters of bubble phase			
Dispersion coefficient of bubble phase[34]	$D_{g.b}$	0.1	m^2/s
Moment 0 at t=0	M_0	100-1,000	# of bubbles/m^3
Moment 1 at t=0	M_1	$0.2 - 2$	m/m^3 of reactor
Moment 2 at t=0	M_2	$4x10^{-4} – 4x10^{-1}$	m^2/m^3 of reactor

Moment 3 at t=0	M_3	$8x10^{-7}$ – $8x10^{-4}$	m^3/m^3 of reactor
Aggregation frequency factor	a_{g0}	10^{-3}	m^6/s
Volume fraction of bubbles for the minimum fluidization velocity	ϵ_{mf}	0.36	m^3 of bubbles/m^3 of reactor
Particle parameters			
Particle radius	r_{p_0}	0.0005-0.002	m
Initial average pore length	l	10^{-9}-$2x10^{-8}$	m
Initial porosity of particle	ε_0	0.0668	m^3 of pore/m^3 of particle
Specific surface area at the beginning of reaction	S_0	$1.2312x10^9$	m^2 of pore /m^3 of particle
Volumetric ash fraction	v_{ash}	0.01-0.1	-
Molar density of solid reactant	ρ_m	$1.67x10^2$	kmol/m^3
Energy equation parameters			
Heat diffusivity of the bubble phase[34]	$D_{Tg.b}$	$1x10^{-4}$	m^2/s
Heat diffusivity of the emulsion phase[34]	$D_{Tg.e}$	$1.84x10^{-6}$	m^2/s
Chemical reaction parameters			
Activation energy	EA	92,500-200,000	kJ/kmol

Pre-exponential factor	A_0	$1.1x10^{-12}$-$3.5x10^{9}$	$\frac{m}{s}(\frac{kmol}{m^3})^{1-n}$
Reaction order	n	0.15-0.41	-

Finally, the parameters k_{E-B}, h_{be}, Cp_b, and Cp_e were calculated as did Chejne et al. [35].

3.4 Results and discussion

The model was initially validated with experimental data obtained from the scientific literature. This validation was further complemented with experimental tests in both a fluidized bed reactor and a thermogravimetric balance. Finally, some model predictions of the steady state bed porosity, mean bubble size, temperature, and pressure fluctuations within the bed were analyzed.

The model predictions in this work were fitted to experimental data reported by Rüdisüli et al.[36,37] obtained in a fluidized bed reactor without chemical reaction. They measured the frequency and distribution of bubbles in a bubbling fluidized bed using optical sensors, finding that bubbles migrated from the walls towards the center of the bed and that larger bubbles tended to be located in the upper part of the bed. The following figures compare the experimental data obtained by Rüdisüli et al[37] and the results of the model developed in this work.

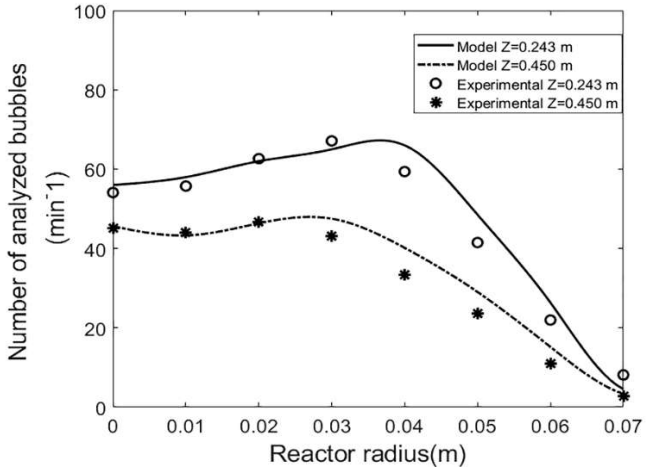

Figure 3-3. Bubble frequency predictions

Figure 3-3 shows that bubbles migrate to the reactor center, as predicted by the additional birth and death terms in the present model related to the migration of bubbles between bins. Figure 3-3 also shows that the number of bubbles is larger at Z=0.243 m that at Z=0.450 m. This is due to the coalescence phenomenon, which leads to a decrease in the number of bubbles with increasing height within the reactor.

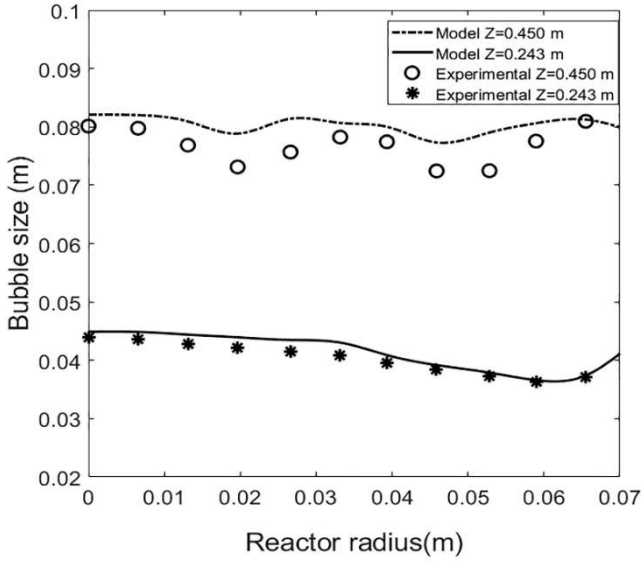

Figure 3-4. Bubble size predictions

Figure 3-4 presents the bubble size profile at two different heights within the bed, showing the model to predict the experimental data remarkably well. This figure (Figure **3-4**) indicates that the bubble size increases with increasing height within the bed. This is due to the coalescence phenomenon, which decreases the number of bubbles while increasing their average radius.

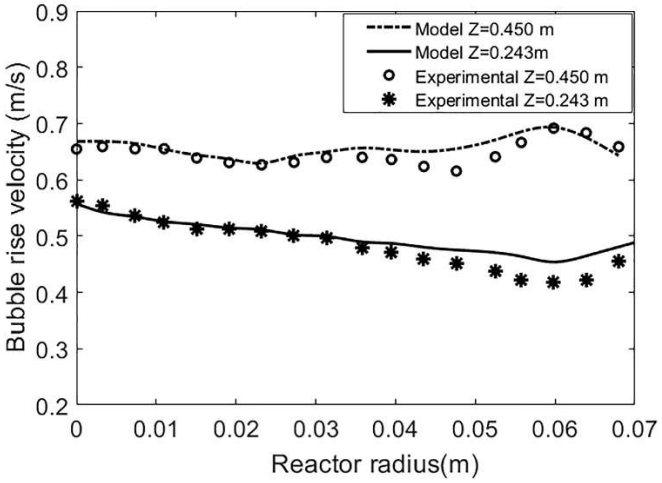

Figure 3-5. Bubble rise velocity predictions

Figure 3-5 presents the bubble rise velocity profile at two reactor heights, showing greater velocity with increasing height within the reactor. This is due to the bubble size increase, and, as observed in Figure 3-4, the largest bubbles are located higher within the reactor.
Subsequently, model predictions were compared with experimental data of the CO_2-char reaction, taken in both a fluidized bed reactor and a thermogravimetric balance. Char gasification experiments were performed at the Aragón Institute for Engineering Research (I3A), Universidad de Zaragoza. In these experiments, char particles were gasified using CO_2 as a gasifying agent at an operating temperature of 900 °C. The material used in this study was obtained from Encino biomass pyrolysis; it was characterized in terms of composition, calorific value and BET specific surface area. Table 3-2 resumes the results of the ultimate and the proximate analyses, the heating value and the specific surface area. Analytical standards and methods used in the characterization of materials are also given in Table 3-2.

The gasification experiments were conducted in a laboratory-scale fluidized bed reactor (1.27m height and 0.04m diameter) operating at atmospheric pressure, as shown in

Figure **3-6**. The reactor heating was assured in N_2 atmosphere, then once temperature reached 900 °C, before solid feeding, the change from N_2 atmosphere to CO_2 was made via gas valves situated in the reactor bottom. Solid was fed from the upper part of the reactor through a double valve feeding system. Small particles of char were retained at the level of

cyclone (at temperature up to 600 ºC) and glass wool hot filter (at 450 ºC). The condensable gases produced were collected in the condenser cooled at 0 ºC through a water-recirculating chiller, then, the small aerosols were retained from non-condensable gases using a cotton filter. The volume of gas produced was measured by a volumetric meter. Gas composition was analyzed continuously using a micro gas chromatograph (Agilent 3000-A). Once the experiment finished, the reactor was allowed cooling under nitrogen atmosphere.

As for raw material, for each fluidized bed gasification experiment, the specific surface area of the produced solid was determined.

Table 3-2. Characterization of char sample

Proximate analysis (wt. % wet basis)		**Analytical standard or equipment**
Moisture	5.55±0.03	EN 14774-3:2010
Ash	12.8±0.3	EN 14775:2010
Volatile matter	29.4±0.1	EN 15148-2010
Fixed carbon	52.3±0.2	By difference
Heating Value (MJ/kg) (dry basis)		
HHV	24.8±42.4	Calorific Bomb IKA C2000
LHV	24.1±42.4	basic
Ultimate analysis (wt. % wet basis)		
C	68.56±0.01	LECO CHN628
H	3.24±0.05	LECO CHN628
N	0.75±0.03	LECO CHN628
S	<0.05	LECO CHN628- 628-S add-
O	14.69±0.03	on
		By difference
Area (m2/g)		Quantachrome Autosorb iQ
		gas sorption
Total area	205.00	

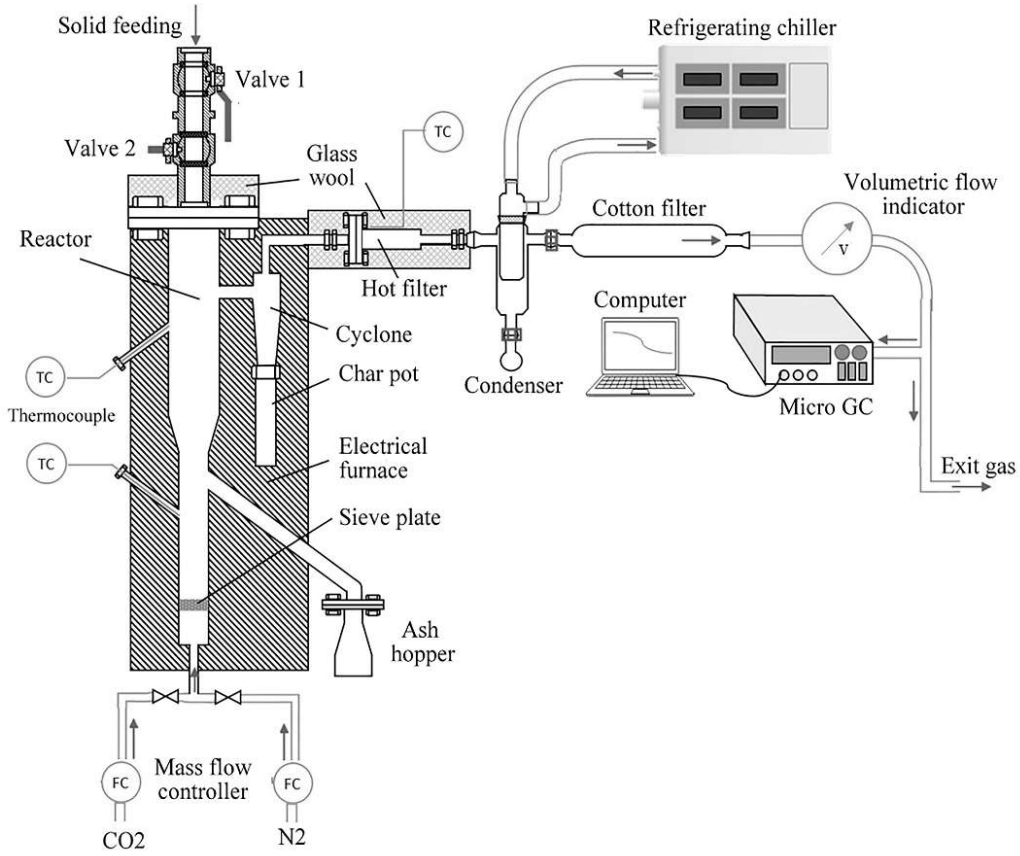

Figure 3-6. Diagram of fluidized bed experimental setup

The present model requires known intrinsic kinetics. Therefore, five tests were carried out in duplicate with a thermogravimetric balance (TGA-DTG, Proteus STA 449 F1 Jupiter-Netzsch) to determine the intrinsic kinetics of the reaction (pre-exponential factor, activation energy and reaction order). During these tests, around 20 mg of the solid sample was heated at a constant heat rate of 10°C/min from ambient temperature to the chosen temperature, then, it was maintained during 1h. The temperature (800, 850 and 900 °C) and composition of the gasifying agent CO_2/N2 (50-50%, 70-30% and 30-70%) were varied and the experimental data were fitted to the model under chemical control conditions. The evolution of both specific surface area with conversion and with the time of particles in the fluidized bed reactor are shown in Figure 3-7(a) and Figure 3-7(b), respectively.

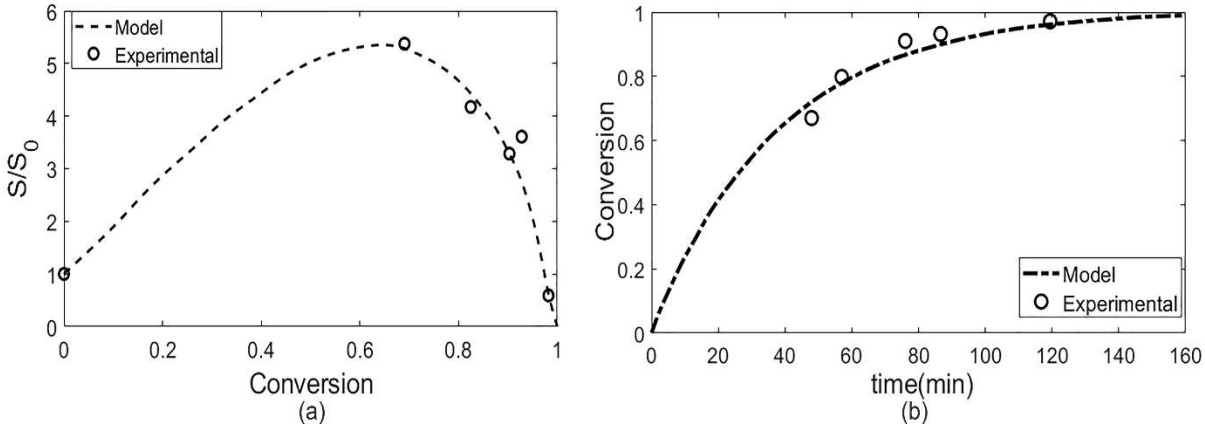

Figure 3-7. a) Evolution of specific surface area with conversion. b) Evolution of char conversion over time.

Figure 3-7(a) shows the evolution of specific surface area with conversion, indicating that it reaches a maximum before decreasing with further conversion. At the initial stages of gasification, the reaction induces pore growth, increasing the specific surface area of the reacting particle. However, as gasification progresses, the pores begin to overlap with adjacent pores. Consequently, there is a moment when pore overlapping becomes dominant, resulting in a decrease of the specific surface area. Figure 3-7(b) presents the evolution of conversion with time, showing that the conversion fraction with the maximum specific surface area (X=0.71) corresponds to 28% of the time required for completing the reaction. Therefore, in order to obtain a char with high specific surface area (for instance, activated coal); long reaction times must be avoided. Finally, some predictions of the present model are analyzed. A fluidized bed reactor was modeled in steady-state at 850 °C with 1 mm diameter char particles. The fluidized bed reactor has a radius of 0.3 m and a bed height of 0.4 m. Results were modeled at a height of 0.3 m above the distributor, predicting the variation of both the bubble size distribution and bed porosity at different ratios of minimum fluidization velocities

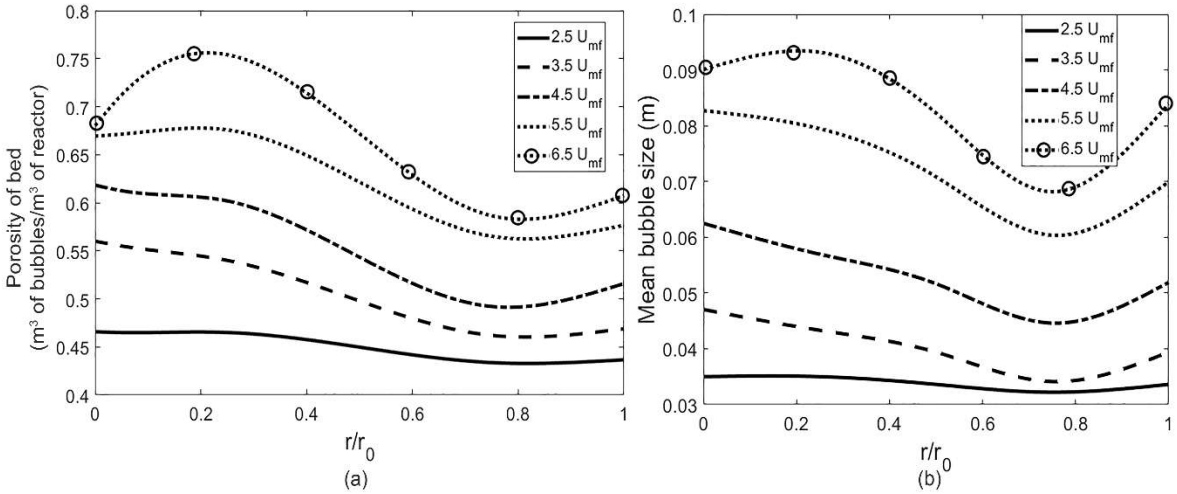

Figure 3-8. (a) Porosity distribution and (b) Average bubble size with radial position for various fluidization velocities

Figure 3-8 (a) presents the porosity profiles for various fluidization velocities. The porosity at the reactor center is larger than that at the reactor walls, due to the bubbles located close to the reactor walls migrating towards the reactor center as coalescence takes place. Furthermore, the porosity in the reactor increases with increasing flow velocity as well. This is due to the excess gas producing a greater number of bubbles. Additionally, a higher gas velocity results in a greater reactivity and consequently increased bubble growth. Figure 3-8 (b) presents the mean bubble size profile. The mean bubble size increases with increasing fluidization velocity, also due to the greater number of bubbles resulting from the excess gas, consequently increasing the aggregation frequency. This figure also shows that larger bubbles are located in the center of the reactor, whereas smaller bubbles are found closer to the reactor wall. This is due to the inter-element coalescence phenomenon, by which bubbles migrate from the wall towards the center of the reactor.

Moreover, temperature profiles of the emulsion for various flow velocities were simulated, as presented in Figure 3-9. The profiles are almost flat, indicating that the radial heat transfer is negligible. On the other hand, the average temperature within the bed increases with increasing gas velocity. This is due to the heat transfer between the bubble and emulsion phases improving with the greater number of bubbles and therefore bubble surface area coming from the distributor as the flow velocity increases.

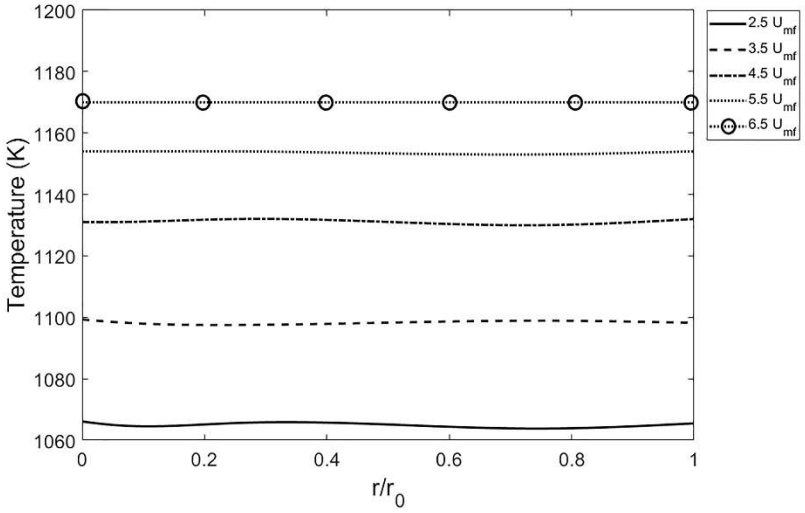

Figure 3-9. Emulsion temperature profiles

Finally, Figure 3-10 presents the pressure with time at z=0.3 m. this pressure drop was calculated by means of moment M_3 and the variation of the bed density. Initially, there is an abrupt drop in pressure near time zero due to the increase in bed porosity with the initial gas flow across the distributor. Subsequently, pressure continues to decrease due to the chemical reaction, exhibiting a greater rate of decrease as the reaction progresses.

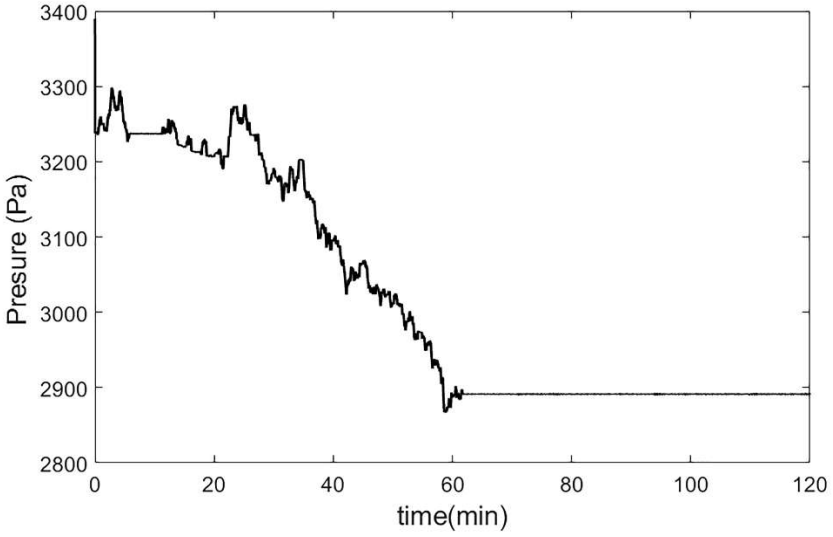

Figure 3-10. Evolution of pressure over time at z=0.3 m.

The above predictions are in agreement with experimental observations of bubble migration from the walls to the reactor center[23–25,38,39]. Particularly, this phenomenon has not been modeled previously, thus, constituting the main scientific contribution of the present work.

3.4.1 Another simulations

This section presents other representative simulations of the model developed in this work. These describe the behavior of the pressure signal of a bubbling fluidized bed due to changes in the porosity of the bed. That is, to the change in the distribution of the size of the bubbles represented in the model as $\frac{4}{3}\pi * M_3$.

Figure 3-11 shows the variation of pressure fluctuations for different minimum fluidization velocities at the same height and under the same initial conditions of the number of bubbles.

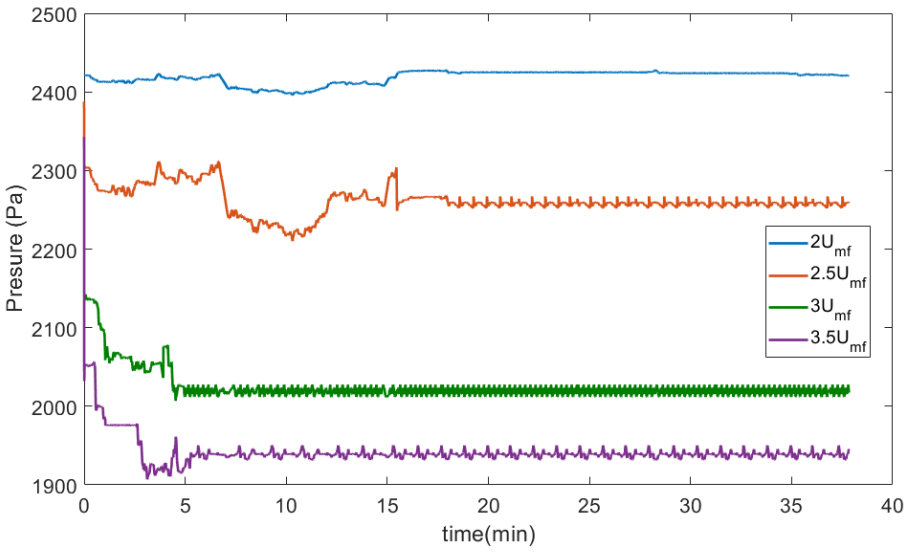

Figure 3-11. Evolution over time of pressure fluctuations at different minimum velocities of fluidization.

Figure 3-11 shows the evolution over time of the pressure fluctuation starting from the static bed at time t = 0, that is, without bubbles. As the bubbles enter the bed, the porosity changes, which is reflected in the behavior of the signal. For velocity of $2U_{mf}$ the bed cannot stabilize and presents incipient fluidization while for a velocity of $3.5U_{mf}$ the bed presents characteristic multiple bubbling fluidization with an abrupt drop in pressure at the

beginning of the process, but with rapid stabilization. In Figure 3-12 the characteristic of the signal is presented in more detail.

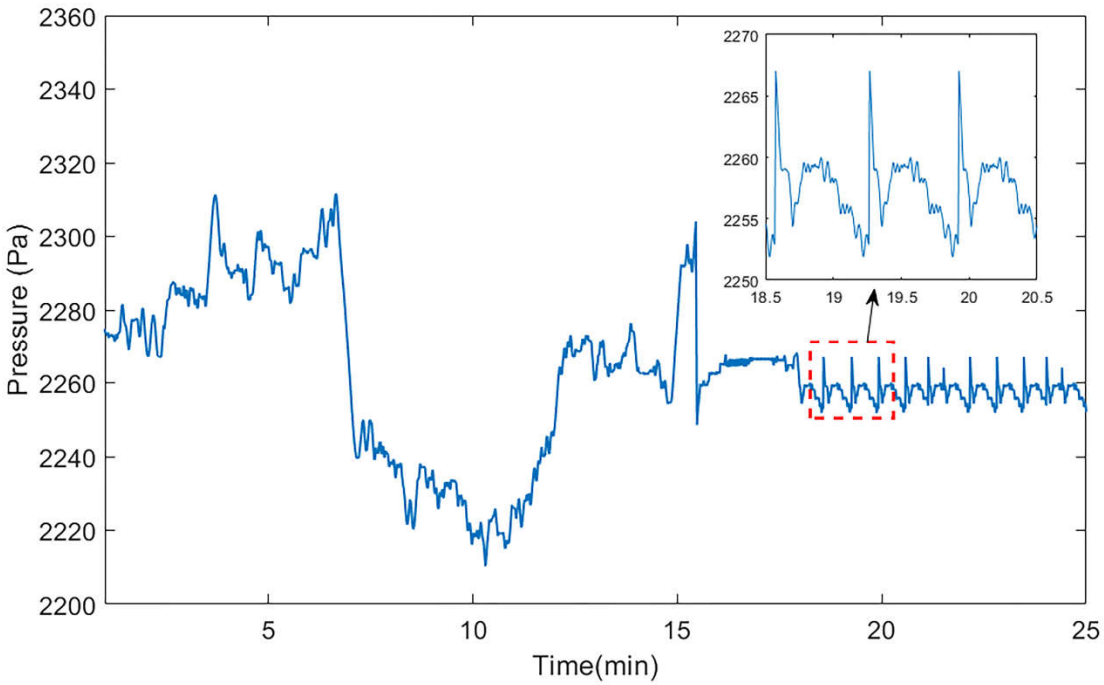

Figure 3-12. Detail of simulation of pressure signal over time.

Figure 3-12 shows the visualization obtained from the pressure signal which gives an idea of the time scale in which the phenomena take place and the complexity of the flow within the bed. Explaining the response of this signal for each interaction is an extremely complex task due to its chaotic nature. However, the magnitude of the pressure drop and the oscillation of the signal corresponds to the data reported in the literature by various authors for this type of reactor[37, 40-42].

Figure 3-13 to Figure 3-15 shows the porosity profiles, mean bubble radius, and number of bubbles within the bed respectively.

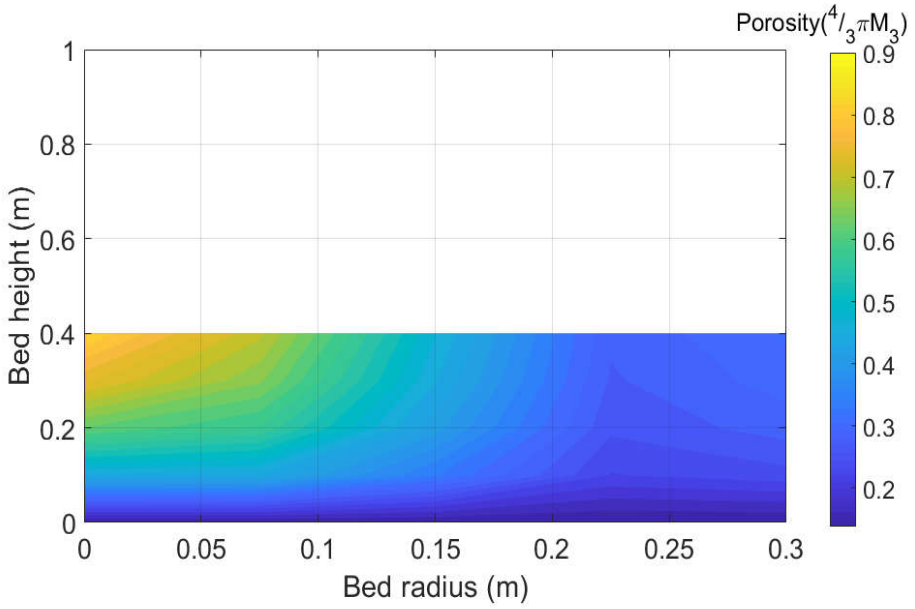

Figure 3-13. Profile of porosity of the bubbling fluidized bed

In Figure 3-13 it is shown that the porosity of the bed is greater in the center than in the walls, this is due to the fact that the bubbles coalesce and migrate towards the center of the reactor. It is also evidenced that some bubbles migrate towards the reactor walls as shown in Figure 3-14.

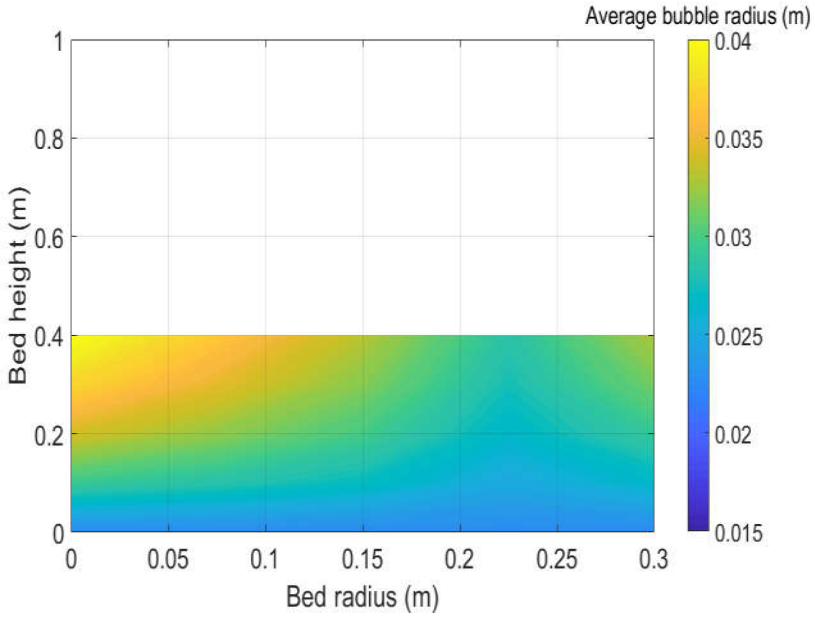

Figure 3-14. Profile of average bubble radius in the bubbling fluidized bed

As mentioned above, the model correctly predicts the axial and radial movement of the bubbles. These migrate to the center of the reactor, coalescing with other bubbles during the vertical and radial ascent within the bed, which explains why larger bubbles are found there as shown in Figure 3-14. In addition, it is observed that in the periphery of the bed, in the upper part, there are bubbles that also increase in size due to wall effects.

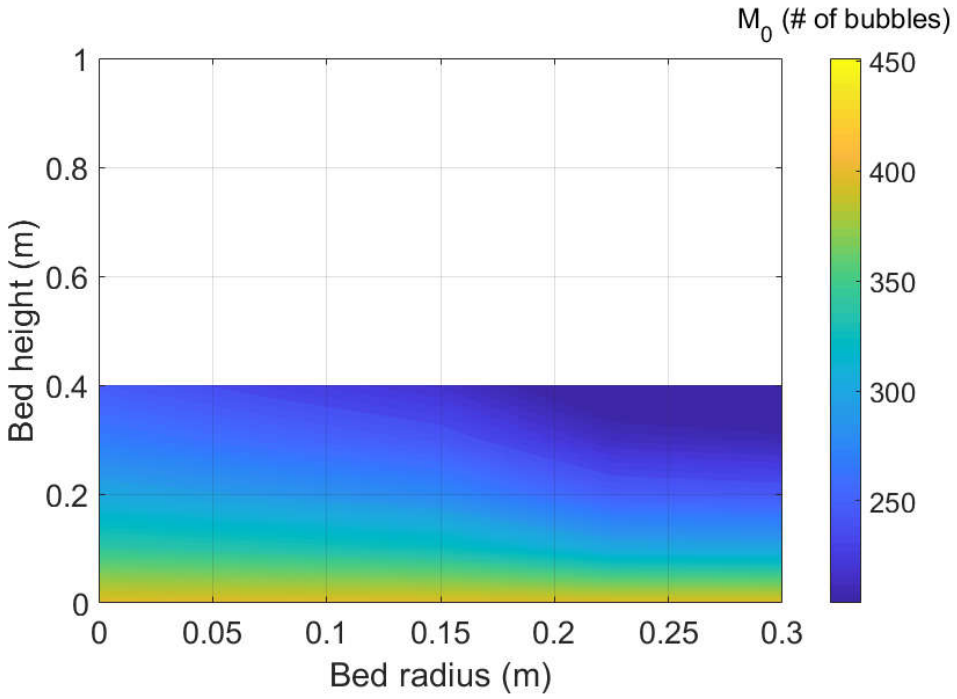

Figure 3-15. Profile of numbers of bubbles in the bubbling fluidized bed

Figure 3-15 shows the profile of the number of bubbles per cubic meter of the reactor (M_0). The initial number of bubbles is given by the configuration of the distributor, which is also taken into account in this model. As the bubbles rise, the coalescence phenomena take place, which leads to the fusion of two or more bubbles, which leads to a low number of bubbles in the upper part of the bed.

Finally, Figure 3-16 shows the evolution over time of the terminal velocity of the particles within the bed for different fluidization velocities.

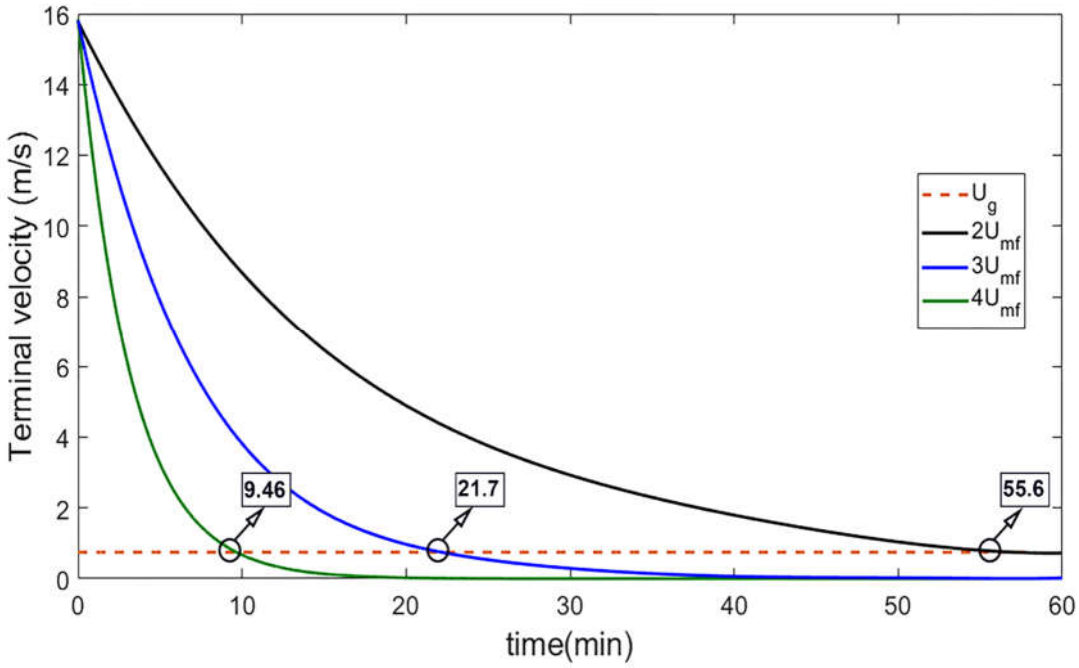

Figure 3-16. Terminal velocity of particles at different minimum velocities of fluidization

The terminal velocity of the particles in this model was calculated taking into account the evolution of the porous structure within the particle. For the same particle size velocities of $2U_{mf}$ to $4U_{mf}$ were simulated. Figure 3-16 shows how the residence time is considerably reduced from 55.6 min to 9.46 min by doubling the fluidization velocity. This is largely due to the asymptotic nature of particle conversion.

3.5 Conclusion

The present work proposes a novel population-balance based model incorporating the effect of bubble coalescence on the evolution of the bubble size distribution. The equations of the developed model were solved simultaneously, integrating reactivity and hydrodynamics as well as energy and mass transfers simulating the dynamics of a bubbling fluidized bed at different scales: pore, particle and reactor. This model was successfully validated with experimental data.

A new mathematical form is proposed for the aggregation frequency, simulating intra-bin and inter-bin coalescence phenomena. This aggregation frequency depends on the bubble density within a given element in the case of intra-element coalescence and on the adjacent element bubble density in the case of inter-element coalescence. The mathematical form proposed in this work predicts the bubble migration from the reactor wall towards the center. This phenomenon has been observed experimentally, however, it had not been modelled previously. Consequently, its successful prediction is a significant contribution of this work. In addition, the aggregation frequency can be used as a parameter for scaling fluidized bed reactors, representing another significant contribution of this work.

3.6 Notation

a_{g0} Aggregation frequency (m3/s)

a Surface area of bubbles per unit volume (m^2/m^3)

B Birth term in the population balance equation

$\mathbb{C}_{i.e}$ Concentration of species *i* in emulsion phase (kmol/m^3 reactor)

$\mathbb{C}_{i.b}$ Concentration of species *i* in bubble phase (kmol/m^3 reactor)

C_{CO_2} Concentration of CO_2 in the particle

Cp_e Average specific heat of the emulsion phase (J/kg-K)

Cp_b Average specific heat of the bubble phase (J/kg-K)

D Death term in the population balance equation

$D_{eff.\mathrm{CO}_2}$ Effective diffusivity of CO_2

$D_{g.i}$ Gaseous dispersion coefficients, axially and radially for emulsion and bubble phase (i=e and i=b) (m^2/s)

$D_{Tg.e}$ Heat diffusivity of gas i in the emulsion phase (m^2/s)

$D_{Tg.b}$ Heat diffusivity of gas i in the bubble phase (m^2/s)

f_b Density distribution function of bubble radius (number of bubbles/m^3 reactor- m of bubble radius)

h_i Specific enthalpy of the gas i (J/kmol)

h_{be} Heat transfer coefficient between bubble and emulsion phases (W/m^2-K)

H Height of bed (m)

k_{E-B} Mass transfer coefficient between emulsion and bubble phases (m/s)

k_1 is the reaction kinetic constant for the CO_2-char reaction

L length (m)

l Average pore length (m)

M_n n-th moment (n=0.1.2.3…) (m^n/m^3 of reactor)

$M_{n.i}$ n-th moment of bin i. m^n/m^3 of reactor

$\dot{N}'''_{p-e.i}$ Flow of the gas i from the particle per unit volume (kmol/m^3-s)

r Radial coordinate within the reactor (m)

r_0 Reactor radius (m)

r_p Radial coordinate of particle

r_b Bubble radius (m)

$\mathrm{r_{p_0}}$ Particle radius (m)

R Radial coordiante within the particle (m)

R_0 Particle radius (m)

S Specific surface area of particle (m^2/m^3)

S_e Specific surface area of the extended pore system (m^2/m^3)

S_0 Specific surface area at the beginning of reaction (m^2/m^3)

T_i Temperature of phase i (i=e and i=b) (K)

u_b Bubble velocity (m/s)

u_g Gas velocity (m/s)

X Conversion

z Axial coordinate of bed height (m)

$\alpha_{i.j}$ Stoichiometric coefficient of the gas i in the reaction j

$\ddot{I}_j$ j-th volumetric reaction rate (kmol/m^3-s)

ΔH_j Heat of reaction j (J/kmol)

ρ_b Density of the bubble phase (kg/m^3)

ρ_e Density of the emulsion phase (kg/m^3)

ϵ_{mf} Volume fraction of bubbles for the minimum fluidization velocity (m^3 of bubbles/m^3 of reactor)

ϵ_b Volume fraction of bubbles within reactor (m^3 of bubbles/m^3 of reactor)

ε Porosity of particle (m^3 of pore/ m^3 of particle)

v_C is the volumetric fraction of carbon in the particle

References

1. Meerman JC, Knoope M, Ramírez A, Turkenburg WC, Faaij APC. The Techno-Economic Potential of Integrated Gasification Co-Generation Facilities with CCS Going from Coal to Biomass. Energy Procedia. 2013;37:6053-6061.
2. Higman C, van der Burgt M. Gasification. Elsevier; 2008.
3. Basu P. Biomass Gasifcation and Pyrolysis Practical Design and Theory. Elsevier; 2010.
4. Rüdisüli M, Schildhauer TJ, Biollaz SM a., van Ommen JR. Scale-up of bubbling fluidized bed reactors — A review. Powder Technology. 2012;217:21-38.
5. Horio M, Nonaka A, Sawa Y, Muchi I. A new similarity rule for fluidized bed scale-up. AIChE Journal. 1986;32(9):1466-1482.
6. Knowlton TM. Fluidized Bed Technologies for Near-Zero Emission Combustion and Gasification. In: Fluidized Bed Technologies for Near-Zero Emission Combustion and Gasification. Elsevier; 2013:481-523.
7. Mahecha-Botero A, Grace JR, Elnashaie SSEH, Lim CJ. Advances in modeling of fluidized-bed catalytic reactors: A comprehensive review. Chemical Engineering Communications. 2009;196(11):1375-1405.
8. Grace JR. An evaluation of models for fluidized bed reactors.Fluidization fundamental studies, solid-fluid reactions, and applications. American Institute of Chemical Engineers. Published online 1971:159-157.
9. Horio M, Wen CY. An assessment of fluidized bed modeling. Fluidization Theories and Applications. 1977;73:9-21.
10. Geldart D. Gas Fluidization Technology. Wiley; 1986.
11. Yang W-C. Handbook of Fluidization and Fluid-Particle Systems. Vol 1.; 2003.
12. Kershenbaun L. Models for flow systems and chemical reactors. International Journal of Heat and Mass Transfer. 1977;20(5):581.
13. Davidson JF (John F, Harrison D (David). Fluidised Particles. University Press; 1963.
14. Gómez-Barea A, Leckner B. Modeling of biomass gasification in fluidized bed. Progress in Energy and Combustion Science. 2010;36(4):444-509.
15. Tomeczek J, Kudzia W, Gradonń B, Remarczyk L. The influence of geometrical factors and feedstock on gasification in a high temperature fluidised bed. The

Canadian Journal of Chemical Engineering. 1987;65(5):785-790.

16. Maya JC, Chejne F, Gómez CA, Bhatia SK, Janna FC. Effect of the CaO sintering on the calcination rate of CaCO3 under atmospheres containing CO2. AIChE Journal. 2018;142(10):3638-3648.
17. Maya JC, Chejne F, Bhatia SK. Novel model for the sintering of ceramics with bimodal pore size distributions: Application to the sintering of lime. AIChE Journal. 2017;63(3):893-902.
18. Maya JC, Chejne F, Bhatia SK. On the modeling of the co2-catalyzed sintering of calcium oxide. AIChE Journal. 2017;63(8):3286-3296.
19. Maya JC, Macías R, Gómez CA, Chejne F. On the evolution of pore microstructure during coal char activation with steam/CO2 mixtures. Carbon. 2020;158:121-130.
20. Bhole MR, Joshi JB, Ramkrishna D. Population balance modeling for bubble columns operating in the homogeneous regime. AIChE Journal. 2007;53(3):579-588.
21. Solsvik J, Jakobsen HA. Bubble Coalescence Modeling in the Population Balance Framework. Journal of Dispersion Science and Technology. 2014;35(11):1626-1642.
22. Ahmadzadeh A, Arastoopour H, Teymour F, Strumendo M. Population balance equations' application in rotating fluidized bed polymerization reactor. Chemical Engineering Research and Design. 2008;86(4):329-343.
23. Muralidhar R, Gustafson S, Ramkrishna D. Population balance modelling of bubbling fluidized beds. II. Axially dispersed dense phase. Sadhana. 1987;10(1-2):69-86.
24. Sweet IR, Gustafson SS, Ramkrishna D. Population balance modelling of bubbling fluidized bed reactors—I. well-stirred dense phase. Chemical Engineering Science. 1987;42(2):341-351.
25. Movahedirad S, Molaei Dehkordi A, Deen NG, van Sint Annaland M, Kuipers JAMH. Novel phenomenological discrete bubble model of freely bubbling dense gas-solid fluidized beds: Application to two-dimensional beds. AIChE Journal. 2012;58(11):3306-3317.
26. Shah BH, Ramkrishna D, Borwanker JD. Simulation of bubble populations in a gas fluidized bed. Chemical Engineering Science. 1977;32(12):1419-1425.
27. Argyriou DT, List HL, Shinnar R. Bubble growth by coalescence in gas fluidized beds. AIChE Journal. 1971;17(1):122-130.

28. Maya JC, Chejne F. Novel model for non catalytic solid–gas reactions with structural changes by chemical reaction and sintering. Chemical Engineering Science. 2016;142:258-268.
29. Gavalas GR. A random capillary model with application to char gasification at chemically controlled rates. AIChE Journal. 1980;26(4):577-585.
30. Bhatia SK, Perlmutter DD. A random pore model for fluid-solid reactions: I. Isothermal, kinetic control. AIChE Journal. 1980;26(3):379-386.
31. Bhatia SK, Perlmutter DD. A random pore model for fluid-solid reactions: II. Diffusion and transport effects. AIChE Journal. 1981;27(2):247-254.
32. Abba IA, Grace JR, Bi HT, Thompson ML. Spanning the flow regimes: Generic fluidized-bed reactor model. AIChE Journal. 2003;49(7):1838-1848.
33. Darton R, LaNauze R, Davidson J, Harrison D. Bubble growth due to coalescence in fluidised beds. Transcripts of the Institute of Chemical Engineering. 1977;55:274-280.
34. NATO ASI Series. Chemical Reactor Design and Technology. Springer Netherlands; 1986.
35. Chejne F, Hernandez JP. Modelling and simulation of coal gasification process in fluidised bed. Fuel. 2002;81(13):1687-1702.
36. Rüdisüli M, Schildhauer TJ, Biollaz SMA, Van Ommen JR. Radial bubble distribution in a fluidized bed with vertical tubes. Industrial and Engineering Chemistry Research. 2012;51(42):13815-13824.
37. Rüdisüli M, Schildhauer TJ, Biollaz SMA, Wokaun A, Ruud van Ommen J. Comparison of bubble growth obtained from pressure fluctuation measurements to optical probing and literature correlations. Chemical Engineering Science. 2012;74:266-275.
38. Kobayashi N, Yamazaki R, Mori S. A study on the behavior of bubbles and solids in bubbling fluidized beds. Powder Technology. 2000;113(3):327-344.
39. Wang H, Lu Y, Xi K. Bubble behavior in gas–solid bubbling fluidized beds based on EMMS model: Comparison of 2D, Q2D, and 3D simulations. Chemical Engineering Research and Design. 2019;149:65-80.
40. Van Ommen JR, Sasic S, Van der Schaaf J, Gheorghiu S, Johnsson F, Coppens MO. Time-series analysis of pressure fluctuations in gas-solid fluidized beds - A review. International Journal of Multiphase Flow. 2011;37(5):403-428.

41. Lu X, Li H. Wavelet analysis of pressure fluctuation signals in a bubbling fluidized bed. Chemical Engineering Journal. 1999;75(2):113-119.
42. Fan LT, Ho T-C, Hiraoka S, Walawender WP. Pressure fluctuations in a fluidized bed. AIChE Journal. 1981;27(3):388-396.

4. Scaling strategy

In this chapter, a new strategy for the scaling of bubbling fluidized bed reactors is presented. This strategy is based on the bubble size distribution, bubble coalescence phenomenon, and the chemical reactivity, allowing to deduct a dimensionless number Φ that must remain constant at different scales to guarantee the fluidization regime. The proposed strategy is validated from computational simulations carried out at different operating conditions. Additionally, limits for the validity of this scaling strategy were determined, which agrees with those reported in the literature.

4.1 Introduction

Fluidized beds are a heterogeneous mixture of gas and solids with irregular shapes, operated at high gas velocities and elevated temperature and/or pressure, its design is a very difficult task since it requires experience and understanding of the phenomena involved.

The implementation of prototypes on a pilot scale based on experimentation at laboratory scale is one of the most used guidelines to reduce risk in the event of a possible scaling to an industrial level [1]. However, even taking these steps into account, considerable failures have happened due to the incorrect understanding of the physical and chemical phenomena involved, as occurred in the 1950s[2] with the expansion of a Fischer-Tropsch fluidized bed synthesis reactor.

Fluidized bed gasifiers have been extensively explored in both experimental and theoretical approaches. With regard to the theoretical investigations, one of the main research topics is scaling, in which the criteria are hydrodynamic similarities and geometric parameters[3]. However, these scaling methods have been questioned by different authors[4,5] because they cannot be applied in a wide range of operating conditions. This is due to the fact that scaling

in the industry is the result of years of development, experimentation, and adjustments to the process [6], that is, scaling has followed an empirical path. Additionally, the mass and heat transfer phenomena occurring in the fluidized bed environment were commonly neglected [7].

Knowlton and Karri [8] studied the scaling of fluidized bed gasifiers by means of empirical techniques and mathematical models relating to certain dimensionless groups. They found that by using Geldart type-A particles, the turbulent fluidized beds operate at higher gas velocities, improving mass transfer and yields. However, the latter approach is empirical since it can only be applied to particular processes, it implies many hours of previous experimentation.

Kunii and Levenspiel [9,10] analyzed the basic problem of “scale-up” and “scale-down,” which lies in the low similarity of fluid-dynamic patterns; this is due to the different bubble formation patterns between Geldart type B particles (100 to 1000 μm) and Geldart type A particles (30 and 100 μm). Finally, they established that fluid dynamics is the main factor affecting bed stability and proposed to use bubbles with similar sizes for every scale.

S. Maure, M. Rüdisüli, *et al.* [11] suggested coupling the hydrodynamic, mass transfer and kinetic phenomena while maintaining constant operating parameters of the scaled reactor. This method yielded fairly accurate predictions for reactors with fixed dimensions; however, the possibility of changing the reactor geometry has not yet been considered. Research with a more phenomenological basis was made by Bo Leckner et. [12], who developed a two-phase model in which the main flow is the gas phase and the particles are the connection between the two phases. They concluded that a correct scaling process can be carried out by considering the fundamental fluid dynamic equations and taking into account the morphological characteristics of particles. On the other hand, Van der Hoef et al. [13] performed a detailed review of fluidized bed reactors scaling by integrating flow models for gases and solids. In this paper, the classical particle model was improved by presenting a new drag force correlation for homogeneous systems.

In the study presented by Maurer et al.[14], the scaling parameters for fluidized and catalytic bed reactors were investigated. They identified the main shortcomings of models reported in the literature and found that the most sensitive parameters on fluidization are the reactor diameter and particle size. They proposed a different approach to the scaling based on

bubble size with which the predictions about selectivity, mass transfer, and stability of the bed height were considerably enhanced.

Works such as that of Matsen [4] studied the scaling based on factors directly affecting fluidization of the bed and studied the effect of minimum fluidization velocity and bed types on the scaling process. They found, by means of empirical correlations based on experimental data, that fluidized beds of different diameters have hydrodynamic similarity if they have a similar Reynolds number, geometry, solid-to-gas ratio, and pattern of bubble interactions.

Glicksman [15] made significant advances in scaling fluidized bed reactors and studied the critical problem of maintaining yields at different scales. The author evaluated the impact of diameter on hydrodynamics and how geometric parameters influence thermal and chemical conditions, residence time, and gas distribution.

Tomeczek et al. [16] explored the geometry by modifying the relationship between diameter, overflow height and reactor size. They studied three different configurations in order to vary residence times for different particle sizes (0.5 mm-1 mm and 1 mm-1.5 mm). They concluded that the variation of geometric parameters mainly affects the residence time of particles in the bed and that the heating value increases with the particle radius.

One of the most important works about scaling laws was carried out by Horio, *et al.* [17]; they developed a hydrodynamic similarity rule for fluidized bed scaling based on bubble equations and gas dynamics. Theoretically, it was shown that it is probable to guarantee the hydrodynamic regime between scales by maintaining the rate of bubble coalescence and the pattern of interstitial flow and bubble division constant. Furthermore, as a significant contribution, if the rule is fulfilled, the longitudinal distribution of the average bubble diameter and the radial distribution of the bubble surface velocity can be maintained in a similar way between different scales.

In more recent studies, Knowlton [18] worked on scaling bubbling fluidized beds and circulating fluidized beds focusing on the most common problems of industrial scale-up. He proposed a methodology that couples the design of the reactors and the mass production, and concluded that there is a significant advancement in scaling fluidized bed reactors. However, the author did not take into account the hydrodynamic effects related with the change in particle size.

As can be seen above, there are many studies and theories proposed for scaling gasification reactors. However, a methodology that couples the hydrodynamics and the chemical kinetics has not yet been developed. Hence, the main objective of this chapter is to develop a scaling methodology integrating both the physical and chemical processes involved in fluidized-bed gasification.

4.2 Fluidized beds modelling for scaling

The aim of scaling a process can be conceived as transferring information from one equipment of a given size to another equipment of different size in such a way that yields are similar or better. During this scaling process, the aim is to avoid economic losses and unsuccessful efforts at all costs, so mathematical models have become a basic scaling tool, according to several authors in recent years [4,19–23]. Frequently, these mathematical models are extremely complex, partly due to the number of equations and parameters describing a bubbling fluidized bed and the high computational effort required even with current technological advances. In this way, several authors [20,21,24–29] have modeled bubbling fluidized beds from basic equations and accepted models such as that of the two-phases model until they get to robust models that take into account the kinetics of reactions and three-phase models. However, most of these models have many simplifications and are empirical or semi-empirical.

With the data reported in the literature, regarding the simulations of the mathematic models [20,30–35], it has been shown that changes associated with the performance and behavior of reactors when moving from an operating scale to a larger scale (i.e., scale-up) are associated with changes in the mechanical and hydrodynamic properties of the fluid such as gas velocity, size and distribution of bubbles, hydrodynamic regime changes, and design details such as the distributor plate [19,36].

One of the strategies used for scaling processes is deriving dimensionless number by using the constitutive equations in their dimensionless form. According to this, some authors[27,37–43] have studied dimensional numbers, and based on them have proposed scale law numbers, which have been successful. These numbers generally describe the hydrodynamics of fluidized beds, mass and heat transfer. This is the case of the commonly known numbers of Reynolds, Froude, Nussel, and Prandalt. Table 4-1 shows some of the most important scaling laws proposed in the literature.

Table 4-1. Sets of scaling law in literature.

Author	Scaling law	Description
Gliksman[15,27]	$psd, \frac{d_p}{D}, \varepsilon_{mf}, \varphi, \frac{D}{H}, \frac{\rho_g}{\rho_p}, \frac{U_0^2}{gD}, \frac{U_0 \rho_g d_p}{\eta}$	Equations of movement and mass conservation. Full description of the system. Quality of fluidization.
Horio et al.[37]	$\frac{u_0 - u_{mf}}{\sqrt{gD}}, \frac{u_0}{\sqrt{gD}}$	Phenomenological model of bubbling fluidized bed. Bubble coalescence.
Van den Bleek and Schouten[44]	$K\sqrt{\frac{H}{g}} \propto \left(\frac{\left(u_0 - u_{mf}\right)^2}{gH}\right)^{15/70} \left(\frac{H}{D}\right)^{-1} D^{16/70}$	Pressure fluctuation, Kolmogorov entropy, Maximum-likehood estimator.
Kelkar and Ng[45]	$N_m = \frac{k_{be} a H}{U_0}$ $N_r = \frac{k_r \varepsilon_p H}{U_0}$	Two-phase model and mass transfer.
M.C. Zhang et al.[41]	$\frac{\beta D}{\rho_s U_0}, \frac{gD}{{U_0}^2}, \frac{P_0}{\rho_s {U_0}^2}$	Gas-solid bubbling fluidized bed, ratio of drag force to particle inertia.
Broadhurst and Becker	$psd, \frac{d_p}{D}, \varepsilon_{mf}, \varphi, \frac{D}{H}, \frac{\rho_g}{\rho_p}, \frac{U_0^2}{gD}, \frac{P_0}{\rho_s {U_0}^2}, \frac{U_0 \rho_g d_p}{\eta}$	Buckinham Pi-theorem
Romeo and Johanson	$\frac{d_p}{D}, \frac{\rho_g}{\rho_p}, \frac{u_{mf}^2}{gD}, \frac{u_{mf} \rho_g d_p}{\eta}$	Buckinham Pi-theorem

Chen et al.[46]	Extension of Gliksman's, α	Internal angle of friction
Gibilaro[47]	$\varepsilon_{mb}, \Delta a$	Bubble hold-up, wave amplitude growth rate
Villa, Guardiola[43]	$K_G = KFr_r$	Kolmogorov entropy, Reynolds number
Zhang et al.[39]	$\boldsymbol{u}^* = \frac{u\tau}{L_c} = \frac{\partial x}{\partial t}\frac{\tau}{L_c}, \left(\frac{\partial C}{\partial \tau^*}\right)_m = \frac{div(D_0^* gradC)}{m^{0.5}}$	Particle-residence-time distribution
Mori and Wen[48]	$\frac{D_{BM-}D_B}{D_{BM-}D_{BO}} = exp\left(-0.3\frac{X}{D}\right)$	Bubble size, height variation
He et al.[49]	$\frac{gd_p}{{U_0}^2}, \frac{U_0\rho_s d_p}{\eta}, \frac{\rho_f}{\rho_s}, \frac{H}{d_p}, \frac{D_c}{d_p}, \varepsilon_0, \varphi, \Phi_s$	Scaling Relationships for Gas-Solid Spouted Bed

Adapted from[50]

Several of the models described above work within the limits defined by the authors; however, it can be seen that there is no dimensionless numbers or correlations that take into account the bubble size distribution and the coalescence phenomenon, which are determinant factors for maintaining the fluidization regime.

One of the main characteristics of fluidized beds is the formation of bubbles, which are bags formed by the excess of gas inside the emulsion when the minimum fluidization velocity is exceeded [1]. Authors such as Davidson and Harrison[51] were pioneers in postulating simple correlations to describe the formation of bubbles; however, there are complex phenomena that these simple models do not adequately describe: this is the case of formation, rupture, and coalescence of bubbles [52–56]. These phenomena are of crucial importance to understand the behavior of fluidized beds and maintain the operating regime from one scale to another [35,37]. In accordance with the described previously, this work proposes a series of dimensionless numbers based on population balance models and those already established in the literature in such a way that they relate the coalescence of bubbles with the other hydrodynamic parameters that describe the behavior of bubbling fluidized beds.

4.3 Dimensionless numbers and scaling methodology

The methodology proposed in this work is based on the modelling of a bubbling fluidized bed through the use of population balances, which had not been done until now. First, consider the following continuity equation for the bubble size distribution function

$$\frac{\partial f}{\partial t}+\frac{\partial(u_b f_b)}{\partial z}=B-D \tag{4-1}$$

Where D and B are the death and birth terms respectively and are given by Eqs. (4-2) and (4-3)

$$B=a_{gf}\left[\frac{1}{2}\int_0^{\infty} f_b\left(r_b{}^3-r_b{}'^3\right)^{1/3} f_b\left(r_b'\right)dr_b'+f_{b\,i-1}\left(r_b\right)\int_0^{\infty} f_{b\,i-1}\left(r_b'\right)dr_b'\right] \tag{4-2}$$

$$D=a_{gf}\left[f_b\left(r_b\right)\int_0^{\infty} f_b\left(r_b'\right)dr_b'+f_{b\,i}\int_0^{\infty} f_{b\,i}\left(r_b'\right)dr_b'\right] \tag{4-3}$$

by assuming a steady-state and replacing B and D from Eqs. (4-2) and (4-3), we obtain

$$\begin{aligned}\frac{\partial(u_b f_b)}{\partial z}=\overline{a_{gf}}\Bigg[&\left(\frac{1}{2}\int_0^{\infty} f_b\left(r_b{}^3-r_b{}'^3\right)^{1/3} f_b\left(r_b'\right)dr_b'\right.\\&\left.+f_{b\,i-1}\left(r_b\right)\int_0^{\infty} f_{b\,i-1}\left(r_b'\right)dr_b'\right)\\&-\left(f_b\left(r_b\right)\int_0^{\infty} f_b\left(r_b'\right)dr_b'+f_{b\,i}\int_0^{\infty} f_{b\,i}\left(r_b'\right)dr_b'\right)\Bigg]\end{aligned} \tag{4-4}$$

It must be said, that in this case averaged aggregation frequency $\overline{a_{gf}}$ aims at deriving dimensionless parameters useful for the scaling up process. The average aggregation frequency is defined by

$$\overline{a_{gf}}=\frac{\int_0^{r_0} a_{gf}\big|_{z=0}\,2\pi r dr}{\pi {r_0}^2} \tag{4-5}$$

From Eq.(4-5) it is inferred that as the reactor radius increases, the average aggregation frequency also increases. Conversely, as the reactor radius decreases, the average aggregation decreases too. The latter suggests that the average aggregation frequency can be used in the scaling up process. Now, the following set of dimensionless variables are defined

$$r_b{}'^{*} = \frac{r_b{}'}{\overline{r_{b_0}}} \; ; \qquad u_b{}^{*} = \frac{u_b}{u_{b\,0}} \; ; \qquad z^{*} = \frac{z}{H} \; ; \qquad r_b{}^{*} = \frac{r_b}{\overline{r_{b_0}}} \; ; \qquad f_b{}^{*}(r_b) = \frac{f_b\,(r_b)}{f_{b\,0}} \tag{4-6}$$

where $\overline{r_{b_0}}$, $u_{b\,0}$ and $f_{b\,0}$ are the average bubble radius, bubble velocity, and bubble radius distribution function at $z = 0$, respectively. By substituting variables of Eq. (4-6) in Eq. (4-4), we have

$$\begin{aligned}\frac{\partial(u^{*} f_b{}^{*})}{\partial z^{*}} = \frac{\overline{a_{gf}} H f_{b\,0} \overline{r_{b\,0}}}{u_{b0}} \Bigg[\Bigg(\frac{1}{2} \int_0^{\infty} f_b{}^{*} \left(r_b{}^{3} - r_b{}'^{3} \right)^{1/3} f_b{}^{*}(r_b{}') dr_b{}'^{*} \\ + f_{b\,i-1}{}^{*}(r_b) \int_0^{\infty} f_{b\,i-1}{}^{*}(r_b{}') dr_b{}'^{*} \Bigg) \\ - \left(f_b{}^{*}(r_b) \int_0^{\infty} f_b{}^{*}(r_b{}') dr_b{}'^{*} + f_{b\,i}{}^{*} \int_0^{\infty} f_{b\,i}{}^{*}(r_b{}') dr_b{}'^{*} \right) \Bigg]\end{aligned} \tag{4-7}$$

In Eq. (4-7), a dimensionless number appears and it is defined as follows

$$\psi_1 = \frac{\overline{a_{gf}} H f_{b_0} \overline{r_{b_0}}}{u_{b_0}} \tag{4-8}$$

This dimensionless number ψ_1 relates the characteristic time for bubble rising $\tau_{rb} = \frac{H}{u_{b_0}}$ with the characteristic time for bubble coalescence $\tau_a = \frac{1}{\overline{a_{gf}} f_{b_0} \overline{r_{b_0}}}$ as follows

$$\psi_1 = \frac{\tau_{rb}}{\tau_a} \tag{4-9}$$

Thus, the dimensionless number ψ_1 allows relating the forces involved with the bubble rising with those related to the bubble migration from the reactor walls to the center. In this sense, it is expected that maintaining this dimensionless number the bubbling regime will be conserved. Now, taking from the mass balance equation for the emulsion phase, it is obtained that

$$\frac{\partial C_e}{\partial t} = \frac{\partial(u C_e)}{\partial z} + \dot{\gamma}''' - k(C_e - C_\infty) + \frac{1}{r} \frac{\partial}{\partial r} (D_r \frac{\partial C_e}{\partial r}) \tag{4-10}$$

Since it is expected that both radial diffusion and inter-phase mass transfer do not significantly affect the residence time of particles, Eq (4-10) in steady state is reduced to

$$0 = \frac{\partial(u_g \mathrm{C_e})}{\partial \mathrm{z}} + \dot{\gamma}''' \tag{4-11}$$

Now, the following variables are defined,

$$u_g^* = \frac{u_g}{u_{g0}}\ ,\ \dot{\gamma}'''^* = \frac{\dot{\gamma}'''}{\dot{\gamma}_0'''}\ ,\ C_e{}^* = \frac{C_e}{C_{e_0}} \tag{4-12}$$

where, u_{g0}, $\dot{\gamma}_0'''$ and C_{e_0} are gas velocity, volumetric reaction rate, and concentration of the reactant gas at $z = 0$, respectively. Replacing the dimensionless variables of Eq.(4-12) in Eq. (4-11), we have

$$\partial \frac{(u_g^* C_e{}^*)}{\partial z^*} = \frac{H\dot{\gamma}_0'''}{u_{g0} C_{e_0}} \dot{\gamma}'''^* \tag{4-13}$$

where

$$\dot{\gamma}_0''' = \dot{\gamma}_0'' S \tag{4-14}$$

where S is the specific surface area and $\dot{\gamma}_0''$ is the reaction rate in surface basis.

The specific surface area is given by

$$S = 4\pi * \int_o^\infty f_{p_o} * r_{p_o}^2 dr_p \tag{4-15}$$

Or for the case of a uniform particle size distribution

$$S = \frac{6}{dp}$$

From the Eq. (4-13), the following dimensionless number appears, which relates the residence time of the gas $\tau_{ug} = \frac{\mathrm{H}}{u_{g0}}$ with the reactivity time in the emulsion $\tau_{rc} = \frac{C_{e0}}{\dot{\gamma}_0'''}$:

$$\psi_2 = \frac{\tau_{ug}}{\tau_{rc}} \tag{4-16}$$

Thus, ψ_2 couples the hydrodynamic and kinetic phenomena in the bubbling fluidized bed. Finally, by coupling the four characteristic times deduced above, we obtain the following dimensionless numbers

$$\Phi = \frac{\tau_{rb}\tau_a}{\tau_{rc}\tau_{ug}} = \frac{u_{g0}\dot{\gamma}_0'' S}{C_{e0} u_{b_0} \overline{a_{gf}} f_{b_0} \overline{r_{b_0}}} \tag{4-17}$$

The dimensionless number Φ suggests that there is an alternative to scaling bubbling fluidized bed reactors using population balance models. In this way, the aggregation frequency becomes a fundamental scaling parameter since it models the dynamics of bubbles in the bed, this being decisive when it comes to preserving the fluidization regime between different reactor scales. Furthermore, the dimensionless number proposed here integrates reactivity and hydrodynamics of bubbling fluidized bed reactors, which had not

been proposed to date. Furthermore, the dimensionless numbers proposed here contain the most used scaling parameters and reported in the literature.

4.3.1 Limits of the scaling methodology

The scaling proposal developed in this work takes into account hydrodynamic phenomena, mass and energy transfer, and chemical reactions that occur in a bubbling fluidized bed reactor. Therefore, this methodology should not be used for reactors belonging to another fluidization regime. In Figure 4-1 limits are shown according to the hydrodynamics and classification of the particles.

.

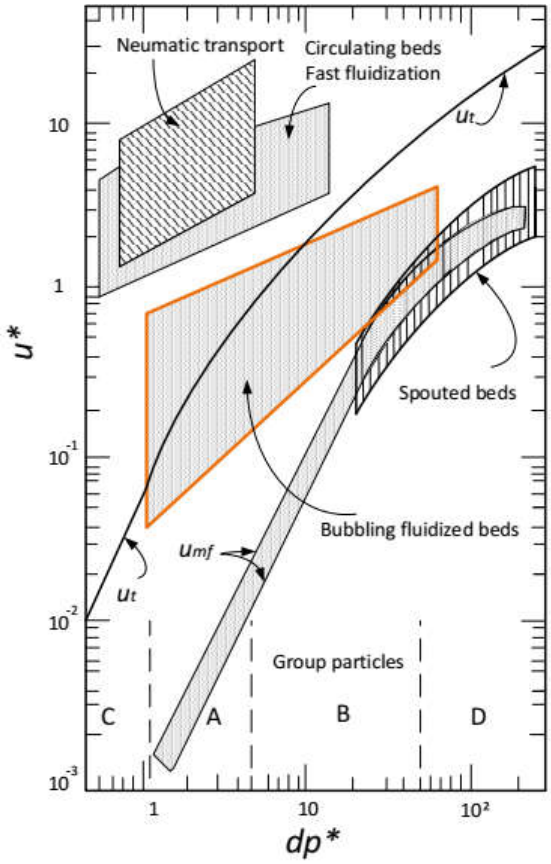

Figure 4-1. Fluidization chart. Adapted from [57]

where,

$$\boldsymbol{d_p^*} = (Ar_{p,mf})^{1/3} = dp\left(\frac{\rho_g(\rho_s - \rho_g)g}{\mu^2}\right)^{1/3} \quad (4\text{-}18)$$

$$\boldsymbol{u^*} = u\left(\frac{{\rho_g}^2}{\mu(\rho_s - \rho_g)g}\right)^{1/3} = \frac{Re_p}{(Ar_{p,mf})^{1/3}} \quad (4\text{-}19)$$

On the other hand, several authors have found, experimentally, [57–62] that for the bubbling regime there is a limit of porosities. Outside these limits, the model loses validity since the behavior of the bed changes from being bubbly to aerated or to a trailing bed. In addition, there are other typical parameters between well-defined limits for the bubbling regime, such as the reactor diameter, the particle size, and the terminal velocity, which is expressed as:

$$u_t = \left(\frac{4g^2(\rho_s - \rho_g)^2}{255\mu_g\rho_g}\right)^{1/3} d_p \quad (4\text{-}20)$$

Thus, Table 4-2 shows a summary of the limits the above-mentioned parameters must be found within in order to ensure that a fluidized bed reactor is in the bubbling regime.

Table 4-2. Scaling limits

Particle size (mm)	0.75 – 2.5
Terminal velocity (m/s)	6.5 – 20.2
Reactor bed diameter (m)	0.4 – 2.2
Bed porosity	0.35 – 0.8

The proposed scaling methodology allows the interconnection of different parameters through dimensionless numbers $\boldsymbol{\tau_{rb}, \tau_a, \tau_{rc}\tau_{ug}}$, which correspond to the characteristic time of bubble rise, bubble coalescence, reactivity, and gas residence, respectively. These numbers are a function of the physical parameters of the bed (particle size, density, viscosity, gas velocity). However, combinations of these numbers can result in a constant Φ parameter and represent an entirely different physical system. That is why scaling limits were proposed to preserve the fluidization regime and therefore the gasifier performance.

4.4 Scaling strategy

A bubbling fluidized bed gasification reactor can be scaled by dimensionless numbers. These must involve the main hydrodynamic parameters on which the process depends, in such a way that when passing from one scale to another they are hydrodynamically similar and their performance is preserved. Thus, the methodology developed is focused on the conservation of these phenomena by proposing a new form of the frequency of aggregation of bubbles and the dimensionless numbers that were deduced as a result of this work. To carry out the scaling of fluidized bed gasification reactors, the following steps are proposed.

I. Use the chart proposed in Figure 4-1 and identify, according to the physical properties of the initial bed (gas velocity, particle size, particle density), the type of regime from the calculation of the dimensionless numbers $\boldsymbol{u}^*$ and $\boldsymbol{dp}^*$.

II. Set the diameter of the new reactor to scale

III. Determine the kinetics of the particles to feed the model and set a constant operating temperature between scales.

IV. Carry out simulations using the mathematical model developed in this work, varying the particle size and gas velocity to later confirm that values are within the limits of bed porosity and terminal velocity of the particles.

V. Calculate the dimensionless numbers $\boldsymbol{\tau_{rb}, \tau_a, \tau_{rc} \tau_{ug}}$

VI. Calculate the number Φ for the two scales: the initial one and the one to be scaled, and confirm that the scaling parameter remains approximately constant. Otherwise it is necessary to repeat the steps and assign new values for the particle size and operating conditions of the reactor.

Calculate the number Φ to validate the aforementioned scaling strategy, the scaling limits proposed in this work were taken (see table Table 4-2). For particle sizes from 0.75mm to 2.5mm and reactor diameter from 0.4m to 2.2m the fluidization regimes were determined as shown in Figure 4-2.

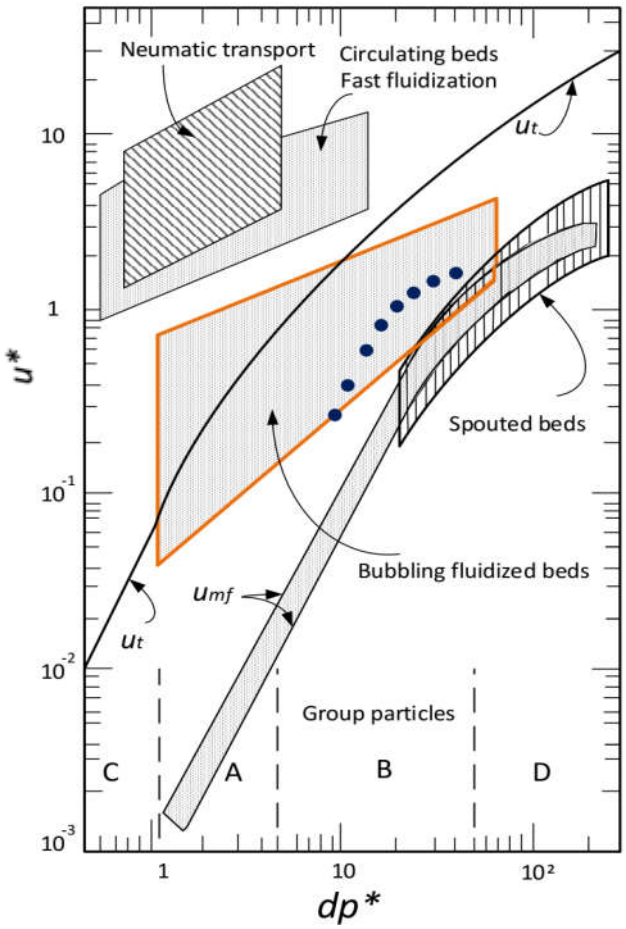

Figure 4-2. Study cases

The operating points indicated in the scaling chart were located from the calculations of $\boldsymbol{u}^*$ y $\boldsymbol{dp}^*$ based on the physical properties of the particle (ρ_s,d_p) and the hydrodynamic parameters of the bed (μ_g, ρ_g, u_{mf}) as indicated in Eqs. (4-18) and (4-19) shows the variation of the parameters dp and dr to obtain the number Φ. As mentioned above, this number relates the characteristic time of bubble rise, the aggregation frequency of bubbles, the reactivity and the residence time of the particles within the bed. Table 4-3 shows the variation of the parameters $\boldsymbol{dp}$ and $\boldsymbol{dr}$ to obtain the number Φ.

Table 4-3. Scaling results

$\boldsymbol{dr(m)}$	0.4	0.6	0.8	1	1.2	1.5	2	2.2
$\boldsymbol{dp\ (*10^{-3}m)}$	0.75	1	1.2	1.5	1.7	2	2.2	2.5
$\boldsymbol{u^*}$	0.235	0.404	0.571	0.856	1.051	1.386	1.605	1.929
$\boldsymbol{dp^*}$	9.11	12.93	15.52	19.39	21.98	25.86	28.45	32.33
$\boldsymbol{\Phi}$	0.447	0.447	0.448	0.450	0.455	0.457	0.458	0.458
time at which terminal velocity is reached $(\boldsymbol{min})$	13.83	19.22	21.79	23.69	27.03	32.83	37.19	40.4
residence time to achieve 80% particle conversion $(\boldsymbol{min})$	13.34	16.42	18.5	20.32	24.67	30.04	34.12	38.64
Gas Flow $(\boldsymbol{m^3/min})$	0.4	1.57	3.9	8	15	26	38	47
Feed $(\boldsymbol{kg/min})$	3.5	6.7	10.6	15.2	20.8	23.1	36.1	38.6

The dp - dr pairs can have a significant number of combinations, however, as mentioned above, it is important to make sure that this combination is consistent with the physical representation of the process. Accordingly, for a reactor diameter of 2.2 m, an interval of particle sizes from 1 mm to 2.5 mm can be chosen for its operation. Similarly, for reactor diameters of 1.2 m particles from 0.75 mm to 1.7 mm can be selected. This would guarantee

the operating regime avoiding hydrodynamic problems from one scale to another, mainly due to wall effects.

Table 4-3 shows how the variation of these two parameters (dp, dR) has a strong influence on the overall hydrodynamics of the bed and on the mass transfer phenomena. It is also observed that the number Φ remains approximately constant between the different scales and therefore the fluidization regime is conserved (see Figure 4-3). Furthermore, for each simulation, it is observed that the conversion of the particles is guaranteed by 80%. The above is explained by the fact that the scaling methodology proposed here involves the terminal velocity, which is directly related to the conversion of the reactive particle.

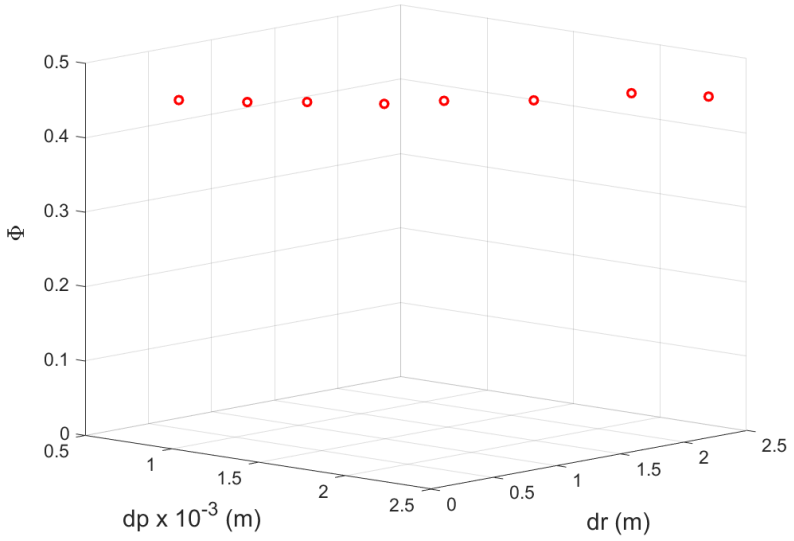

Figure 4-3. Scaling results

Figure 4-3 shows that the ***Φ*** number remains constant for the scaling of reactors ranging from 0.4 m to 2.2 m with variations in particle size, which also allows the reactor performance to be maintained. In addition, Figure 4-3 constitutes an important tool to scale-up or scale down within the established limits.

Since the study case presents a wide range of reactor sizes, the number ***Φ*** was analyzed for each of them using statistical parameters in order to establish correlations between variables.

The maximum value of number ***Φ*** is 0.458 an the minimum value 0.447 with a median of 0.452. These data do not present values far from the median (outliers). Similarly, the ***Φ***

number was evaluated using Student's t-test to verify the dispersion of the data. A significance value α=0.25 resulting in a confidence interval of 0.452±0.0057, which indicates that the data set of the Φ number is included in the said interval and does not present a significant dispersion.

Since the Φ number is represented by multiple variables, a statistical analysis was necessary. This was evaluated using Pearson's linear correlation coefficient, since it allows estimating the reciprocity between two variables and thus determining which of them has greater sensitivity when scaling, resulting in the particle size as a fundamental factor to when keeping the Φ number constant between scales. See appendix A.

4.5 Concluding remarks

In this work, it was proposed a scaling strategy for bubbling fluidized bed gasification reactors based on a novel model that groups chemical kinetics, hydrodynamics, and population balances into the dimensionless number Φ. This strategy allows the scaling of reactors while keeping the reaction yields and hydrodynamic regime within established limits.

The dimensionless Φ number allows to relate both reactivity and hydrodynamics. In this latter, by the very first time, are taken into account the bubble movement in both axial and radial directions, by using the mass equation and a population balance for bubble coalescence, respectively. Thus, the inclusion for the first time of coalescence phenomenon in the scaling of fluidized bed gasification reactors constitutes one of the main contributions of this work, which had not been made so far.

By means of the scaling methodology proposed in this work, it was possible to establish the limits at which the bubbling fluidization regime takes place. It was made by combining the above mentioned methodology with experiments *in silico* based on a comprehensive gasification model described in previous chapters.

References

1. Grace J, Bi X, Ellis N. Essentials of Fluidization Technology. (Grace J, Bi X, Ellis N, eds.). Wiley; 2020.

2. Squires AM. Origins of the Fast Fluid Bed. Advances in Chemical Engineering. 1994;20(C):1-37.

3. Glicksman LR, McAndrews G. The effect of bed width on the hydrodynamics of large particle fluidized beds. Powder Technology. 1985;42(2):159-167.

4. Matsen JM. Scale-up of fluidized bed processes: Principle and practice. Powder Technology. 1996;88(3):237-244.

5. Glicksman LR, Hyre MR, Farrell P a. Dynamic similarity in fluidization. International Journal of Multiphase Flow. 1994;20(94):331-386.

6. Sanderson J, Wang S, Rhodes MJ, Lim KS. An investigation of fluidized bed scaling laws by DEM simulation. In: The 12th International Conference on Fluidization - New Horizons in Fluidization Engineering. ; 2007:671-678.

7. Wu W, Agarwal PK. Heat Transfer to an Isolated Bubble Rising in a High-Temperature Incipiently Fluidized Bed. The Canadian Journal of Chemical Engineering. 2008;82(2):399-405.

8. Knowlton TM, Karri SBR, Issangya a. Scale-up of fluidized-bed hydrodynamics. Powder Technology. 2005;150(2):72-77.

9. Kunii D, Levenspiel O. Circulating fluidized-bed reactors. Chemical Engineering Science. 1997;52(15):2471-2482.

10. Kunii D, Levenspiel O. The RTD and Size Distribution of Solids in Fluidized Beds. Elsevier; 1991.

11. Maurer S, Rüdisüli M. Scale-up of bubbling fluidized bed reactors with vertical internals: A new approach accounting for chemistry and hydrodynamics. The 14th International Conference on Fluidization - From Fundamentals to Products. Published online 2013.

12. Leckner B, Szentannai P, Winter F. Scale-up of fluidized-bed combustion – A review. Fuel. 2011;90(10):2951-2964.

13. van der Hoef MA, Ye M, van Sint Annaland M, Andrews AT, Sundaresan S, Kuipers JAM. Multiscale Modeling of Gas-Fluidized Beds. Advances in Chemical Engineering. 2006;31:65-149.

14. Maurer S, Schildhauer TJ, Ruud van Ommen J, Biollaz SM a., Wokaun A. Scale-up of fluidized beds with vertical internals: Studying the sectoral approach by means of optical probes. Chemical Engineering Journal. 2014;252:131-140.

15. Glicksman LR. Fluidized Bed Scale-up. In: Fluidization, Solids Handling, and Processing. Elsevier; 1998:1-110.

16. Tomeczek J, Kudzia W, Gradonń B, Remarczyk L. The influence of geometrical factors and feedstock on gasification in a high temperature fluidised bed. The Canadian Journal of Chemical Engineering. 1987;65(5):785-790.

17. Horio M, Nonaka A, Sawa Y, Muchi I. A new similarity rule for fluidized bed scale-up. AIChE Journal. 1986;32(9):1466-1482.

18. Knowlton TM. Fluidized Bed Technologies for Near-Zero Emission Combustion and Gasification. In: Fluidized Bed Technologies for Near-Zero Emission Combustion and Gasification. Elsevier; 2013:481-523.

19. Werther J. Scale-up modeling for fluidized bed reactors. Chemical Engineering Science. 1992;47(9-11):2457-2462.

20. Gómez-Barea a., Leckner B. Modeling of biomass gasification in fluidized bed. Progress in Energy and Combustion Science. 2010;36(4):444-509.

21. van der Hoef M a., Ye M, van Sint Annaland M, Andrews a. T, Sundaresan S, Kuipers J a M. Multiscale Modeling of Gas-Fluidized Beds. Advances in Chemical Engineering. Published online 2006.

22. Lungu M, Wang J, Yang Y. Numerical simulations of a bubbling fluidized bed reactor with an energy minimization multiscale bubble based model: Effect of the mesoscale. Industrial and Engineering Chemistry Research. 2014;53(42):16204-16221.

23. Xu M, Ellis N, Ryu HJ, Lim CJ. Modeling of an interconnected fluidized bed reactor for chemical looping combustion. In: 2007 ECI Conference on The 12th Int Conf on Fluidization – New Horizons in Fluidization Engineering. ; 2007.

24. Chejne F, Lopera E, Londoño CA. Modelling and simulation of a coal gasification process in pressurized fluidized bed. Fuel. 2011;90(1):399-411.

25. Chejne F, Hernandez JP. Modelling and simulation of coal gasification process in fluidised bed. Fuel. 2002;81(13):1687-1702.

26. Davidson JF (John F, Harrison D (David). Fluidised Particles,. University Press; 1963.

27. Glicksman LR, Hyre M, Woloshun K. Simplified scaling relationships for fluidized beds. Powder Technology. 1993;77(2):177-199.

28. Natale G, Galgano A, Di Blasi C. Modeling particle population balances in fluidized-bed wood gasifiers. Biomass and Bioenergy. 2014;62:123-137.

29. Abba IA, Grace JR, Bi HT, Thompson ML. Spanning the flow regimes: Generic fluidized-bed reactor model. AIChE Journal. 2003;49(7):1838-1848.

30. Jain AA, Mehra A, Ranade V V. Modeling and simulation of a fluidized bed gasifier. Asia-Pacific Journal of Chemical Engineering. 2018;13(1):1-17.

31. Safarian S, Unnþórsson R, Richter C. A review of biomass gasification modelling. Renewable and Sustainable Energy Reviews. 2019;110:378-391.

32. Farshi A, Boroojerdi S. Modelling of Catalytical Bubbling Fluidized Bed on Pilot Scale. Petroleum & Coal. 2005;(1973).

33. Saxena SC. Mathematical models for fluidized-bed coal combustion and sulfur retention. Energy. 1988;13(7):557-607.

34. Jain MP, Sathiyamoorthy D, Rao VG. A new model for bubbling fluidized bed reactors. Chemical Engineering Research and Design. 2014;92(3):471-480.

35. Sanderson J, Rhodes M. Bubbling fluidized bed scaling laws: Evaluation at large scales. AIChE Journal. 2005;51(10):2686-2694.

36. Chiba T, Terashima K, Kobayashi H. Behaviour of bubbles in gas-solids fluidized beds: initial formation of bubbles. Chemical Engineering Science. 1972;27(5):965-972.

37. Horio M, Nonaka A, Sawa Y, Muchi I. A new similarity rule for fluidized bed scale-up. AIChE Journal. 1986;32(9):1466-1482.

38. van Ommen JR, Teuling M, Nijenhuis J, van Wachem BGM. Computational validation of the scaling rules for fluidized beds. Powder Technology. 2006;163(1-2):32-40.

39. Zhang J, Xu G. Scale-up of bubbling fluidized beds with continuous particle flow based on particle-residence-time distribution. Particuology. Published online October 2014.

40. Di Felice R, Rapagnà S, Foscolo PU. Dynamic similarity rules: Validity check for bubbling and slugging fluidized beds. Powder Technology. 1992;71(3):281-287.

41. Zhang MC, Yang RYK. On the scaling laws for bubbling gas-fluidized bed dynamics. Powder Technology. 1987;51(2):159-165.

42. Mithani R, Shenoi S, Fan LT, Walawender WP. Ranking dimensionless groups in fluidized-bed reactor scale-up. International Journal of Approximate Reasoning. 1990;4(1):69-85.

43. Villa Briongos J, Guardiola J. New methodology for scaling hydrodynamic data from a 2D-fluidized bed. Chemical Engineering Science. 2005;60(18):5151-5163.

44. Schouten JC, Vander Stappen MLM, Van Den Bleek CM. Scale-up of chaotic fluidized bed hydrodynamics. Chemical Engineering Science. 1996;51(10):1991-2000.

45. Kelkar V V., Ng KM. Development of fluidized catalytic reactors: Screening and scale-up. AIChE Journal. 2002;48(7):1498-1518.

46. Yang W-C. Handbook of Fluidization and Fluid-Particle Systems. Vol 1.; 2003.

47. Gibilaro LG. Fluidization-dynamics : the formulation and applications of a predictive theory for the fluidized state. Published online 2001:xxiv, 232 p.-xxiv, 232 p.

48. Mori S, Wen CY. Estimation of bubble diameter in gaseous fluidized beds. AIChE Journal. 1975;21(1):109-115.

49. He YL, Lim CJ, Grace JR. Scale-up studies of spouted beds. Chemical Engineering Science. 1997;52(2):329-339.

50. Rüdisüli M, Schildhauer TJ, Biollaz SM a., van Ommen JR. Scale-up of bubbling fluidized bed reactors — A review. Powder Technology. 2012;217:21-38.

51. Davidson JF (John F, Harrison D (David). Fluidised Particles,. University Press; 1963.

52. Muralidhar R, Gustafson S, Ramkrishna D. Population balance modelling of bubbling fluidized beds. II. Axially dispersed dense phase. Sadhana. 1987;10(1-2):69-86.

53. Darton R, LaNauze R, Davidson J, Harrison D. Bubble growth due to coalescence in fluidised beds. Transcripts of the Institute of Chemical Engineering. 1977;55:274-280.

54. Argyriou DT, List HL, Shinnar R. Bubble growth by coalescence in gas fluidized beds. AIChE Journal. 1971;17(1):122-130.

55. Mori S, Wen CY. Estimation of bubble diameter in gaseous fluidized beds. AIChE Journal. 1975;21(1):109-115.

56. Solsvik J, Jakobsen HA. Bubble Coalescence Modeling in the Population Balance Framework. Journal of Dispersion Science and Technology. 2014;35(11):1626-1642.

57. Grace JR. Gas-Solid and Other Two-Phase Suspensions. The Canadian Journal of Chemical Engineering. 1986;64(June):353-363.

58. Almendros-Ibáñez JA, Pallarès D, Johnsson F, Santana D. Voidage distribution around bubbles in a fluidized bed: Influence on throughflow. Powder Technology. 2010;197(1-2):73-82.

59. Basu P. Combustion and Gasification in Fluidized Beds.; 2006.

60. Wang D, Fan L-S. Fluidized Bed Technologies for Near-Zero Emission Combustion

and Gasification. Elsevier; 2013.

61. Miao Q, Wang C, Wu C, Yin X, Zhu J. Fluidization of sawdust in a cold model circulating fluidized bed: Experimental study. Chemical Engineering Journal. 2011;167(1):335-341.

62. Bakker PJ, Heertjes PM. Porosity distributions in a fluidized bed. Chemical Engineering Science. 1960;12(4):260-271.

A. Appendix: Pearson's correlation coefficient

According to the parameters that define dimensionless numbers, it was found that there is a strong correlation between the number $\boldsymbol{\Phi}$ and the particle size $\boldsymbol{dp}$. Similarly, this correlation is presented for the number $\boldsymbol{\Phi}$ and size of reactor $\boldsymbol{dr}$. This was evaluated using Pearson's linear correlation coefficient since it allows estimating the reciprocity between two variables, taking into account that values close to +1 indicate a strong and direct correlation. Additionally, since the data sample is small, an adjustment was made for the Pearson correlation with Kendall's tau coefficient in the Matlab R2019b software as shown in Eqs. 1 to 3. Kendall's tau is based on counting the number of pairs (i, j), for i <j, that are concordant, that is, for which $\boldsymbol{\Phi_{a,i}} - \boldsymbol{\Phi_{a,j}}$ and $\boldsymbol{dp_{b,i}} - \boldsymbol{dp_{b,j}}$ have the same sign. For a matrix composed of a column of values $\boldsymbol{\Phi}$ and another column of values $\boldsymbol{dp}$ and in the same way for a column of values $\boldsymbol{\Phi}$ and another column of values $\boldsymbol{dr}$ el Kendall's tau coeffcient has the form

$$\tau = \frac{2K}{n(n-1)} \tag{1}$$

where

$$K = \sum_{i=1}^{n-1} \sum_{j=i+1}^{n} \xi * (\boldsymbol{\Phi_{a,i}}, \boldsymbol{\Phi_{a,j}}, \boldsymbol{dp_{b,i}}, \boldsymbol{dp_{b,j}}) \tag{2}$$

$$\xi * \left(\boldsymbol{\Phi_{a,i}}, \boldsymbol{\Phi_{a,j}}, \boldsymbol{dp_{b,i}}, \boldsymbol{dp_{b,j}}\right) = \begin{cases} 1 \;\; if \;\; (\boldsymbol{\Phi_{a,i}} - \boldsymbol{\Phi_{a,j}})(\boldsymbol{dp_{b,i}} - \boldsymbol{dp_{b,j}}) > 0 \\ 0 \;\; if \;\; (\boldsymbol{\Phi_{a,i}} - \boldsymbol{\Phi_{a,j}})(\boldsymbol{dp_{b,i}} - \boldsymbol{dp_{b,j}}) = 0 \\ -1 \;\; if \;\; (\boldsymbol{\Phi_{a,i}} - \boldsymbol{\Phi_{a,j}})(\boldsymbol{dp_{b,i}} - \boldsymbol{dp_{b,j}}) < 0 \end{cases} \tag{3}$$

Figure A1 shows the polynomial fit between the dimensionless number $\boldsymbol{\Phi}$ and the particle size

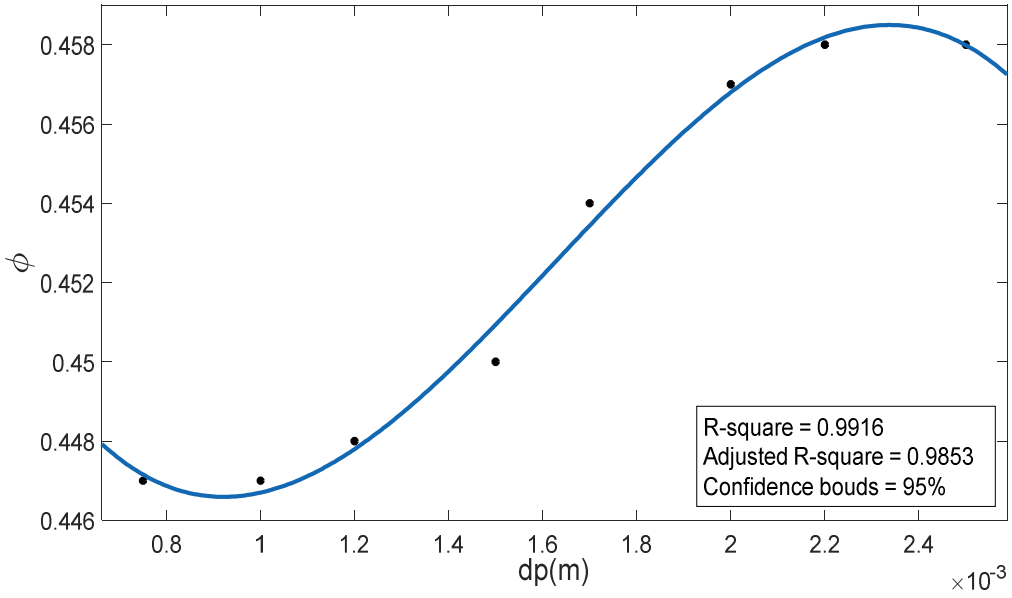

Figure A1.. Data fit for the $\boldsymbol{\Phi} - \boldsymbol{dp}$ pair

with equation

$$\boldsymbol{\Phi} = p_1 * {d_p}^3 + p_2 * {d_p}^2 + p_3 * d_p + p_4 \quad (4)$$

where

$$p_1 = -0.00189,\ p_2 = 0.0002111,\ p_3 = 0.007668,\ \ p_4 = 0.4523 \quad (5)$$

This correlation has a value of 0.9636 for the pair $\boldsymbol{\Phi} - \boldsymbol{dp}$ which indicates a strong and direct relationship between the analyzed variables with a p-val of 1.9845 e-4, this value being below 0.05, indicating that the result of the correlation is trustworthy. Similarly, Figure A2 shows the polynomial fit between the dimensionless number $\boldsymbol{\Phi}$ and the size of the reactor $\boldsymbol{dr}$

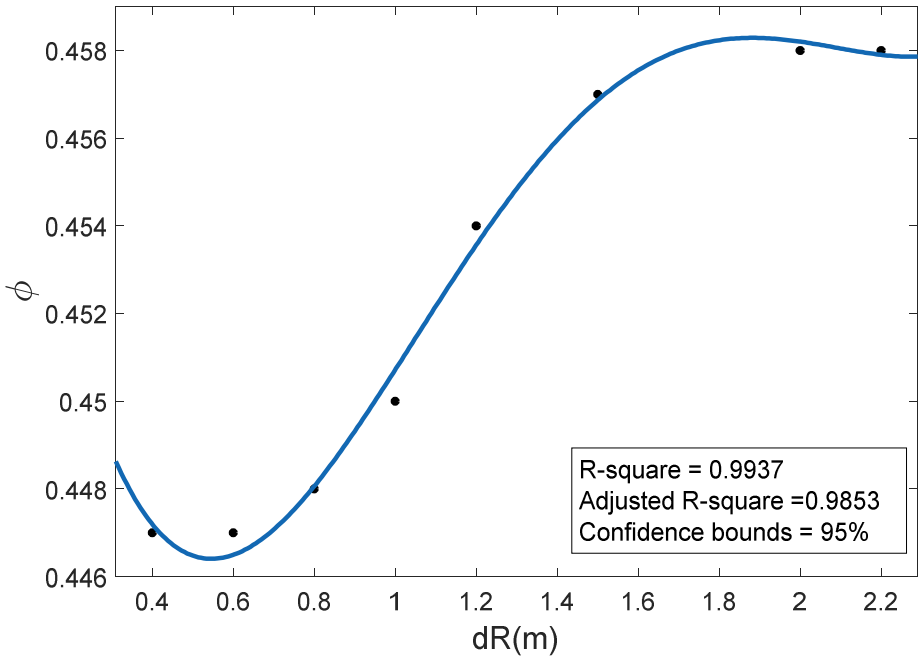

Figure A2. Data fit for the $\boldsymbol{\Phi - dR}$ pair

with equation

$$\boldsymbol{\Phi} = p_1 * dR^4 + p_2 * dR^3 + p_3 * dR^2 + p_4 * dR + p_5 \quad (6)$$

where

$$p_1 = 0.001236,\ p_2 = -0.00271,\ p_3 = -0.002615,\ p_4 = 0.008643,\ p_5 = 0.4537 \quad (7)$$

This correlation has a value of 0.953 for the pair $\boldsymbol{\Phi - dr}$, which indicates a strong and direct relationship between the analyzed variables with a p-val of 2.4651e-4, this value being below 0.05 indicating that the result of the correlation is trustworth